GLYCOSYLATION AT THE CHOROID PLEXUS MODULATES INFLAMMATION STATUS IN ALZHEIMER'S DISEASE

by

DAVID NIX

(Under the Direction of Michael Tiemeyer)

ABSTRACT

Cell surface glycans on glycoproteins and glycolipids modulate cellular interactions in development and disease. Interactions between specific glycans and their cognate glycan binding proteins enhance or suppress inflammatory responses in many vertebrate tissues. Many of these interactions occur at epithelial surfaces, such as the epithelial lining of the airway and the digestive tract. This thesis describes enhanced methods to analyse subsets of glycoprotein glycans that frequently participate in inflammatory responses and applies these methods to the characterization of normal human airway epithelial cells grown and differentiated at an air-liquid interface. This thesis also describes the first comprehensive glycomic characterization of an aggressive mouse model of Alzheimer's disease (AD) and identifies a previously uncharacterized change in the expression of anti-inflammatory glycans at the epithelial interface between the vascular system and the cerebrospinal fluid (CSF). To assess the glycomic changes associated with amyloidopathy of AD, we characterized protein and lipid

glycosylation in the highly aggressive 5xFAD mouse model and detected broad changes in glycoprotein and glycolipid glycosylation by multi-dimensional mass spectrometry. These changes were verified and extended orthogonally using structurally specific plant lectin probes on blots and in tissue sections. We also detected changes in the expression of glycan structures recognized by SIGLEC-F, an anti-inflammatory glycan binding protein expressed on mouse macrophages, eosinophils. microglia, and subsets of T-cells. Engagement of SIGLEC-F by its glycan ligands induces apoptosis in eosinophilic asthma models and supports anti-inflammatory polarization of macrophages. Significantly increased expression of SIGLEC-F glycan ligands was detected in the 5xFAD mouse at the apical surface of the epithelial cells of the choroid plexus (ChP), the ventricular structure responsible for forming CSF and for modulating immune cell trafficking into the brain (Meeker et al. 2012; Lehtinen et al. 2013). Glycan-based immunoprecipitation to identify brain glycoproteins that carry glycans recognized by SIGLEC-F identified two candidate SIGLEC-F counter-receptor proteins, Lipoprotein Receptor Related Protein 1 (LRP1) and Versican (VC). While LRP-1 is significantly increased at the interface between the basal surface of ChP epithelial and endothelial cells in the 5xFAD mouse, it does not colocalize with the distribution of SIGLEC-F ligands. Nonetheless, glycoform differences were detected in comparing the PNGaseF sensitivity and antibody epitope masking of LRP1 in 5xFAD mouse brain compared to control. Like LRP1, VC is also strongly expressed at the endothelial face of the ChP but does not colocalize with SIGLEC-F ligands. Thus, these two proteins likely function as major SIGLEC-F

counter-receptors in whole brain, but the specific counter-receptor at the ChP epithelium remains to be determined. Significant increases in the extravasation of bone marrow derived M2 macrophages (anti-inflammatory macrophages) were detected in the 5xFAD mouse ChP, indicating that the glycomic changes at this essential epithelial interface may mediate recruitment or differentiation of specific inflammatory cells.

INDEX WORDS: Alzheimer's, glycosylation, innate immunity, choroid plexus, Siglecs, inflammation, leukocytes, airway, NHBE, bronchus

GLYCOSYLATION AT THE CHOROID PLEXUS MODULATES INFLAMMATION STATUS IN ALZHEIMER'S DISEASE

by

DAVID NIX

BS, Georgia College and State University, 2006

MS, Georgia College and State University, 2010

A Dissertation Submitted to the Graduate Faculty of The University of Georgia in Partial Fulfillment of the Requirements for the Degree

DOCTOR OF PHILOSOPHY

ATHENS, GEORGIA

2017

GLYCOSYLATION AT THE CHOROID PLEXUS MODULATES INFLAMMATION STATUS IN ALZHEIMER'S DISEASE

by

DAVID NIX

Major Professor: Michael Tiemeyer
Committee: Richard Steet
Lance Wells
Robert Sabatini

Electronic Version Approved:

Suzanne Barbour
Dean of the Graduate School
The University of Georgia
May 2017

DEDICATION

This is for my wife Chelsea. I hope to never know life without you.

ACKNOWLEDGEMENTS

Having to thank those who have helped you along the way is an arduous task. In saying that I don't mean it's difficult to say thank you, rather it's impossible to properly assess the situation and not be hasty. I know without any doubt that I will be forgetting most of those who helped me since my memory is a rusty sieve trying to contain sand. Nevertheless, let me start with my wife Chelsea. She has been a constant source of inspiration and love to help me through this journey towards being over qualified for all jobs except those you don't receive. She has given me the best years of my life and has a contractual obligation to continue to do so. My daughter Calloway is responsible for giving my life purpose and I must thank her for that. It's impossible to know happiness until it shows up at your door screaming and energetic at 3am. My mother is, of course, a big reason why I am here today. She provided me with the ability to make a life when no one else would consider me worthy of a second chance. I would be remiss if I didn't point out how generous and supportive she can be after you track her down. Lastly I want to thank my advisor Mike. He is the source of, and solution to, all of my professional anxiety and stress. I believe he possess the ability to inspire a creative and curious view of scientific problems that others see as impossible, to persevere in the face of difficult objectives without giving up hope, and leave you with absolutely zero solutions since you have to do that by yourself. He also, unexpectedly, inspired an even greater appreciation of

diversity and fostered an expectation of being welcome. Everyone in the Tiemeyer lab is where he or she should be, home, whether that is temporarily or permanently, they are home. I would also like to thank the entire Tiemeyer lab, past and present. Everyone during my tenure here has been incredibly helpful and friendly, making coming to work that much easier.

TALBE OF CONTENTS

Page

LIST OF TABLES

Page

LIST OF FIGURES

Page

Chapter 1

Introduction and Literature Review

Glycosylation is a vital part of life and is involved in many cellular processes and interactions. This has been demonstrated by decades of research in addition to experiments of nature. Defects in glycosylation have been known for decades; however, little therapeutic value has been extracted from research over this period. My goal in research is to add value to the knowledge of inflammatory disease in the search for potential therapeutics. The scope of this dissertation covers changes in glycosylation due to disease or age and the impact this has on inflammation and disease progression.

This chapter will discuss glycosylation in the context of disease. My main thesis project covers alterations of glycosylation in Alzheimer's disease and its role in inflammation and disease progression, so these topics will be covered in great detail. Additional topics covered will include sialic acid binding lectins (Siglecs) and the Choroid Plexus' role as the intersection between the immune system and the brain. I will also discuss the role cellular differentiation has on infection of airway bronchus as it relates to complex glycosylation and siglec binding. Many of the topics covered in the introduction do not have clear relationships, yet all are required for a proper understanding of chapters 2 & 3.

Mammalian Glycosylation

Complex carbohydrates (glycans) are found on the exterior of most vertebrate cells in a fuzzy layer commonly termed the glycocalyx. This thick blanket of diverse glycoproteins, glycolipids, and proteoglycans are essential to life and provide detailed information relative to each cell and their environment. Often cell or tissue specific glycosylation provides a label or unique identifier that is read by nearby cells and provides direct instructions for interaction. These interactions can be direct cell-cell interaction, para- juxta- endo-crine signaling, immune surveillance, and leukocyte extravasation to name a few. These interactions are mediated by several distinct classes of glycans: glycosphingolipids (GSL), glypiation, and C- O- N-linked glycosylation; here I will focus on GSL, O- and N-glycans and their building blocks N-Acetyl-Galactosamine (GalNAc), Mannose (Man), Fucose (Fuc), Glucose (Glc), or N-Acetyl-Glucosamine (GlcNAc) (Moremen et al. 2012).

Modifying glycan structures to achieve specific epitopes is highly regulated and has implications in nearly every biological process. For example, the ABO blood groups were identified in the early twentieth century but were not attributed to the presence of glycan epitopes on red blood cells until 1959 (Watkins and Morgan 1959). We now know that there are two genomic loci that encode the ABO and H determinants. The ABO locus has three possible alleles: allele A and B differ by several single nucleotide polymorphisms (SNP) that result in a difference of four amino acids and change the type of monosaccharide transferred while the O allele encodes a catalytically inactive glycosyltransferase.

These alleles are not expressed throughout the body but are restricted to red blood cells, vascular endothelium, platelets, and various epitheliums. The H blood antigen (commonly called type O) is defined by the addition of a α1-2 fucose to *N*-acetyllactosamine (LacNAc) and is the basis of both A and B blood types. Therefore, if a person doesn't express either the A or B allele then they have type O blood. The addition of a single GalNAc to the H antigen results in type A blood while the addition of a single Gal results in type B blood. While these differences appear minor, a patient with type A blood that receives a transfusion of type B blood will reject the blood, most likely through complement activated hemolysis. This illustrates the point that glycosylation is highly regulated and tissue specific and should be regarded as a functionally relevant post-translational modification in medicine and disease.

N-linked glycosylation

Protein translation at the endoplasmic reticulum (ER) is often modified by the addition of glucose terminated oligomannose glycan(s), $Glc_3Man_9GlcNAc_2$, to asparagine when the consensus motif Asn-X-Ser/Thr is recognized by oligosaccharyltransferase (OST) (Pless and Lennarz 1977; Dempski and Imperiali 2002). The glycans are transferred *en bloc* from a dolichol phosphate precursor, or lipid linked oligosaccharide (LLO), to the nascent polypeptide resulting in a N-linked glycoprotein (Burda and Aebi 1999). The composition of this glycan is highly specific for OST in mammals and plays a role in protein folding. Following the removal of two terminal glucose residues, resulting in

$GlcMan_9GlcNAc_2$, the protein becomes a ligand for the membrane bound or soluble chaperones calreticulin and calnexin (Schrag et al. 2003; Moremen et al. 2012). If the protein does not fold properly then it enters a loop where a glucose is removed by glucosidase II, followed by addition of glucose by UDP-Glc:glycoprotein glucosyltransferase (UGGT1) (Helenius and Aebi 2004). This is necessary since neither chaperone binds the protein backbone and are unable to recognize improperly folded proteins. Interestingly, UGGT1 does recognize globular, unfolded proteins and acts as the signal for entering the “calnexin cycle” (D'Alessio et al. 2010). Proteins that are unable to properly fold are marked for degradation by trimming two mannoses, resulting in $Man_7GlcNAc_2$, before being shuttled to the cytosol for proteasomal degradation (Moremen and Molinari 2006).

The N-linked glycans on folded proteins are further trimmed by glucosidase II resulting in a high mannose glycan $Man_9GlcNAc_2$ that can be further modified through the sequential removal and addition of sugar residues in the Golgi. Prior to leaving the ER, high mannose N-glycans may be trimmed by ER mannosidase I. Once in the Golgi, further trimming can occur by Golgi Mannosidase I to produce $Man_5GlcNAc_2$, which is the starting point for creating both hybrid and complex type N-glycans. This glycan is distinct in structure since the 6-arm retains two mannose residues while the 3-arm is fully trimmed. It is here that the 3-arm may be extended by N-Acetyl-Glucosamine transferase I (GnT-I) to create hybrid N-glycans. If the 6-arm mannose residues are removed

by Golgi Mannosidase II and extended by GnT-II, the glycan is now called complex (**Figure 1.1**).

N-glycans are required for more than assisting in protein folding in the ER. The loss of hybrid and complex N-glycans by deletion of GnT-I in mice is embryonic lethal (Stanley and Ioffe 1995). Whereas, if all N-glycans are lost, through a recessive deletion of UDP-GlcNAc: dolichol phosphate N-acetylglucosamine-1-phosphate transferase, an enzyme required for production of LLO, then embryos are lost during peri-implantation (Marek et al. 1999). Defects in N-glycosylation commonly result in Congenital Disorders of Glycosylation (CDGs) (Freeze and Aebi 2005), dysfunction in cytokine and growth factor signaling (Partridge et al. 2004; Wang et al. 2006), impaired glucose transport (Ohtsubo et al. 2005), and defects in cell differentiation and proliferation (Lau et al. 2007).

Figure 1.1: N-glycosylation

Processing of N-glycans begins in the ER prior to protein folding. Glucosidase and mannosidase enzymes remove residues before transport to the Golgi where final processing happens. The destruction and re-building of the glycan can result in various oligomannose forms or elongated hybrid and complex structures.

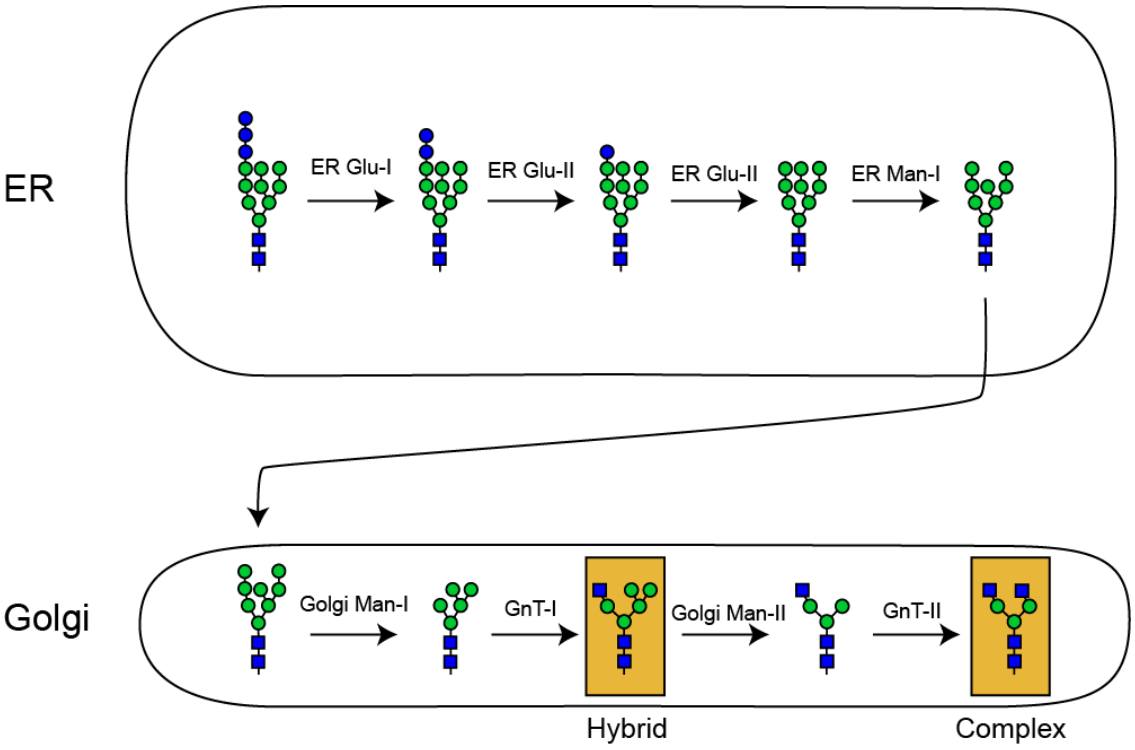

O-Glycans

O-linked glycosylation is the addition of a sugar residue(s) to serine or threonine and can be initiated by GalNAc, Man, Fuc, Glc, or GlcNAc (**Figure 1.2**). O-glycans are not transferred *en bloc* like N-linked glycans; rather they are processively elongated by the addition of single monosaccharides. Only mannose initiated O-glycosylation relies on a lipid-linked precursor, all others utilize nucleotide sugars. The smallest addition that has function is a single GlcNAc addition to nucleocytoplasmic and mitochondrial targeted proteins. These O-GlcNAc proteins are often involved in disease state signaling, nutrient sensing, enzymatic regulation, and processes that can be antagonized by phosphorylation (Bond and Hanover 2015). GalNAc O-glycans are the major extracellular vertebrate O-glycan and are commonly referred to as Mucin-type. O-GalNAc glycans can be classified into 8 categories, or cores, with cores 1-4 being common and widely expressed while cores 5-8 are rarely found (**Figure 1.2**). Initiated in ERGIC or *cis*-Golgi these glycans can be greatly elongated, branched, and contain fucose and Sialic acid (Neu5Ac). The core structure that is made depends on the quantitative expression of the GalNAc-transferase (GalNAc-Ts) enzymes in a particular tissue, since many members of the large GalNAc-T family share overlapping substrate specificity (Gill et al. 2011). For example, Core 1 GalNAc-T (C1GalT) is widely expressed throughout the body while C3GalT is specifically expressed at high levels in gastrointestinal tissues producing core 3 and 4 structures (Gill et al. 2011). The presence of heavily O-GalNAc modified glycoproteins, often mucin protein family members, in airway

and intestine luminal spaces are thought to play a role in innate immunity by providing a sticky barrier to capture pathogens (Linden et al. 2008). The O-glycans found on mucins may also interact with extravasating leukocytes and induce apoptosis in the airway to limit the amount of inflammation during an infection or allergic attack (Kiwamoto et al. 2015). Fucose and glucose initiated O-glycans are highly regulated and only have a few structures (**Figure 1.2**). O-fucose glycans are very often tetrasaccharides that are capped with sialic acid and attached to Notch, however, the length of the glycan determines its function. Each O-fucose modification is site specific and has a function associated with the amount of elongation at that site (Bruckner et al. 2000; Moloney et al. 2000; Taylor et al. 2014). Therefore, each modification has a potential function associated with Notch activity and signaling. To date, the regulation of O-fucose modification and function is not well understood. Interestingly, both O-fucose and O-glucose glycan modifications of Notch are essential and knockouts of either initiating enzyme, *Pofut1* and *Rumi*, result in a similar phenotype. Similar to O-fucose elongation, the addition of xylose to O-glucose also modifies Notch activity (Stanley and Okajima 2010; Takeuchi and Haltiwanger 2014). O-Mannose glycans are expressed in all tissues and categorized into four classes: M0, M1, M2, and M3 (Manya et al. 2006; Praissman and Wells 2014). The best-described O-mannosylated protein is alpha-dystroglycan (α-DG), where proper glycosylation of α-DG is required for interaction with laminin domains in the extracellular matrix. Here, M3 type O-mannose glycans, which are only found at two sites on α-DG in the human proteome based on consequence sequence, are

phosphorylated at the 6-position of the core mannose and extended by a repeating disaccharide of xylose-glucuronic acid (Praissman et al. 2016). If α-DG isn't glycosylated in this way it results in one of the congenital muscular dystrophies (CMD). There are four types of CMDs that can result from a defect in glycosylation, one of which also occurs due to a loss of α-DG.

Figure 1.2: O-glycosylation

O-glycosylation can be initiated by five monosaccharides. GalNAc can be categorized by extension into four common cores and is the most common type of extracellular O-glycosylation. GlcNAc is typically not extended and found on intracellular proteins. Glucose is commonly extended by two xylose residues and found on EGF repeats. Fucose is often a tetrasaccharide and found along side glucose on EGF repeats. Mannose can also be categorized by its extension and has an essential function in the extracellular matrix.

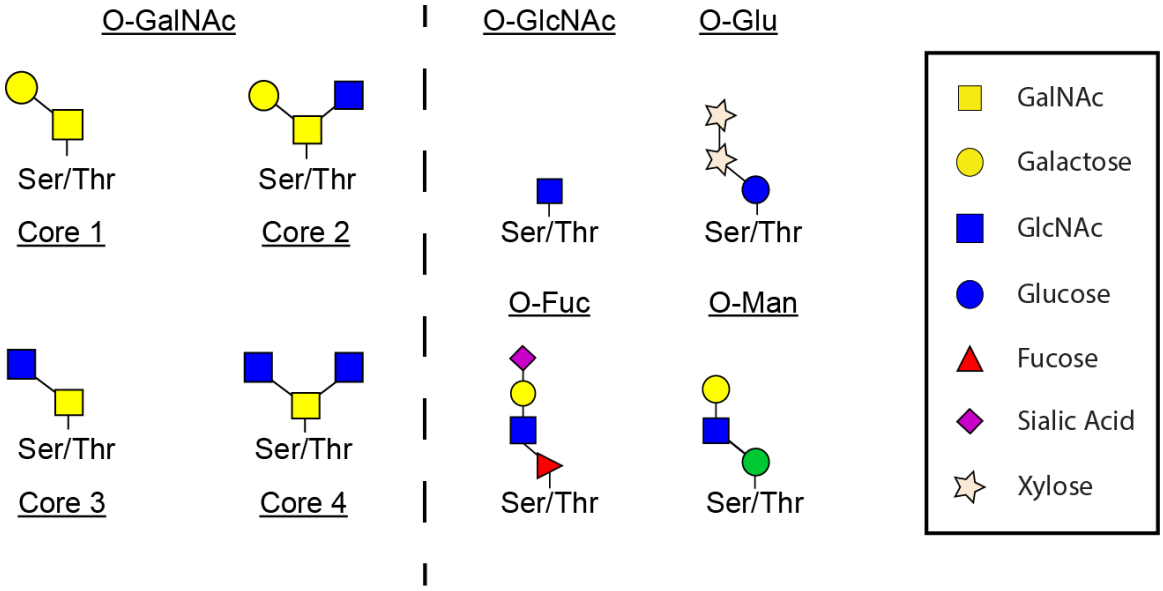

Glycosphingolipids

GSLs are initiated by the transport of ceramide to the cytosolic side of the ER by Ceramide transport protein (CERT) before subsequent CERT independent movement to the Golgi. On the luminal face of the Golgi GlucosylCeramide (GlcCer) synthase adds glucose to ceramide before a flippase orients the monosaccharide towards the lumen of the Golgi (Ishibashi et al. 2013). Production of GalactosylCeramide (GalCer) is slightly different and more restricted. GlcCer is produced throughout the body while GalCer is seemingly restricted to and highly expressed in the brain and kidney. Synthesis is performed by GalCer synthase on the luminal side of the ER (Ichikawa and Hirabayashi 1998). GalCer extension is limited to the addition of either 3-linked sulfate or α3 sialic acid. GlcCer however is much more diverse in possible extentions. There are six categories for the core glycan structure: Lacto, Lactoneo, Globo, Isoglobo, Ganglio, and Muco (**Figure 1.3**). Each category has unique core structures which dictates how the glycan can be extended. The lacto and lactoneo categories share the core glycan structure, Gal-GlcNAc-Gal-Glc-Ceramide, but differ in the linkage between the terminal and penultimate monosaccharides. This is also true for the globo and isoglobo series but the linkage difference is between the second and third monosaccharides. The ganglio and muco series are structurally distinct but share a common core disaccharide with all six categories. The ganglio series is perhaps the most diverse in possible terminal extentions leading to a wide array of similar but different glycans that share a processive enzymatic pathway.

Figure 1.3 Glycosphingolipids

Glycosphingolipids are categorized into eight categories based on two criteria: the extension of the reducing lactose and their linkages. Six of the categories are predominantly neutral, one is predominantly charged (Ganglio), and one is charged by the addition of sulfate (Sulfatides).

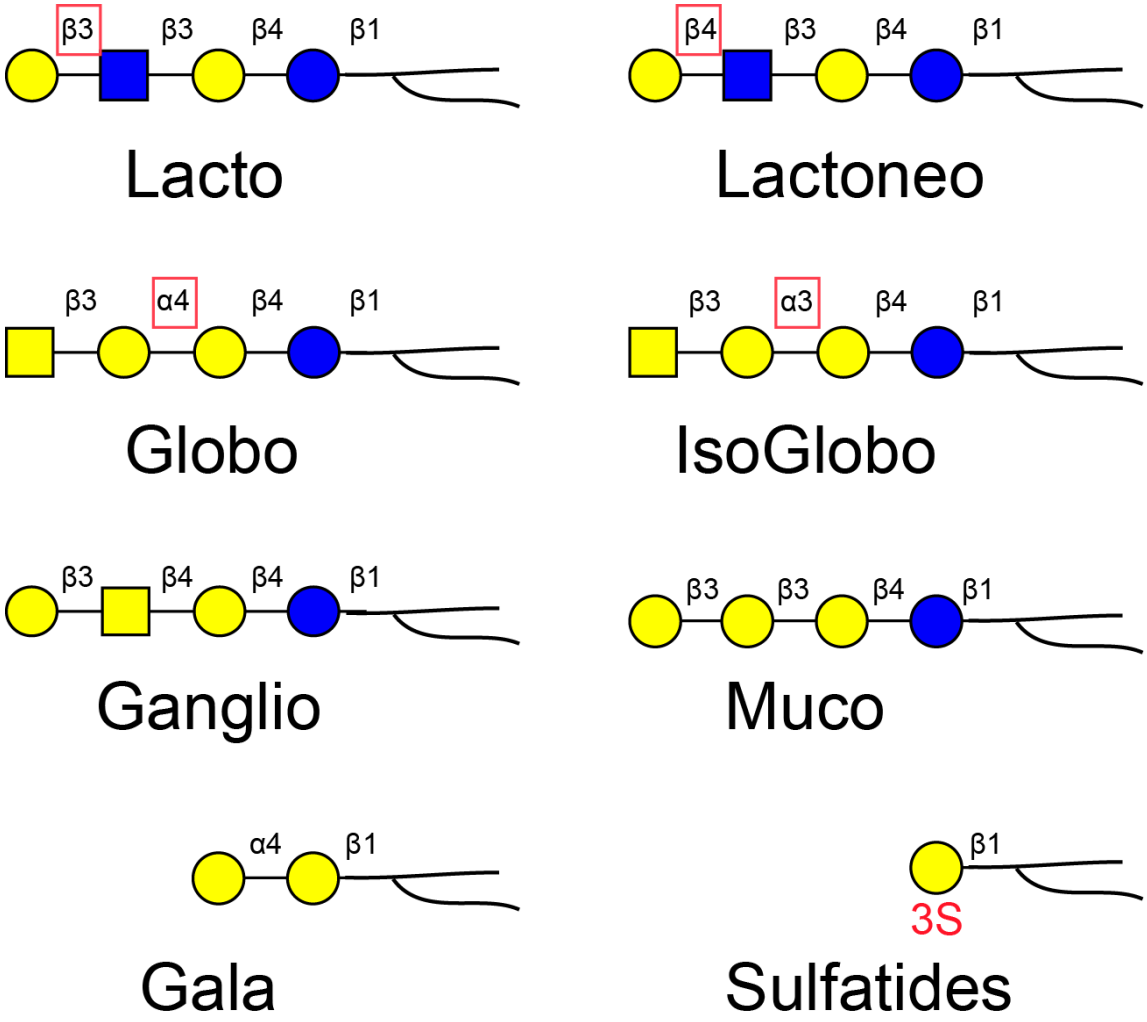

Alzheimer's Disease

Alzheimer's disease is the sixth leading cause of death affecting 6 million Americans and represents the only top ten cause of death without any ability to slow or prevent pathological progression (Xu JQ 2016). There are two classifications for the disease: familial and sporadic. Familial Alzheimer's disease is very early onset and is heritable through mutations in amyloid precursor protein (APP) or presenilin 1 (PS1). Genetic testing provides a highly reliable diagnosis but is rarely useful since familial Alzheimer's accounts for less than 5% of cases. There are no diagnostic tests for sporadic onset Alzheimer's; instead physicians rely on family history and cognitive tests for patients' aged 65 and over. This is a major dilemma in the clinical treatment and diagnosis of Alzheimer's disease since the vast majority of cases are sporadic. Recently a new imaging technique has been developed and approved by the U.S. Food and Drug Administration (FDA). This method relies on tracer molecules (Amyvid (florbetapir F-18), Vizamyl (flutametamol F18), and Neuraceq (florbetaben F18)) that bind to Aβ in the brain and are visualized by Positron Emission Tomography (PET) scanning to identify plaques in a living brain. This method is informative but limited in use.

The prevailing theory for why the disease occurs is the amyloid cascade hypothesis. Simply stated, fragments of APP that bind together and form insoluble oligomers are the cause of the disease (Hardy and Higgins 1992). Processing of APP occurs outside of the disease state in healthy individuals by α-secretase, an extracellular protease, followed by cleavage at a site buried in

the lipid bilayer by γ-secretase. γ-secretase is a protein complex whose catalytic domain is formed by one of the presenilin proteins, PSEN1 or PSEN2. This produces an intracellular fragment that is benign and readily degraded. If α-secretase is replaced by β-secretase (BACE1), the peptide produced is extracellular and varied in length with 1-42aa being the most amyloidogenic. These peptides bind together and form large, extracellular, insoluble deposits that are toxic and induce cell death. Most patients diagnosed with Alzheimer's disease post-mortem show significant deposition of these plaques throughout the brain. However, these amyloid plaques are not unique to Alzheimer's patients. Healthy, non-affected individuals who die of old age also show these deposits, just fewer in number. This is the largest hurdle for PET imaging to overcome since positive identification of Aβ plaques is not sufficient for a diagnosis. Recent research, along with an increasing number of failed clinical trials for biologics targeting amyloid fragments and plaques, are producing stress fractures in the amyloid cascade hypothesis (Herrup 2015; Wisniewski and Goni 2015). Many clinical trials are centered upon removal of Aβ from the brain and blood plasma in hopes of improved cognitive function (**Table 1.1**). Unfortunately, the mostly likely outcome for these trials is unaffected cognitive function with negative clinical side effects, such as micro-hemorrhages, amyloid related imaging abnormalities – edema (ARIA-E), or encephalitis.

Table 1.1: Clinical trails of biologics, their outcomes, and targets

Trial	Stage	Status	Target
AN1792	Phase II	Terminated; No improvement; encephalitis	Aggregated Aβ1-42
CAD106	Phase II	Completed; No safety concerns; Starting new phase II	Aβ1-40 Aβ1-42; Bacteriophage Qβ carrier; T-cell response
ACC-001	Phase II	Completed; No change; Abondoned	Fibrillar brain Aβ
AFFITOPE AD02	Phase II	Completed; No cognitive change	Unmodified N-terminus of Aβ
AADvac1	Phase I	Completed; High IgG titres acheived	Synthetic tau peptide coupled to KLH-ALUM
Bapineuzumab AAB-001	Phase III	Abondoned; No changes; ARIA-E; Micro-hemmorages	Human 3D6 anti-Aβ1-5 monoclonal
Bapineuzumab AAB-003	Phase I	Complete; Increased plasma Aβ; ARIA-E	Reduced Fc of Human 3D6

Alzheimer's disease is generally split into three clinical categories: mild (early-stage), moderate (middle-stage), and severe (late-stage). Common symptoms for the early stage of the disease are often ignored or confused with the pressures of daily life. The most common symptoms include trouble remembering names or recalling a specific word, immediately forgetting newly read material, and losing valuable objects. All of these symptoms can be attributed to almost anyone and are poor indicators of early disease highlighting the need for improved diagnostics and biomarkers. Moderate or middle-stage disease is the most common form since this stage can last for many years to decades. The symptoms are similar to early-stage but more exaggerated with several new and often debilitating complications, such as an increase in mood swings and feeling withdrawn, being unable to recall information like their spouses name, and being unable to control their bladder and bowels. This is commonly where a diagnosis of dementia is reached if there aren't any familial gene mutations. The final stage of the disease renders the person completely helpless making them require constant attention and care. Here a person will commonly be unable to respond to their environment, lose the ability to walk, chew or swallow, and become more susceptible to opportunistic infections.

The first Alzheimer's mouse model was made in 1995 through the insertion of a single mutation at V717F in human APP (Games et al. 1995). This mouse displayed for the first time many of the hallmark symptoms associated with the disease in humans. Current research is often performed with a mouse model that has 5 mutations, the 5xFAD mouse.

5xFAD Mouse Model

Model organisms are indispensable for biomedical research, nowhere more so than for a disease that is intractable in clinical trials (**Table 1.2**). For Alzheimer's disease the most widely utilized mouse model is 5xFAD, named for harboring 5 genetic mutations identified in familial Alzheimer's patients – three in APP [K670N/M671L (Swedish) + I716V (Florida) + V717I (London)] and two in PS1 [M146L + L286V]. These mice have a greatly accelerated pathology showing intraneuronal amyloid at 1.5 months, extraneuronal amyloid plaques at 2 months, memory deficits at 4 months, and neuron loss at 9 months (Oakley et al. 2006; Eimer and Vassar 2013). RNA sequencing was done on the frontal cortex, an area commonly affected in Alzheimer's disease, and the cerebellum, an area uncommonly affected, on 7-week old mice in early stages of the disease. Notably there was an increase in expression of Transthyretin (TTR) in the frontal cortex and a decrease in the cerebellum. This is of interest since TTR is secreted into the CSF by the ChP and binds thyroid hormone, vitamin A, and is associated with amyloidosis (Westermark et al. 1990). There were also RNA transcript variants for Tau-tubulin kinase 1 (TTBK1) and Tau-tubulin kinase 2 (TTBK2) seen in the 5xFAD mice that were not observed in WT littermates. Both TTBK1 and TTBK2 are capable of phosphorylating Tau on serine residues while only TTBK1 can phosphorylate Tau on threonine and tyrosine and induce Tau aggregation (Sato et al. 2006; Bouskila et al. 2011). Interestingly, TTBK2 is a central regulator of ciliogenesis and Sonic Hedgehog (SHH) signaling during neurogenesis (Goetz et al. 2012).

Table 1.2: Alzheimer's disease mouse models

The first mouse model was made using a transgene with a mutation at the γ-secretase cleavage site. Since, many other mouse models have been made using transgenes, multi-transgenes, intracerebroventricular injected Aβ, and severely inbred populations. All models have their virtues, but most lack a central tenet of the disease. Adapted from Puzzo et al (Puzzo et al. 2014).

Name/Genotype	Phenotype	Notes
APP (Mutations at γ-secretase cleavage site 717)	Increased γ-secretase cleavage. More diffuse plaques.	Yes: Amyloid plaques (9-12 mo.), synaptic defects, memory loss No: Tau tangles, neuron loss
APP (Mutations at β-secretase cleavage site 670/671)	Increased β-secretase cleavage. More tau hyperphosphorylation and dense Aβ plaques.	Yes: Amyloid plaques (9-12 mo.), synaptic defects, memory loss No: Tau tangles, neuron loss
APP (Mutations within sequence 692/693)	Increased Aβ oligomerization, significant cerebral amyloid angiopathy	Yes: Amyloid plaques (9-12 mo.), synaptic defects, memory loss No: tau tangles, neuron loss
Single transgene (Presenilin-1). FAD point mutations or exon 9 deletion from human PS1	Altered APP cleavage. Increased Aβ 42:40 ratio. Accelerated neurodegeneration in older mice	Yes: Synaptic defects, neuron loss No: Plaques, tau tangles, neuron loss
Double transgenic (APP/Tau)	Accelerated phenotype and pathology, minimal neurodegeneration	Yes: Plaques (3-6 mo.), tau tangles, neuron loss, synaptic defects, memory loss
3xTg (APP/PS1/Tau)	Accelerated phenotype and pathology	Yes: Plaques (3-6 mo.), tau tangles, neuron loss, synaptic defects, memory loss
Intracerebroventricular injected Aβ into dorsal hippocampus and lateral ventricle	Localized Aβ accumulation. From cell culture media, purified human dimers, and synthetic oligomers	Yes: Synaptic defects, memory loss No: Plaques, tau tangles, neuron loss

SHH signaling is required for proper development of many tissues and organs, is dependent upon the primary cilium for signaling, and required for maintaining the neural stem cell population at the sub-ventricular zone - the region where neurogenesis occurs giving rise to the cortical plate during development and forms new neurons throughout adult life (Ahn and Joyner 2005; Goetz and Anderson 2010).

Leukocyte homing is central to the immune surveillance of tissues. The 5xFAD mouse has decreased expression of four determinants that are central to leukocyte trafficking into the CNS in response to damage: intercellular adhesion molecule 1 (ICAM1), vascular cell adhesion molecule 1 (VCAM1), C-X-C motif chemokine 10 (CXCL10) and chemokine C-C motif ligand 2 (CCL2) (Baruch et al. 2015). This deficit reduces the capability of leukocytes, specifically monocytes, to infiltrate the CNS and resolve inflammation.

Inflammation in AD

The inflammatory response is one of the first lines of defense for the immune system. Upon injury, cytokines are released by resident antigen presenting cells stimulating capillary endothelium to express selectins within the vascular space. Peripheral leukocytes bind these selectins through cell surface glycans that promote a low affinity interaction, which results in “rolling” along the endothelium surface. This interaction promotes integrin expression on leukocytes that bind endothelial receptors such as ICAM or VCAM thereby slowing the rolling and preventing further movement. These cells can now extravasate

through the tight junctions between endothelium as a result of Mast cell degranulation. This movement of leukocytes and blood into the tissue is the basis of the inflammatory response. There are many secreted factors involved in leukocyte recruitment, most of which are cytokines and chemokines. Since the number of known cytokines and chemokines quickly deviates from the scope of this dissertation, an excellent review of their role in inflammatory disease is recommended (Turner et al. 2014).

In Alzheimer's disease there are many factors that affect the overall inflammatory status that include both pro- and anti-inflammatory pathways (**Table 1.3**). There are six pro-inflammatory molecules that are well described in exacerbating inflammation in Alzheimer's disease: Aβ, chromogranin A, chemokines, cytokines, cyclooxygenases, and nitric oxide. Conversely, there is only one molecular system that is not pro-inflammatory, the complement system. Complement directly affects or phagocytosis labeled substrates without the secretion of cytokines. Also listed are NSAIDS, the only therapeutic documented to have any effect on the onset and accumulation of Aβ. How NSAIDS slow the accumulation of Aβ is not known, nor are they equally efficacious for all patients, but their lack of detrimental or adverse side effects coupled with availability and low cost make them very attractive.

The most important molecule that affects the inflammatory status in Alzheimer's disease is Aβ. The detrimental effect of Aβ has long been appreciated and involves many pathways through direct interaction or signaling molecules (Rogers et al. 1992; Yan et al. 1998; Bate et al. 2004; Fassbender et

al. 2004; Simard et al. 2006; Maier et al. 2008; Griciuc et al. 2013). The production of Aβ is neurotoxic and leads to continued production of Aβ in a positive feedback loop which doesn't seem to have an endogenous method of limitation. There are several cell surface receptors on microglia that can bind Aβ, including CD36, α6β1 integrin, and Toll-like receptors (TLR2, TLR4, TLR6, and TLR9) (Heneka et al. 2015). Microglia and blood derived macrophages are capable of phagocytosis upon receptor ligation but are not a complete means of regulating Aβ plauqe accumulation (Paresce et al. 1996). While the accumulation of Aβ plauqes directly influences the amount of systemic or chronic inflammation, the type of plauqes present is key. Diffuse plauqes that do not exhibit strong immunohistochemical staining *in vivo* are not responsible for propagating inflammation (Eikelenboom and Veerhuis 1996). Instead it is the fibrillar Aβ plauqes, also called classical or neuritic plaques, that cause inflammation through binding microglia and macrophages (Itagaki et al. 1989).

Table 1.3: Proteins, small molecules, and drugs known to modulate inflammation in Alzheimer's disease.

Name	Effect	Reference
Amyloid Beta	Pro-inflammatory. Activates microglia through scavenger receptors and pattern recognition receptors.	(Rogers et al. 1992; Yan et al. 1998; Bate et al. 2004; Fassbender et al. 2004)
Chromogranin A	Pro-inflammatory. Activates microglia and causes neuronal death	(Taupenot et al. 1996; Ciesielski-Treska et al. 1998)
Complement	Anti-inflammatory. Reduction of plaques, neurodegeneration.	(Botto 1998; Taylor et al. 2000; Wyss-Coray et al. 2002; Fonseca et al. 2004; Maier et al. 2008)
Chemokines	Both pro-inflammatory and anti-inflammatory. Recruit microglia, astrocytes, monocytes, leukocytes, and lymphocytes.	(Xia and Hyman 1999; Stalder et al. 2005; Charo and Ransohoff 2006; Simard et al. 2006)
Cytokines	Both pro-inflammatory and anti-inflammatory. Lengthen intensity of immune response or reduce immune response.	(Wyss-Coray et al. 2000; Tuppo and Arias 2005; Rota et al. 2006)
Cyclooxygenases	Both pro-inflammatory and anti-inflammatory. Expressed by microglia, astrocytes, monocytes, and neurons	(Bauer et al. 1997; Yermakova et al. 1999; Shie et al. 2005)
Nitric Oxide	Pro-inflammatory. Induced in macrophages, microglia, astrocytes by LPS or cytokine stimulation	(Corradin et al. 1993; Vodovotz et al. 1996; Heneka et al. 2001)
NSAIDs	Pharmacological treatment, anti-inflammatory. Several potential effects including prevention of amyloid formation and alteration of APP processing	(Thomas et al. 2001; Agdeppa et al. 2003; Sastre et al. 2003; Sastre et al. 2006)

Chemokines are a class of secreted proteins that direct the migration of lymphocytes and other immune cells to a site of injury or damage through the production of a chemo-attractant gradient. Many chemokines have been implicated or shown to be involved in Alzheimer's disease, most notably CCL2, CCR3, CCL4, and CCR5 (Ishizuka et al. 1997; Xia et al. 1998; Xia and Hyman 1999). More recently, chemokines have been implicated in various other processes such as neuron loss, microglial activation, Aβ plauqe deposition, and astrocyte activation (Kiyota et al. 2009; Fuhrmann et al. 2010; Lee et al. 2010; Cho et al. 2011; Hwang et al. 2016).

Another class of secreted proteins involved in the immune response is cytokines, which simply influence the activity and function of other cells through binding cell-surface receptors. Their contribution to neuroinflammation is substantial and their secretion by microglia and astrocytes often results from binding Aβ. In fact, the accumulation of Aβ in TgAPPsw and PS1/APPsw mice leads to secretion of TNFα, interleukin 6, interleukin 1α, and GM-CSF (Patel et al. 2005). This reinforces the idea that Aβ accumluation is the chief protagonist of neuroinflammation. There are anti-inflammatory cytokines associated with Alzheimer's disaase, such as IL-1, IL-4, IL-10, and TGF-β, but they do not appear to have any appreciable affect.

Neurodegeneration is the most common outcome of the chronic inflammation seen in Alzheimer's disease. The most pronounced change is a reduction in the surface area and cell density of the cerebral cortex, which is responsible for higher thought, planning, and memory. The sulci, or the valleys in

the folded appearance of the brain, become more pronounced as the brain shrinks due to neuron loss. The hippocampus, a sub-structure of the cortex involved in memory formation, also has exaggerated neuron loss and shrinks in size. Directly adjacent to the hippocampus are the lateral ventricles, which also increase in size and contain more CSF. This is different from hydrocephalus where an increase in ventricle size is not accompanied by shrinkage of the cerebral cortex, although the two conditions have overlapping symptoms. The rate of cell loss at the hippocampus has been extimated by MRI to be 26.5 ± 4.5 mm^3/year, or 1.6% ± 0.2%/year, when normalized to unaffacted seniors (Schuff et al. 2009).

Siglecs

Immune receptors are classically known for binding cell-surface or secreted proteins that initiate a cascade of downstream events. However, there are several classes of glycan binding receptors, or lectins, that are also innate immune receptors. The Siglec (sialic-acid-binding immunoglobulin-like lectins) family of lectins is broadly expressed on many cell types, typically leukocytes and lymphocytes, with varying consequences (i.e. apoptosis, sequester surface receptor, etc.) upon ligand binding (Vyas et al. 2002; Tateno et al. 2007; Bochner 2009; Kawasaki et al. 2010; McMillan et al. 2014; Kiwamoto et al. 2015). Siglecs are type-1 membrane proteins that bind sialic acid containing glycans through V-set immunoglobulin like domains and typically signal through immunoreceptor tyrosine-based inhibitory motifs (ITIM domains) (**Figure 1.4**) (Crocker et al. 2007;

Macauley et al. 2014). The Siglec family can be divided into two groups: common and CD33-related. The common group includes sialoadhesin (Siglec-1), CD22 (Siglec-2), MAG (Siglec-4), and Siglec-15 (Macauley et al. 2014). These four receptors show low sequence similarity and have orthologous in all mammals that have been examined. The CD33-related Siglecs, however, show high sequence similarity between the receptors but have undergone rapid evolution producing paralogs within the same species. Between humans and mice there are similarities between several of the CD33-related Siglecs, but much is still unknown.

Figure 1.4: Sialic acid binding immunoglobulin-like lectins (Siglecs)

Siglecs bind a broad range of glycans that are terminated in sialic acid, some of which require specific epitopes or modifications for binding. These lectins generally display immunoreceptor tyrosine-based inhibitory motifs (ITIM) on their intracellular domain, and so far each results in a unique outcome.

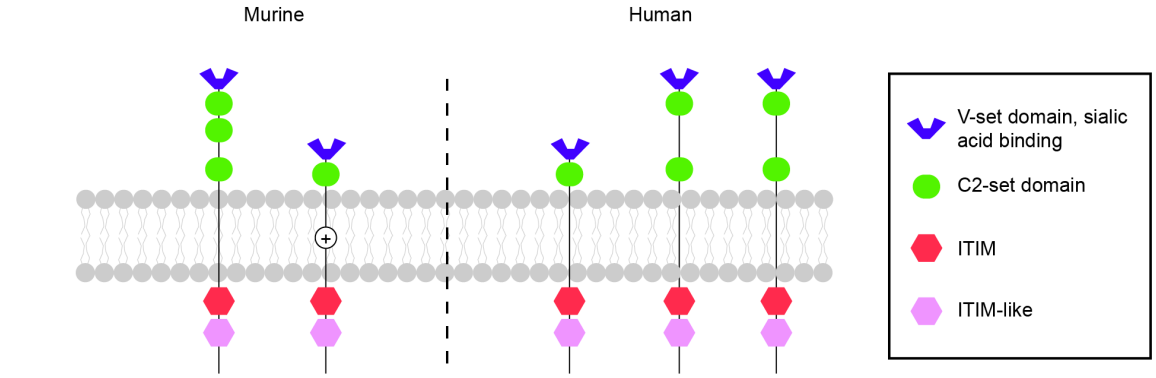

Name	Siglec-F	CD33 (Siglec-3)	CD33 (Siglec-3)	Siglec-8	Siglec-9
Cell Type	Eo, MΦ MiG	N, MΦ	MΦ, MyP, MiG	Eo, Ba, MC	N,MΦ, NK

A majority of the Siglecs are endocytic and functionally differentiate between “self” and “non-self”. Through this recognition of “self”, CD22 was identified to bind *cis* ligands thereby allowing B-cell Receptor (BCR) signaling to occur. However, if CD22 associates with the BCR it cannot aggregate and form membrane-signaling domains (**Figure 1.5)** (Nitschke et al. 1997; Razi and Varki 1998). Interestingly, subtypes of B-cells also express another Siglec that functions as an inhibitory receptor and antagonist to CD22. Siglec-G, or its human paralog Siglec-10, relies on binding sialic acid to associate with the BCR and inhibit signaling (Hutzler et al. 2014; Muller and Nitschke 2014). This ability to function as a co-receptor and function through multiple schemes is the basis for Siglec interactions in the innate immune system. These receptors are important in many diseases and infections, such as viral infections, osteoporosis, bacterial infections, chronic lung inflammation, and neuroinflammation (Crocker et al. 2007; Macauley et al. 2014; Schnaar 2016). However, the prism through which Siglecs are viewed in disease depends on the cell type(s) involved and their expression pattern, making every instance unique.

Figure 1.5: CD22 inhibits B-cell signaling

CD22 preferentially binds *cis* α2-6 sialylated LacNAc and self aggregates allowing the B-cell receptor (BCR) to oligomerize and activate downstream signaling pathways (A). If CD22 is allowed to interact with the BCR then it prevents oligermerization and downstream signaling (B).

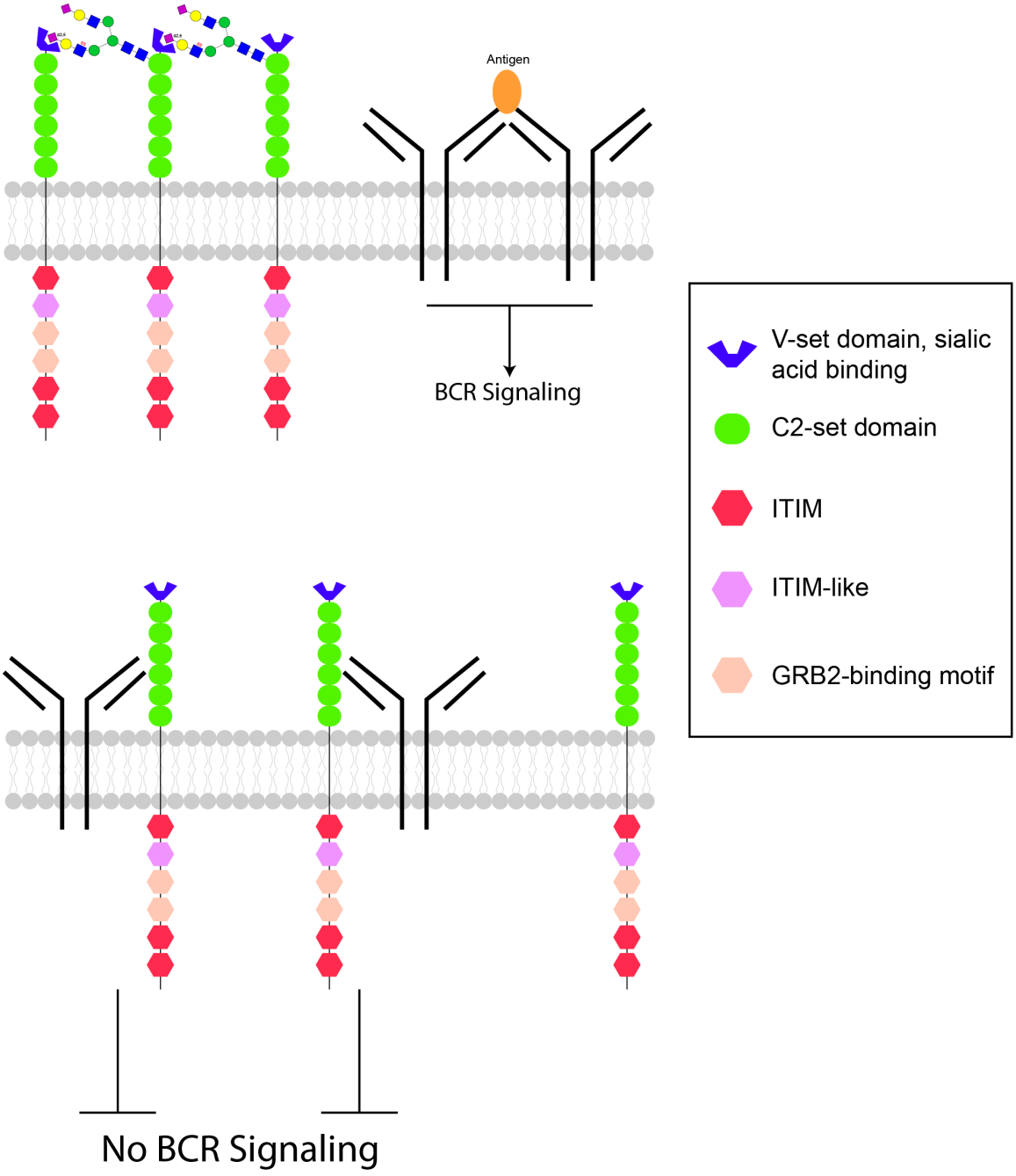

CD33 is primarily found on monocytes and myeloid progenitors, but not granulocytes. The ligand for CD33 is mainly α2-6 sialic acid with weak binding to α2-3 sialic acid (Brinkman-Van der Linden et al. 2003). CD33 is an inhibitory receptor that binds *cis* ligands preventing release of pro-inflammatory cytokines, namely IL-1β, TNF- α, and IL-8 (Lajaunias et al. 2005). CD33 is involved in neurodegeneration through binding amyloid beta and has been associated with Alzheimer's disease through GWAS studies. A single nucleotide polymorphism was identified that reduces the amount of CD33 at the cell surface resulting in lower quantities of insoluble amyloid beta in the brain (Griciuc et al. 2013).

Siglec-F is a CD33-related siglec that is typically expressed on immune cells, namely eosinophils, microglia, and macrophages (Bochner 2009; Hussell and Bell 2014; Schneider et al. 2014). When an eosinophil binds both IL-5 and a glycan ligand for Siglec-F, the cell undergoes apoptosis without producing ROS or signaling through SHP-1 and the Src family of kinases (Mao et al. 2013). This is contradictory of apoptosis signaled through Siglec-8 (Nutku et al. 2003; Nutku et al. 2005; Nutku-Bilir et al. 2008; Hudson et al. 2009). The endogenous ligand for Siglec-F is still unknown, however, glycan array binding data shows that 6′ sulfated sialyl Lewis X (6′-sulfo-sLex or NeuAcα2-3Galβ1-4(Fucα1-3)(6-O-sulfo)GlcNAc) binds with high selectivity (Bochner et al. 2005; Tateno et al. 2005). Siglec-F has also been shown to be a marker for intestinal M cells and is induced in microglia upon amyloidosis (Lunnon et al. 2011; Gicheva et al. 2016). The human paralog for Siglec-F is thought to be Siglec-8 due to its preference for similar ligands; it is however much more restricted in what it will bind versus the

promiscuous Siglec-F (Guo et al. 2011; Patnode et al. 2013; Kiwamoto et al. 2015; Schnaar 2016). Siglec-8 shows a very similar function in eosinophils when co-stimulated with IL-5 by mediating apoptosis through a β2 integrin-dependent mechanism. Despite the functional correlation between Siglec-F and Siglec-8, there are discussions of Siglec-9 being the paralog of Siglec-F due to similar ligand binding profiles on glycan arrays and trachea.

LRP1

Low-density lipoprotein 1 (LRP1) is a major receptor for lipoproteins originally identified as a binding partner for apolipoprotein E (Apo E) (Beisiegel et al. 1989). LRP1 is an endocytic receptor that binds over 40 ligands and is involved in many different biological processes and diseases, making it multi-functional (Lillis et al. 2008). LRP1 is translated as a single polypeptide with a mass of 600-kD that is cleaved by Furin into an extracellular 515-kD α-chain and an intracellular 85-kD β-chain. The α-chain is comprised of 31 complement like repeats, 22 cysteine rich EGF-like domains, and 8 β-propeller domains while the β-chain has a transmembrane domain followed by two NPxY motifs, two dileucine repeats, and a YXXL motif that are responsible endocytosis and downstream signalling (**Figure 1.6**) (Li et al. 2000; Auderset et al. 2016). Domains II and IV are responsible for binding most ligands, making receptor associated protein (RAP) a unique ligand for domain III, while the EGF-like domains and the β-propeller domains promote ligand release at low pH (Bu and Rennke 1996; Jeon et al. 2001; De Nardis et al. 2017). The protein is extensively

modified through 52 N-linked glycosylation sites on the α-chain resulting in many differentially modified variants of the protein which do not have an associated funciton (Van Leuven et al. 1993; De Nardis et al. 2017).

Figure 1.6: LRP1 structure and glycosylation

LRP1 has an extracellular 515-kD α-chain and an intracellular 85-kD β-chain. The α-chain is comprised of 31 complement like repeats, 22 cysteine rich EGF-like domains, and 8 β-propeller domains while the β-chain has a transmembrane domain followed by two NPxY motifs, two dileucine repeats, and a YXXL motif. There are 52 predicted N-glycosylation sites found on the extracellular domain that may be involved in ligand binding. The α-chain is non-covalently bound to the intracellular β-chain allowing shedding to occur in the blood and cerebrospinal fluid.

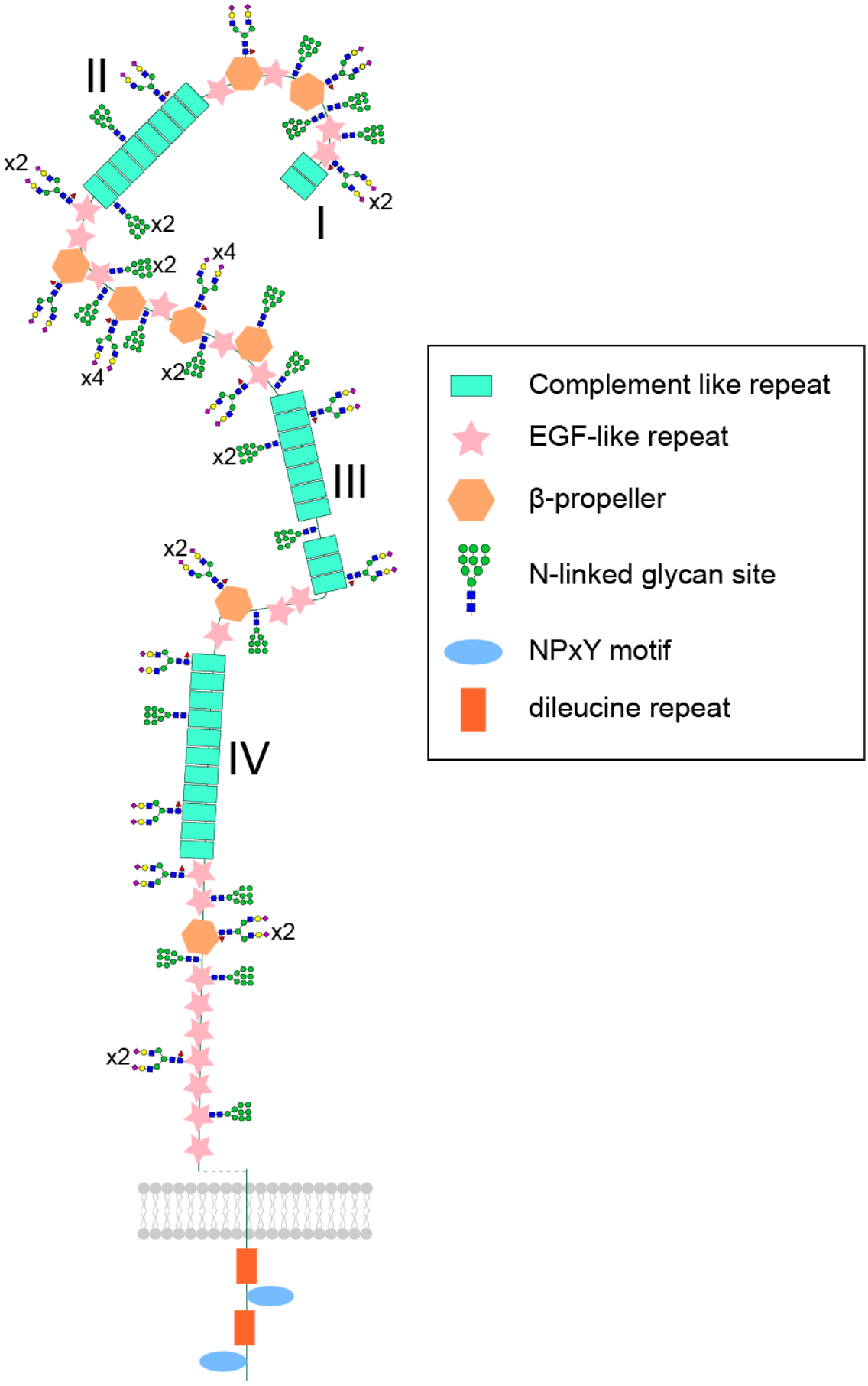
II
I
III
IV
x2
x2
x2
x4
x4
x2
x2
x2
x2
x2
x2
Complement like repeat
EGF-like repeat
β-propeller
N-linked glycan site
NPxY motif
dileucine repeat

The best described function of LRP1 is in the liver where it works alongside the LDL receptor to remove left-over lipoproteins from the blood. These left-over lipoproteins result from degrading large aggregates of dietary lipids, cholesterol, and fat soluble vitamins called chylomicrons (Cooper 1997). The LDL receptor can directly bind the chylomicrons for uptake and degradation. In the absence of the LDL receptor any remnant lipoproteins are bound by ApoE and endocytosed by LRP1 (**Figure 1.7**) (Willnow et al. 1995).

Disruption of the LRP1 gene in mice is lethal for LRP1-/- embryos, most likely during implantation (Herz et al. 1992). This isn't entirely surprising since LRP1 is involved in such a large number of diverse biological functions. To overcome this obstacle, LRP1 floxed mice were generated that didn't show any developmental delays or complications in homozygous or heterozygous pups (Rohlmann et al. 1996). Targeted mating with mice engineered for Cre recombinase expression yielded viable pups that are tissue specific knockouts. Hepatic knockout animals show lower high density lipoproteins (HDL) levels in plasma when fed a normal diet (Basford et al. 2011). This study suggested that the reduced secretion of HDL from hepatocytes is indirect and likely due to activation of lysosomal enzymes. Wnt signaling is disrupted in fibroblasts deficient for LRP1 leading to accumulation of cholesterol when differentiated to adipocytes (Terrand et al. 2009). Interestingly, adipose specific knockouts show delayed lipid processing, lower body weight, and improved glucose tolerance highlighting its role in energy usage and maintenance (Hofmann et al. 2007).

Figure 1.7: LRP1 ligands

Over 40 ligands have been described for LRP1 and can be classified into six categories: lipoprotein metabolism, proteases, intracellular proteins, growth factors, matrix proteins, and other. The multi-active protein binds most ligands in the second and fouth complement repeat domains. Only receptor associated protein (RAP) can bind the third complement domain.

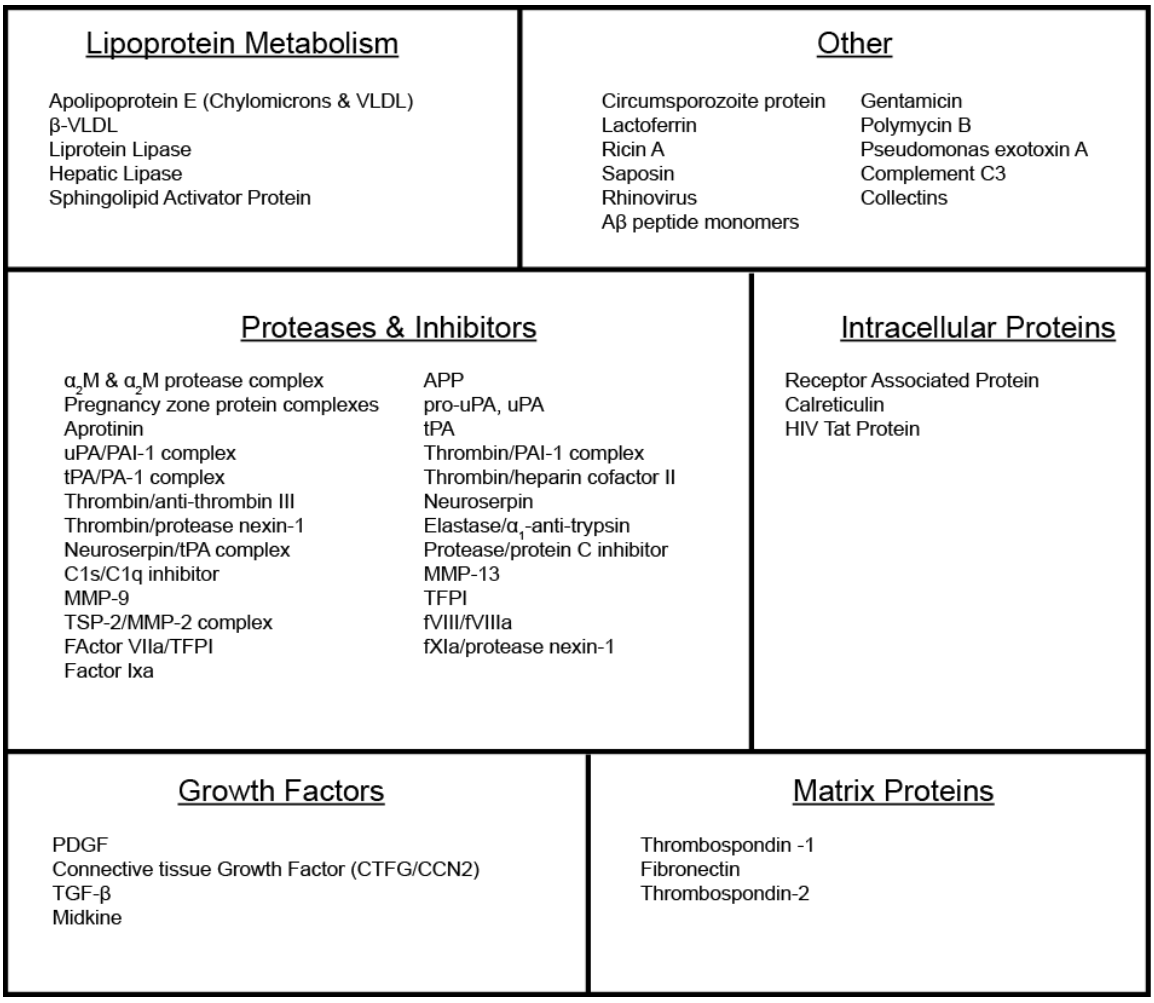

In the brain LRP1 has been shown to have many functions, including axon guidance through chemoattractants, regulating neural stem cell proliferation and differentiation in postnatal cerebellum through SHH signaling, regulator of oligodendrogenesis, their progenitors, and the function of newly formed oligodendrocytes since it is highly upregulated in these cells types (Vaillant et al. 2007; Hennen et al. 2013; Zhang et al. 2014; Landowski et al. 2016). Mice with a neuronal LRP1 knockout show altered behavior, physical trembling, motor disfunction, neuroinflammation, neurodegeneration, and premature death (May et al. 2004; Mulder et al. 2004; Liu et al. 2010). LRP1 has also been shown to influence the endocytic, retrograde transport of APP through adapter protein Fe65 binding the intracellular domains of LRP1 and APP. This association places APP where most experts believe BACE1 activity is highest thereby promoting the amyloidogenic pathway (Ulery et al. 2000; Pietrzik et al. 2002; Pietrzik et al. 2004).

Expression of LRP1 in the CNS is found in neurons, microglia, astrocytes, pericytes, and endothelium. The effect Alzheimer's disease has on LRP1's expression profile and function is still debated in all of these cell types, however, very little is known about its role in choroid plexus epithelium.

Choroid Plexus and Brain Development

The choroid plexus (ChP) is a free floating structure comprised of specialized ependymal epithelium, the cells that line the ventricles, that is found in all ventricles of the brain and secretes the cerebral spinal fluid (CSF). The cells

are first visible in development at embryonic day 11 (E11) as pseudostratified cells that are ciliated but do not have any folds in the tissue. By E13 the cells have changed to columnar epithelium with minimal folds present. The cells are starting to take on their final adult form by E15 showing more folding and have changed shape to cuboidal epithelium (Sturrock 1979). The adult form is highly folded cuboidal epithelium with basal nuclei (Lun et al. 2015). The structure of choroid plexus is similar to other secretory tissues where the basal surface is spaced apart from capillaries by parenchyma, or stroma (**Figure 1.8**). The capillaries are highly fenestrated allowing for increased movement of particles and immune cells into the stroma. The tight junctions between ChP epithelium are less restrictive, or looser, than typical epithelium allowing for increased immune surveillance of the CNS. This CSF-blood barrier (CBB) is a major intersection between the CNS and the immune system where many leukocytes and lymphocytes enter the brain since the blood-brain barrier (BBB) is much more restrictive. The apical surface of ChP cells are highly ciliated and in direct contact with the CSF. These cilia are not motile and serve as a signaling structure. The CSF is secreted into the ventricular system, which is lined by ependymal cells that are also highly ciliated and function by moving the CSF between the ventricles in an ordered manner. Histology of brains during early embryogenesis shows large ventricles with greatly exaggerated connections between the lateral, third, and fourth ventricles and a very thin layer of cortical neurons. These oversized ventricles disappear by E18.5 and have a morphology that resembles an adult brain.

Figure 1.8: Structure of the choroid plexus

The Choroid plexus is a modified form of ependyma that is found in the ventricular system of the CNS and secretes the cerebrospinal fluid (CSF). The basal surface borders stromal tissue and highly fenestrated capillaries allowing immune surveillance of the CNS. The apical surface is highly modified with non-motile cilia involved in signaling for growth and differentiation at the ependymal surface.

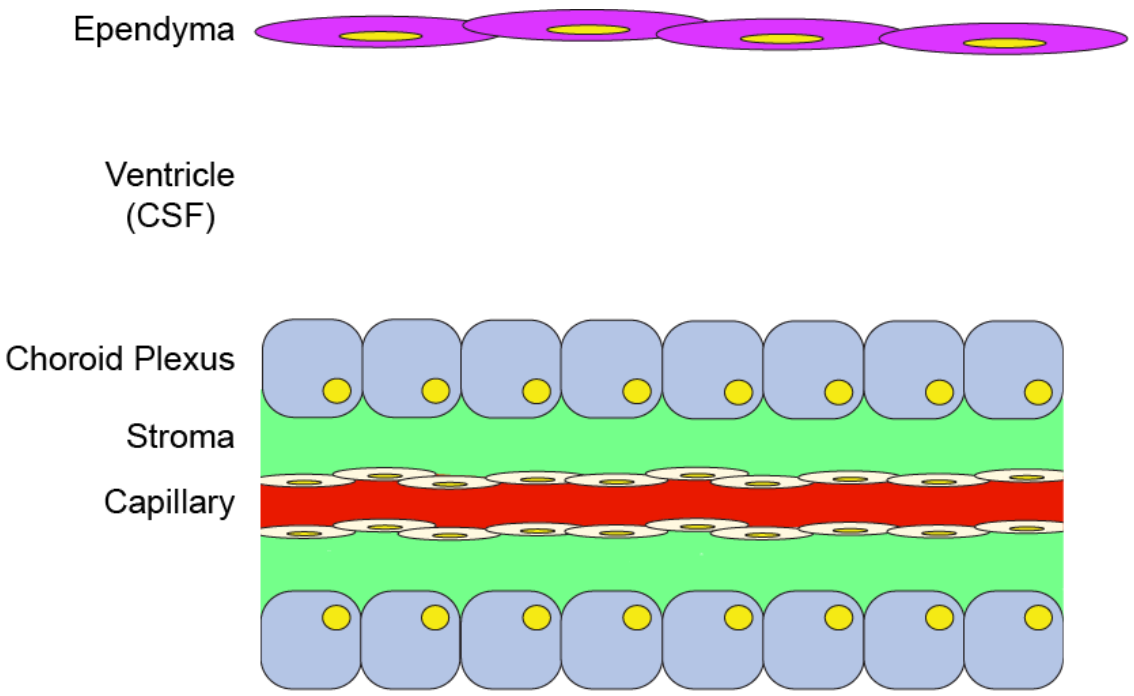

The mammalian brain has thick layers of highly evolved cortical neurons, called the cortical plate, that surround the brain and are responsible for all higher order thought. A stem cell niche found in the apical ventricular zone, with is adjacent to the surface lining ependyma, that surrounds the lateral ventricles produces these cortical layers. Neurons are formed at this ventricular-CSF boundary and migrate towards the cortical plate, away from the ventricle, along radial glia, passing all previously formed neurons. In this way the cortical layers are formed from the “inside-out” producing the most outer layer of neurons last. This neurogenesis is the result of signals received from the CSF that are unique to the embryonic state. An elegantly designed experiment shows that cortical plate formation and growth doesn’t occur when brain explants from E16 embryos are incubated with artificial CSF, but resembles explants from E17 embryos when grown using CSF extracted from E17 embryos (Lehtinen et al. 2011). Choroid plexus cells are highly variable and are often referred to as mosaic due to their expression pattern. The lateral ventricles are adjacent to the hippocampus and contain choroid plexus that is highly similar, if not identical in expression, and are a direct extension of the ependyma. This similarity changes with position in the brain, age, and developmental state.

CSF can pass from the lateral ventricles to the third ventricle through the foramina of Munro. Moving into the third ventricle the overall morphology is consistent but the cells seem to branch out from a central locus, or budding point. ChP cells in the third ventricle are not very well described in the literature but they are expected to differ from the lateral ventricles and the fourth ventricle.

CSF can flow from the third ventricle to the fourth ventricle in the narrow aqueduct of Sylvius. The fourth ventricle begins near the intersection of the brain and the brain stem and contains ChP that is again entirely different. These differences have only been recently described, as the prevailing thought was that all ChP was identical and served the same function. Recently the transcriptome of the lateral ventricles and the fourth ventricle was described for the first time. Striking differences emerged showing regional expression of genes involved in growth and maturation of cells, homeostasis, and signaling to distal parts of the brain. The largest group of enriched genes in both the lateral and fourth ventricles is secreted proteins followed by extracellular region and matrix proteins. Interestingly, the fourth ventricle has a large enrichment of glycoproteins being expressed that have yet to be identified or have defined function. A detailed analysis of proteins found in the CSF identified 598 proteins of which ~5% did not show corresponding gene expression in ChP. The large overlap of proteins identified in the CSF and the gene expression profile for ChP describes the unique function of the ChP and reinforces the hypothesis that the vast majority of the CSF is produced by the ChP. Grouping the identified proteins into functional groups using DAVID analysis identified vesicle associated proteins as the most highly expressed in lateral ventricles. The fourth ventricle was enriched in proteins involved with protein biosynthesis and vesicle associated proteins. A large proportion of the identified proteins were found in CSF from both the lateral and fourth ventricles. Approximately ~7% of all identified proteins were unique to a specific ventricle. CSF in the fourth ventricle continues to flow

through the foramina of Magendie and Luschka into the spinal canal and subarachnoid space before filtering back into the venous system via the arachnoid villi. An adult typically circulates 150 mL of CSF through this pathway and produces three to four volumes each day.

Overall, the ChP is a highly vascularized epithelial tissue that is highly folded and produces CSF. Similar to other secretory epithelium throughout the body, such as airway bronchus, it is a primary intersection with the immune system.

Airway Bronchus

The human airway consists of three main types of cells: basal cells, ciliated epithelial cells, and secretory cells. The basal cells underlie the airway interacting cells and are traditionally thought of as stem cell niche. Columnar epithelial cells line the airway and function as a physical barrier preventing allergens and pathogens from reaching the underlying parenchyma. They are highly ciliated and work to move the secreted mucus thereby expelling allergens and pathogens. Goblet cells are the main secretory cells in the large airways and constitutively secrete mucus. Serous cells and Clara cells are found in the large airways but dominate the secretory landscape in smaller branches.

Allergens such as diesel exhaust, cigarette smoke, and pollen can cause localized inflammation in the airway reducing the airflow to the lungs. A result of this inflammation is excessive mucus production that further obstructs airflow.

Chronic insults, normally due to habitual cigarette smoking, result in chronic obstructive pulmonary disorder (COPD) causing a lowered gas exchange rate in the lungs and a narrowing of the bronchi.

Normal Human Bronchus Epithelium (NHBE) is primary cells that can be cultured from postmortem explants of airway tissue. These cells are difficult to maintain using submerged culture methods due to altered morphology and secretions that do not mirror intact tissue. Therefore, an Air-Liquid Interface (ALI) culture method was developed to allow basic research on these primary cells. ALI culture utilizes a porous mesh insert coated with purified extracellular matrix proteins, like collagen, as a growth surface. These inserts are typically placed in a six well plate and sit 5-10 mm above the bottom of a well. Growth media is placed below the well, providing growth factors and nutrients, to mimic the highly vascularized nature of the airway. Above the insert, an initial addition of growth media is added to facilitate membrane attachment and proliferation that is removed after one week. ALI culture beings after this initial week when growth media is only added below the insert. This culture method results in airway cells that morphologically resemble intact airway and secrete mucus.

Secreted mucins are densely O-glycosylated and represent upwards of 80% of their molecular weight. These mucins are thought to be a physical barrier to pathogens through glycan ligand mimicry and their gelatinous form. The epithelium is also glycosylated on the apical surface and display unique sets of glycans for each region of the airway as determined by Lectin histochemistry (Dorscheid et al. 1999). These differences in glycosylation relate to infection sites

for various bacteria and viruses in the airway. For example, trachea and bronchus are reported to express mainly α2-6 sialic acid making them susceptible to human influenza infection while the lung mainly displays α2-3 sialic acid and is resistant to infection (Viswanathan et al. 2010). Therefore, understanding glycosylation patterns in the airway will aid therapeutic design, illustrating the need for in depth glycomic analysis.

Summary and Scope of Dissertation

This chapter provides a detailed background on the topics that are central to this dissertation. A detailed understanding of glycosylation in a mammalian system is required since we use mouse models and human tissues for our studies. In chapter two, N-glycosylation is a central theme since we found changes in glycosylation in the whole brain and specific tissues. Chapter three details the broad changes in glycosylation as NHBE cells are differentiated. In addition, a general background on Alzheimer's disease is required as well as specific details on the inflammatory status and it's regulation by Siglecs. The structure and function of LRP1 was explored due to its central role in the ventricular system, in particular at the choroid plexus. Finally, a second secretory tissue was described and cell culture methods for its study.

Chapter two describes an alteration in tissue specific glycosylation in Alzheimer's disease that modulates the inflammatory status of the CNS. This novel finding suggests that glycosylation may be pivotal in dampening inflammation that results from the neurotoxic effects of Aβ. This is particularly intriguing since this glyco-epitope is widely expressed throughout the whole mouse yet has very distinct, and different, consequences depending on which cell type it binds.

Chapter three in this dissertation presents an overview of glycosylation in NHBE cells as they differentiate. These changes also correlate to changes in epitopes for anti-inflammatory receptors that have a known function in the airway. These changes are hypothesized to correlate with susceptibility to infection for various bacterial and viral pathogens. These data also highlight the importance of glycosylation in the airway and how differences may impact therapeutic design.

Chapter four describes a novel method for isolation and identification of O-glycans from glycoproteins that have been separated by SDS-PAGE. This is an important advance since there are often unknown proteins that bear interesting O-glycans where there is no other means of analysis. In addition, we show that sulfated O-glycans can be subsequently separated using an organic partitioning method so that they may be analyzed by negative mode MS^n.

This dissertation aims to provide a narrative centered upon glycosylation in inflammatory mediated diseases. Alzheimer's disease is exacerbated by chronic inflammation while airway infection and allergic disease increases local inflammation and lowers gas exchange in the lung. Here I present analytic and biochemical data that may provide insight into limiting infection or disease in the future.

References

Agdeppa, E.D., Kepe, V., Petri, A., Satyamurthy, N., Liu, J., Huang, S.C., Small, G.W., Cole, G.M. and Barrio, J.R. (2003). "In vitro detection of (S)-naproxen and ibuprofen binding to plaques in the Alzheimer's brain using the positron emission tomography molecular imaging probe 2-(1-[6-[(2-[(18)F]fluoroethyl)(methyl)amino]-2-naphthyl]ethylidene)malononitrile." Neuroscience **117**(3): 723-730.

Ahn, S. and Joyner, A.L. (2005). "In vivo analysis of quiescent adult neural stem cells responding to Sonic hedgehog." Nature **437**(7060): 894-897.

Auderset, L., Landowski, L.M., Foa, L. and Young, K.M. (2016). "Low Density Lipoprotein Receptor Related Proteins as Regulators of Neural Stem and Progenitor Cell Function." Stem Cells Int **2016**: 2108495.

Baruch, K., Rosenzweig, N., Kertser, A., Deczkowska, A., Sharif, A.M., Spinrad, A., Tsitsou-Kampeli, A., Sarel, A., Cahalon, L. and Schwartz, M. (2015). "Breaking immune tolerance by targeting Foxp3(+) regulatory T cells mitigates Alzheimer's disease pathology." Nat Commun **6**: 7967.

Basford, J.E., Wancata, L., Hofmann, S.M., Silva, R.A., Davidson, W.S., Howles, P.N. and Hui, D.Y. (2011). "Hepatic deficiency of low density lipoprotein receptor-related protein-1 reduces high density lipoprotein secretion and plasma levels in mice." J Biol Chem **286**(15): 13079-13087.

Bate, C., Veerhuis, R., Eikelenboom, P. and Williams, A. (2004). "Microglia kill amyloid-beta1-42 damaged neurons by a CD14-dependent process." Neuroreport **15**(9): 1427-1430.

Bauer, M.K., Lieb, K., Schulze-Osthoff, K., Berger, M., Gebicke-Haerter, P.J., Bauer, J. and Fiebich, B.L. (1997). "Expression and regulation of cyclooxygenase-2 in rat microglia." Eur J Biochem **243**(3): 726-731.

Beisiegel, U., Weber, W., Ihrke, G., Herz, J. and Stanley, K.K. (1989). "The LDL-receptor-related protein, LRP, is an apolipoprotein E-binding protein." Nature **341**(6238): 162-164.

Bochner, B.S. (2009). "Siglec-8 on human eosinophils and mast cells, and Siglec-F on murine eosinophils, are functionally related inhibitory receptors." Clin Exp Allergy **39**: 317-324.

Bochner, B.S., Alvarez, R.A., Mehta, P., Bovin, N.V., Blixt, O., White, J.R. and Schnaar, R.L. (2005). "Glycan array screening reveals a candidate ligand for Siglec-8." J Biol Chem **280**(6): 4307-4312.

Bond, M.R. and Hanover, J.A. (2015). "A little sugar goes a long way: the cell biology of O-GlcNAc." J Cell Biol **208**(7): 869-880.

Botto, M. (1998). "C1q knock-out mice for the study of complement deficiency in autoimmune disease." Exp Clin Immunogenet **15**(4): 231-234.

Bouskila, M., Esoof, N., Gay, L., Fang, E.H., Deak, M., Begley, M.J., Cantley, L.C., Prescott, A., Storey, K.G. and Alessi, D.R. (2011). "TTBK2 kinase substrate specificity and the impact of spinocerebellar-ataxia-causing mutations on expression, activity, localization and development." Biochem J **437**(1): 157-167.

Brinkman-Van der Linden, E.C., Angata, T., Reynolds, S.A., Powell, L.D., Hedrick, S.M. and Varki, A. (2003). "CD33/Siglec-3 binding specificity, expression pattern, and consequences of gene deletion in mice." Mol Cell Biol **23**(12): 4199-4206.

Bruckner, K., Perez, L., Clausen, H. and Cohen, S. (2000). "Glycosyltransferase activity of Fringe modulates Notch-Delta interactions." Nature **406**(6794): 411-415.

Bu, G. and Rennke, S. (1996). "Receptor-associated protein is a folding chaperone for low density lipoprotein receptor-related protein." J Biol Chem **271**(36): 22218-22224.

Burda, P. and Aebi, M. (1999). "The dolichol pathway of N-linked glycosylation." Biochim Biophys Acta **1426**(2): 239-257.

Charo, I.F. and Ransohoff, R.M. (2006). "The many roles of chemokines and chemokine receptors in inflammation." N Engl J Med **354**(6): 610-621.

Cho, S.H., Sun, B., Zhou, Y., Kauppinen, T.M., Halabisky, B., Wes, P., Ransohoff, R.M. and Gan, L. (2011). "CX3CR1 protein signaling modulates microglial activation and protects against plaque-independent cognitive deficits in a mouse model of Alzheimer disease." J Biol Chem **286**(37): 32713-32722.

Ciesielski-Treska, J., Ulrich, G., Taupenot, L., Chasserot-Golaz, S., Corti, A., Aunis, D. and Bader, M.F. (1998). "Chromogranin A induces a neurotoxic phenotype in brain microglial cells." J Biol Chem **273**(23): 14339-14346.

Cooper, A.D. (1997). "Hepatic uptake of chylomicron remnants." J Lipid Res **38**(11): 2173-2192.

Corradin, S.B., Mauel, J., Donini, S.D., Quattrocchi, E. and Ricciardi-Castagnoli, P. (1993). "Inducible nitric oxide synthase activity of cloned murine microglial cells." Glia **7**(3): 255-262.

Crocker, P.R., Paulson, J.C. and Varki, A. (2007). "Siglecs and their roles in the immune system." Nat Rev Immunol **7**(4): 255-266.

D'Alessio, C., Caramelo, J.J. and Parodi, A.J. (2010). "UDP-GlC:glycoprotein glucosyltransferase-glucosidase II, the ying-yang of the ER quality control." Semin Cell Dev Biol **21**(5): 491-499.

De Nardis, C., Lossl, P., van den Biggelaar, M., Madoori, P.K., Leloup, N., Mertens, K., Heck, A.J. and Gros, P. (2017). "Recombinant Expression of the Full-length Ectodomain of LDL Receptor-related Protein 1 (LRP1) Unravels pH-dependent Conformational Changes and the Stoichiometry of Binding with Receptor-associated Protein (RAP)." J Biol Chem **292**(3): 912-924.

Dempski, R.E., Jr. and Imperiali, B. (2002). "Oligosaccharyl transferase: gatekeeper to the secretory pathway." Curr Opin Chem Biol **6**(6): 844-850.

Dorscheid, D.R., Conforti, A.E., Hamann, K.J., Rabe, K.F. and White, S.R. (1999). "Characterization of cell surface lectin-binding patterns of human airway epithelium." Histochem J **31**(3): 145-151.

Eikelenboom, P. and Veerhuis, R. (1996). "The role of complement and activated microglia in the pathogenesis of Alzheimer's disease." Neurobiol Aging **17**(5): 673-680.

Eimer, W.A. and Vassar, R. (2013). "Neuron loss in the 5XFAD mouse model of Alzheimer's disease correlates with intraneuronal Abeta42 accumulation and Caspase-3 activation." Mol Neurodegener **8**: 2.

Fassbender, K., Walter, S., Kuhl, S., Landmann, R., Ishii, K., Bertsch, T., Stalder, A.K., Muehlhauser, F., Liu, Y., Ulmer, A.J., Rivest, S., Lentschat, A., Gulbins, E., Jucker, M., Staufenbiel, M., Brechtel, K., Walter, J., Multhaup, G., Penke, B., Adachi, Y., Hartmann, T. and Beyreuther, K. (2004). "The LPS receptor (CD14) links innate immunity with Alzheimer's disease." FASEB J **18**(1): 203-205.

Fonseca, M.I., Zhou, J., Botto, M. and Tenner, A.J. (2004). "Absence of C1q leads to less neuropathology in transgenic mouse models of Alzheimer's disease." J Neurosci **24**(29): 6457-6465.

Freeze, H.H. and Aebi, M. (2005). "Altered glycan structures: the molecular basis of congenital disorders of glycosylation." Curr Opin Struct Biol **15**(5): 490-498.

Fuhrmann, M., Bittner, T., Jung, C.K., Burgold, S., Page, R.M., Mitteregger, G., Haass, C., LaFerla, F.M., Kretzschmar, H. and Herms, J. (2010). "Microglial Cx3cr1 knockout prevents neuron loss in a mouse model of Alzheimer's disease." Nat Neurosci **13**(4): 411-413.

Games, D., Adams, D., Alessandrini, R., Barbour, R., Berthelette, P., Blackwell, C., Carr, T., Clemens, J., Donaldson, T., Gillespie, F. and et al. (1995). "Alzheimer-type neuropathology in transgenic mice overexpressing V717F beta-amyloid precursor protein." Nature **373**(6514): 523-527.

Gicheva, N., Macauley, M.S., Arlian, B.M., Paulson, J.C. and Kawasaki, N. (2016). "Siglec-F is a novel intestinal M cell marker." Biochem Biophys Res Commun.

Gill, D.J., Clausen, H. and Bard, F. (2011). "Location, location, location: new insights into O-GalNAc protein glycosylation." Trends Cell Biol **21**(3): 149-158.

Goetz, S.C. and Anderson, K.V. (2010). "The primary cilium: a signalling centre during vertebrate development." Nat Rev Genet **11**(5): 331-344.

Goetz, S.C., Liem, K.F., Jr. and Anderson, K.V. (2012). "The spinocerebellar ataxia-associated gene Tau tubulin kinase 2 controls the initiation of ciliogenesis." Cell **151**(4): 847-858.

Griciuc, A., Serrano-Pozo, A., Parrado, A.R., Lesinski, A.N., Asselin, C.N., Mullin, K., Hooli, B., Choi, S.H., Hyman, B.T. and Tanzi, R.E. (2013). "Alzheimer's Disease Risk Gene CD33 Inhibits Microglial Uptake of Amyloid Beta." Neuron.

Guo, J.P., Brummet, M.E., Myers, A.C., Na, H.J., Rowland, E., Schnaar, R.L., Zheng, T., Zhu, Z. and Bochner, B.S. (2011). "Characterization of Expression of Gylcan Ligands for Siglec-F in Normal Mouse Lungs." Am J Respir Cell and Molec Biol **44**: 238-243.

Hardy, J.A. and Higgins, G.A. (1992). "Alzheimer's disease: the amyloid cascade hypothesis." Science **256**(5054): 184-185.

Helenius, A. and Aebi, M. (2004). "Roles of N-linked glycans in the endoplasmic reticulum." Annu Rev Biochem **73**: 1019-1049.

Heneka, M.T., Carson, M.J., El Khoury, J., Landreth, G.E., Brosseron, F., Feinstein, D.L., Jacobs, A.H., Wyss-Coray, T., Vitorica, J., Ransohoff, R.M., Herrup, K., Frautschy, S.A., Finsen, B., Brown, G.C., Verkhratsky, A., Yamanaka, K., Koistinaho, J., Latz, E., Halle, A., Petzold, G.C., Town, T., Morgan, D., Shinohara, M.L., Perry, V.H., Holmes, C., Bazan, N.G., Brooks, D.J., Hunot, S., Joseph, B., Deigendesch, N., Garaschuk, O., Boddeke, E., Dinarello, C.A., Breitner, J.C., Cole, G.M., Golenbock, D.T. and Kummer, M.P. (2015). "Neuroinflammation in Alzheimer's disease." Lancet Neurol **14**(4): 388-405.

Heneka, M.T., Wiesinger, H., Dumitrescu-Ozimek, L., Riederer, P., Feinstein, D.L. and Klockgether, T. (2001). "Neuronal and glial coexpression of argininosuccinate synthetase and inducible nitric oxide synthase in Alzheimer disease." J Neuropathol Exp Neurol **60**(9): 906-916.

Hennen, E., Safina, D., Haussmann, U., Worsdorfer, P., Edenhofer, F., Poetsch, A. and Faissner, A. (2013). "A LewisX glycoprotein screen identifies the

low density lipoprotein receptor-related protein 1 (LRP1) as a modulator of oligodendrogenesis in mice." J Biol Chem **288**(23): 16538-16545.

Herrup, K. (2015). "The case for rejecting the amyloid cascade hypothesis." Nat Neurosci **18**(6): 794-799.

Herz, J., Clouthier, D.E. and Hammer, R.E. (1992). "LDL receptor-related protein internalizes and degrades uPA-PAI-1 complexes and is essential for embryo implantation." Cell **71**(3): 411-421.

Hofmann, S.M., Zhou, L., Perez-Tilve, D., Greer, T., Grant, E., Wancata, L., Thomas, A., Pfluger, P.T., Basford, J.E., Gilham, D., Herz, J., Tschop, M.H. and Hui, D.Y. (2007). "Adipocyte LDL receptor-related protein-1 expression modulates postprandial lipid transport and glucose homeostasis in mice." J Clin Invest **117**(11): 3271-3282.

Hudson, S.A., Bovin, N.V., Schnaar, R.L., Crocker, P.R. and Bochner, B.S. (2009). "Eosinophil-selective binding and proapoptotic effect in vitro of a synthetic Siglec-8 ligand, polymeric 6'-sulfated sialyl Lewis x." J Pharmacol Exp Ther **330**(2): 608-612.

Hutzler, S., Ozgor, L., Naito-Matsui, Y., Klasener, K., Winkler, T.H., Reth, M. and Nitschke, L. (2014). "The ligand-binding domain of Siglec-G is crucial for its selective inhibitory function on B1 cells." J Immunol **192**(11): 5406-5414.

Hwang, C.J., Park, M.H., Hwang, J.Y., Kim, J.H., Yun, N.Y., Oh, S.Y., Song, J.K., Seo, H.O., Kim, Y.B., Hwang, D.Y., Oh, K.W., Han, S.B. and Hong, J.T. (2016). "CCR5 deficiency accelerates lipopolysaccharide-induced astrogliosis, amyloid-beta deposit and impaired memory function." Oncotarget **7**(11): 11984-11999.

Ichikawa, S. and Hirabayashi, Y. (1998). "Glucosylceramide synthase and glycosphingolipid synthesis." Trends Cell Biol **8**(5): 198-202.

Ishibashi, Y., Kohyama-Koganeya, A. and Hirabayashi, Y. (2013). "New insights on glucosylated lipids: metabolism and functions." Biochim Biophys Acta **1831**(9): 1475-1485.

Ishizuka, K., Kimura, T., Igata-yi, R., Katsuragi, S., Takamatsu, J. and Miyakawa, T. (1997). "Identification of monocyte chemoattractant protein-1 in senile plaques and reactive microglia of Alzheimer's disease." Psychiatry Clin Neurosci **51**(3): 135-138.

Itagaki, S., McGeer, P.L., Akiyama, H., Zhu, S. and Selkoe, D. (1989). "Relationship of microglia and astrocytes to amyloid deposits of Alzheimer disease." J Neuroimmunol **24**(3): 173-182.

Jeon, H., Meng, W., Takagi, J., Eck, M.J., Springer, T.A. and Blacklow, S.C. (2001). "Implications for familial hypercholesterolemia from the structure of the LDL receptor YWTD-EGF domain pair." Nat Struct Biol **8**(6): 499-504.

Kawasaki, N., Rademacher, C. and Paulson, J.C. (2010). "CD22 regulates adaptive and innate immune responses of B cells." J Innate Immun **3**(4): 411-419.

Kiwamoto, T., Katoh, T., Evans, C.M., Janssen, W.J., Brummet, M.E., Hudson, S.A., Zhu, Z., Tiemeyer, M. and Bochner, B.S. (2015). "Endogenous airway mucins carry glycans that bind Siglec-F and induce eosinophil apoptosis." J Allergy Clin Immunol **135**(5): 1329-1340 e1321-1329.

Kiyota, T., Yamamoto, M., Xiong, H., Lambert, M.P., Klein, W.L., Gendelman, H.E., Ransohoff, R.M. and Ikezu, T. (2009). "CCL2 accelerates microglia-mediated Abeta oligomer formation and progression of neurocognitive dysfunction." PLoS One **4**(7): e6197.

Lajaunias, F., Dayer, J.M. and Chizzolini, C. (2005). "Constitutive repressor activity of CD33 on human monocytes requires sialic acid recognition and phosphoinositide 3-kinase-mediated intracellular signaling." Eur J Immunol **35**(1): 243-251.

Landowski, L.M., Pavez, M., Brown, L.S., Gasperini, R., Taylor, B.V., West, A.K. and Foa, L. (2016). "Low-density Lipoprotein Receptor-related Proteins in a Novel Mechanism of Axon Guidance and Peripheral Nerve Regeneration." J Biol Chem **291**(3): 1092-1102.

Lau, K.S., Partridge, E.A., Grigorian, A., Silvescu, C.I., Reinhold, V.N., Demetriou, M. and Dennis, J.W. (2007). "Complex N-glycan number and degree of branching cooperate to regulate cell proliferation and differentiation." Cell **129**(1): 123-134.

Lee, S., Varvel, N.H., Konerth, M.E., Xu, G., Cardona, A.E., Ransohoff, R.M. and Lamb, B.T. (2010). "CX3CR1 deficiency alters microglial activation and reduces beta-amyloid deposition in two Alzheimer's disease mouse models." Am J Pathol **177**(5): 2549-2562.

Lehtinen, M.K., Zappaterra, M.W., Chen, X., Yang, Y.J., Hill, A.D., Lun, M., Maynard, T., Gonzalez, D., Kim, S., Ye, P., D'Ercole, A.J., Wong, E.T., LaMantia, A.S. and Walsh, C.A. (2011). "The cerebrospinal fluid provides a proliferative niche for neural progenitor cells." Neuron **69**(5): 893-905.

Li, Y., Marzolo, M.P., van Kerkhof, P., Strous, G.J. and Bu, G. (2000). "The YXXL motif, but not the two NPXY motifs, serves as the dominant endocytosis signal for low density lipoprotein receptor-related protein." J Biol Chem **275**(22): 17187-17194.

Lillis, A.P., Van Duyn, L.B., Murphy-Ullrich, J.E. and Strickland, D.K. (2008). "LDL receptor-related protein 1: unique tissue-specific functions revealed by selective gene knockout studies." Physiol Rev **88**(3): 887-918.

Linden, S.K., Sutton, P., Karlsson, N.G., Korolik, V. and McGuckin, M.A. (2008). "Mucins in the mucosal barrier to infection." Mucosal Immunol **1**(3): 183-197.

Liu, Q., Trotter, J., Zhang, J., Peters, M.M., Cheng, H., Bao, J., Han, X., Weeber, E.J. and Bu, G. (2010). "Neuronal LRP1 knockout in adult mice leads to impaired brain lipid metabolism and progressive, age-dependent synapse loss and neurodegeneration." J Neurosci **30**(50): 17068-17078.

Lun, M.P., Monuki, E.S. and Lehtinen, M.K. (2015). "Development and functions of the choroid plexus-cerebrospinal fluid system." Nat Rev Neurosci **16**(8): 445-457.

Lunnon, K., Teeling, J.L., Tutt, A.L., Cragg, M.S., Glennie, M.J. and Perry, V.H. (2011). "Systemic inflammation modulates Fc receptor expression on microglia during chronic neurodegeneration." J Immunol **186**(12): 7215-7224.

Macauley, M.S., Crocker, P.R. and Paulson, J.C. (2014). "Siglec-mediated regulation of immune cell function in disease." Nat Rev Immunol **14**(10): 653-666.

Maier, M., Peng, Y., Jiang, L., Seabrook, T.J., Carroll, M.C. and Lemere, C.A. (2008). "Complement C3 deficiency leads to accelerated amyloid beta plaque deposition and neurodegeneration and modulation of the microglia/macrophage phenotype in amyloid precursor protein transgenic mice." J Neurosci **28**(25): 6333-6341.

Manya, H., Chiba, A., Margolis, R.U. and Endo, T. (2006). "Molecular cloning and characterization of rat Pomt1 and Pomt2." Glycobiology **16**(9): 863-873.

Mao, H., Kano, G., Hudson, S.A., Brummet, M., Zimmermann, N., Zhu, Z. and Bochner, B.S. (2013). "Mechanisms of Siglec-F-induced eosinophil apoptosis: a role for caspases but not for SHP-1, Src kinases, NADPH oxidase or reactive oxygen." PLoS One **8**(6): e68143.

Marek, K.W., Vijay, I.K. and Marth, J.D. (1999). "A recessive deletion in the GlcNAc-1-phosphotransferase gene results in peri-implantation embryonic lethality." Glycobiology **9**(11): 1263-1271.

May, P., Rohlmann, A., Bock, H.H., Zurhove, K., Marth, J.D., Schomburg, E.D., Noebels, J.L., Beffert, U., Sweatt, J.D., Weeber, E.J. and Herz, J. (2004). "Neuronal LRP1 functionally associates with postsynaptic proteins and is required for normal motor function in mice." Mol Cell Biol **24**(20): 8872-8883.

McMillan, S.J., Sharma, R.S., Richards, H.E., Hegde, V. and Crocker, P.R. (2014). "Siglec-E Promotes beta2-Integrin-dependent NADPH Oxidase Activation to Suppress Neutrophil Recruitment to the Lung." J Biol Chem **289**(29): 20370-20376.

Moloney, D.J., Panin, V.M., Johnston, S.H., Chen, J., Shao, L., Wilson, R., Wang, Y., Stanley, P., Irvine, K.D., Haltiwanger, R.S. and Vogt, T.F. (2000). "Fringe is a glycosyltransferase that modifies Notch." Nature **406**(6794): 369-375.

Moremen, K.W. and Molinari, M. (2006). "N-linked glycan recognition and processing: the molecular basis of endoplasmic reticulum quality control." Curr Opin Struct Biol **16**(5): 592-599.

Moremen, K.W., Tiemeyer, M. and Nairn, A.V. (2012). "Vertebrate protein glycosylation: diversity, synthesis and function." Nat Rev Mol Cell Biol **13**(7): 448-462.

Mulder, M., Jansen, P.J., Janssen, B.J., van de Berg, W.D., van der Boom, H., Havekes, L.M., de Kloet, R.E., Ramaekers, F.C. and Blokland, A. (2004). "Low-density lipoprotein receptor-knockout mice display impaired spatial memory associated with a decreased synaptic density in the hippocampus." Neurobiol Dis **16**(1): 212-219.

Muller, J. and Nitschke, L. (2014). "The role of CD22 and Siglec-G in B-cell tolerance and autoimmune disease." Nat Rev Rheumatol **10**(7): 422-428.

Nitschke, L., Carsetti, R., Ocker, B., Kohler, G. and Lamers, M.C. (1997). "CD22 is a negative regulator of B-cell receptor signalling." Curr Biol **7**(2): 133-143.

Nutku, E., Aizawa, H., Hudson, S.A. and Bochner, B.S. (2003). "Ligation of Siglec-8: a selective mechanism for induction of human eosinophil apoptosis." Blood **101**(12): 5014-5020.

Nutku, E., Hudson, S.A. and Bochner, B.S. (2005). "Mechanism of Siglec-8-induced human eosinophil apoptosis: role of caspases and mitochondrial injury." Biochem Biophys Res Commun **336**(3): 918-924.

Nutku-Bilir, E., Hudson, S.A. and Bochner, B.S. (2008). "Interleukin-5 priming of human eosinophils alters siglec-8 mediated apoptosis pathways." Am J Respir Cell Mol Biol **38**(1): 121-124.

Oakley, H., Cole, S.L., Logan, S., Maus, E., Shao, P., Craft, J., Guillozet-Bongaarts, A., Ohno, M., Disterhoft, J., Van Eldik, L., Berry, R. and Vassar, R. (2006). "Intraneuronal beta-amyloid aggregates, neurodegeneration, and neuron loss in transgenic mice with five familial Alzheimer's disease mutations: potential factors in amyloid plaque formation." J Neurosci **26**(40): 10129-10140.

Ohtsubo, K., Takamatsu, S., Minowa, M.T., Yoshida, A., Takeuchi, M. and Marth, J.D. (2005). "Dietary and genetic control of glucose transporter 2 glycosylation promotes insulin secretion in suppressing diabetes." Cell **123**(7): 1307-1321.

Paresce, D.M., Ghosh, R.N. and Maxfield, F.R. (1996). "Microglial cells internalize aggregates of the Alzheimer's disease amyloid beta-protein via a scavenger receptor." Neuron **17**(3): 553-565.

Partridge, E.A., Le Roy, C., Di Guglielmo, G.M., Pawling, J., Cheung, P., Granovsky, M., Nabi, I.R., Wrana, J.L. and Dennis, J.W. (2004). "Regulation of cytokine receptors by Golgi N-glycan processing and endocytosis." Science **306**(5693): 120-124.

Patel, N.S., Paris, D., Mathura, V., Quadros, A.N., Crawford, F.C. and Mullan, M.J. (2005). "Inflammatory cytokine levels correlate with amyloid load in transgenic mouse models of Alzheimer's disease." J Neuroinflammation **2**(1): 9.

Patnode, M.L., Cheng, C.W., Chou, C.C., Singer, M.S., Elin, M.S., Uchimura, K., Crocker, P.R., Khoo, K.H. and Rosen, S.D. (2013). "Galactose 6-o-sulfotransferases are not required for the generation of siglec-f ligands in leukocytes or lung tissue." J Biol Chem **288**(37): 26533-26545.

Pietrzik, C.U., Busse, T., Merriam, D.E., Weggen, S. and Koo, E.H. (2002). "The cytoplasmic domain of the LDL receptor-related protein regulates multiple steps in APP processing." EMBO J **21**(21): 5691-5700.

Pietrzik, C.U., Yoon, I.S., Jaeger, S., Busse, T., Weggen, S. and Koo, E.H. (2004). "FE65 constitutes the functional link between the low-density lipoprotein receptor-related protein and the amyloid precursor protein." J Neurosci **24**(17): 4259-4265.

Pless, D.D. and Lennarz, W.J. (1977). "Enzymatic conversion of proteins to glycoproteins." Proc Natl Acad Sci U S A **74**(1): 134-138.

Praissman, J.L. and Wells, L. (2014). "Mammalian O-mannosylation pathway: glycan structures, enzymes, and protein substrates." Biochemistry **53**(19): 3066-3078.

Praissman, J.L., Willer, T., Sheikh, M.O., Toi, A., Chitayat, D., Lin, Y.Y., Lee, H., Stalnaker, S.H., Wang, S., Prabhakar, P.K., Nelson, S.F., Stemple, D.L., Moore, S.A., Moremen, K.W., Campbell, K.P. and Wells, L. (2016). "The functional O-mannose glycan on alpha-dystroglycan contains a phospho-ribitol primed for matriglycan addition." Elife **5**.

Puzzo, D., Lee, L., Palmeri, A., Calabrese, G. and Arancio, O. (2014). "Behavioral assays with mouse models of Alzheimer's disease: practical considerations and guidelines." Biochem Pharmacol **88**(4): 450-467.

Razi, N. and Varki, A. (1998). "Masking and unmasking of the sialic acid-binding lectin activity of CD22 (Siglec-2) on B lymphocytes." Proc Natl Acad Sci U S A **95**(13): 7469-7474.

Rogers, J., Cooper, N.R., Webster, S., Schultz, J., McGeer, P.L., Styren, S.D., Civin, W.H., Brachova, L., Bradt, B., Ward, P. and et al. (1992). "Complement activation by beta-amyloid in Alzheimer disease." Proc Natl Acad Sci U S A **89**(21): 10016-10020.

Rohlmann, A., Gotthardt, M., Willnow, T.E., Hammer, R.E. and Herz, J. (1996). "Sustained somatic gene inactivation by viral transfer of Cre recombinase." Nat Biotechnol **14**(11): 1562-1565.

Rota, E., Bellone, G., Rocca, P., Bergamasco, B., Emanuelli, G. and Ferrero, P. (2006). "Increased intrathecal TGF-beta1, but not IL-12, IFN-gamma and IL-10 levels in Alzheimer's disease patients." Neurol Sci **27**(1): 33-39.

Sastre, M., Dewachter, I., Landreth, G.E., Willson, T.M., Klockgether, T., van Leuven, F. and Heneka, M.T. (2003). "Nonsteroidal anti-inflammatory drugs and peroxisome proliferator-activated receptor-gamma agonists modulate immunostimulated processing of amyloid precursor protein through regulation of beta-secretase." J Neurosci **23**(30): 9796-9804.

Sastre, M., Dewachter, I., Rossner, S., Bogdanovic, N., Rosen, E., Borghgraef, P., Evert, B.O., Dumitrescu-Ozimek, L., Thal, D.R., Landreth, G., Walter, J., Klockgether, T., van Leuven, F. and Heneka, M.T. (2006). "Nonsteroidal anti-inflammatory drugs repress beta-secretase gene promoter activity by the activation of PPARgamma." Proc Natl Acad Sci U S A **103**(2): 443-448.

Sato, S., Cerny, R.L., Buescher, J.L. and Ikezu, T. (2006). "Tau-tubulin kinase 1 (TTBK1), a neuron-specific tau kinase candidate, is involved in tau phosphorylation and aggregation." J Neurochem **98**(5): 1573-1584.

Schnaar, R.L. (2016). "Glycobiology simplified: diverse roles of glycan recognition in inflammation." J Leukoc Biol **99**(6): 825-838.

Schrag, J.D., Procopio, D.O., Cygler, M., Thomas, D.Y. and Bergeron, J.J. (2003). "Lectin control of protein folding and sorting in the secretory pathway." Trends Biochem Sci **28**(1): 49-57.

Schuff, N., Woerner, N., Boreta, L., Kornfield, T., Shaw, L.M., Trojanowski, J.Q., Thompson, P.M., Jack, C.R., Jr. and Weiner, M.W. (2009). "MRI of hippocampal volume loss in early Alzheimer's disease in relation to ApoE genotype and biomarkers." Brain **132**(Pt 4): 1067-1077.

Shie, F.S., Montine, K.S., Breyer, R.M. and Montine, T.J. (2005). "Microglial EP2 is critical to neurotoxicity from activated cerebral innate immunity." Glia **52**(1): 70-77.

Simard, A.R., Soulet, D., Gowing, G., Julien, J.P. and Rivest, S. (2006). "Bone marrow-derived microglia play a critical role in restricting senile plaque formation in Alzheimer's disease." Neuron **49**(4): 489-502.

Stalder, A.K., Ermini, F., Bondolfi, L., Krenger, W., Burbach, G.J., Deller, T., Coomaraswamy, J., Staufenbiel, M., Landmann, R. and Jucker, M. (2005). "Invasion of hematopoietic cells into the brain of amyloid precursor protein transgenic mice." J Neurosci **25**(48): 11125-11132.

Stanley, P. and Ioffe, E. (1995). "Glycosyltransferase mutants: key to new insights in glycobiology." FASEB J **9**(14): 1436-1444.

Stanley, P. and Okajima, T. (2010). "Roles of glycosylation in Notch signaling." Curr Top Dev Biol **92**: 131-164.

Sturrock, R.R. (1979). "A morphological study of the development of the mouse choroid plexus." J Anat **129**(Pt 4): 777-793.

Takeuchi, H. and Haltiwanger, R.S. (2014). "Significance of glycosylation in Notch signaling." Biochem Biophys Res Commun **453**(2): 235-242.

Tateno, H., Crocker, P.R. and Paulson, J.C. (2005). "Mouse Siglec-F and human Siglec-8 are functionally convergent paralogs that are selectively expressed on eosinophils and recognize 6-sulfo-sialyl Lewis X as a preferred glycan ligand." Glycobiology **15**: 1125-1135.

Tateno, H., Li, H., Schur, M.J., Bovin, N., Crocker, P.R., Wakarchuk, W.W. and Paulson, J.C. (2007). "Distinct endocytic mechanisms of CD22 (Siglec-2) and Siglec-F reflect roles in cell signaling and innate immunity." Mol Cell Biol **27**(16): 5699-5710.

Taupenot, L., Ciesielski-Treska, J., Ulrich, G., Chasserot-Golaz, S., Aunis, D. and Bader, M.F. (1996). "Chromogranin A triggers a phenotypic transformation and the generation of nitric oxide in brain microglial cells." Neuroscience **72**(2): 377-389.

Taylor, P., Takeuchi, H., Sheppard, D., Chillakuri, C., Lea, S.M., Haltiwanger, R.S. and Handford, P.A. (2014). "Fringe-mediated extension of O-linked fucose in the ligand-binding region of Notch1 increases binding to mammalian Notch ligands." Proc Natl Acad Sci U S A **111**(20): 7290-7295.

Taylor, P.R., Carugati, A., Fadok, V.A., Cook, H.T., Andrews, M., Carroll, M.C., Savill, J.S., Henson, P.M., Botto, M. and Walport, M.J. (2000). "A hierarchical role for classical pathway complement proteins in the clearance of apoptotic cells in vivo." J Exp Med **192**(3): 359-366.

Terrand, J., Bruban, V., Zhou, L., Gong, W., El Asmar, Z., May, P., Zurhove, K., Haffner, P., Philippe, C., Woldt, E., Matz, R.L., Gracia, C., Metzger, D., Auwerx, J., Herz, J. and Boucher, P. (2009). "LRP1 controls intracellular cholesterol storage and fatty acid synthesis through modulation of Wnt signaling." J Biol Chem **284**(1): 381-388.

Thomas, T., Nadackal, T.G. and Thomas, K. (2001). "Aspirin and non-steroidal anti-inflammatory drugs inhibit amyloid-beta aggregation." Neuroreport **12**(15): 3263-3267.

Tuppo, E.E. and Arias, H.R. (2005). "The role of inflammation in Alzheimer's disease." Int J Biochem Cell Biol **37**(2): 289-305.

Turner, M.D., Nedjai, B., Hurst, T. and Pennington, D.J. (2014). "Cytokines and chemokines: At the crossroads of cell signalling and inflammatory disease." Biochim Biophys Acta **1843**(11): 2563-2582.

Ulery, P.G., Beers, J., Mikhailenko, I., Tanzi, R.E., Rebeck, G.W., Hyman, B.T. and Strickland, D.K. (2000). "Modulation of beta-amyloid precursor protein processing by the low density lipoprotein receptor-related protein (LRP). Evidence that LRP contributes to the pathogenesis of Alzheimer's disease." J Biol Chem **275**(10): 7410-7415.

Vaillant, C., Michos, O., Orolicki, S., Brellier, F., Taieb, S., Moreno, E., Te, H., Zeller, R. and Monard, D. (2007). "Protease nexin 1 and its receptor LRP

modulate SHH signalling during cerebellar development." Development **134**(9): 1745-1754.

Van Leuven, F., Stas, L., Raymakers, L., Overbergh, L., De Strooper, B., Hilliker, C., Lorent, K., Fias, E., Umans, L., Torrekens, S. and et al. (1993). "Molecular cloning and sequencing of the murine alpha-2-macroglobulin receptor cDNA." Biochim Biophys Acta **1173**(1): 71-74.

Viswanathan, K., Chandrasekaran, A., Srinivasan, A., Raman, R., Sasisekharan, V. and Sasisekharan, R. (2010). "Glycans as receptors for influenza pathogenesis." Glycoconj J **27**(6): 561-570.

Vodovotz, Y., Lucia, M.S., Flanders, K.C., Chesler, L., Xie, Q.W., Smith, T.W., Weidner, J., Mumford, R., Webber, R., Nathan, C., Roberts, A.B., Lippa, C.F. and Sporn, M.B. (1996). "Inducible nitric oxide synthase in tangle-bearing neurons of patients with Alzheimer's disease." J Exp Med **184**(4): 1425-1433.

Vyas, A.A., Patel, H.V., Fromholt, S.E., Heffer-Lauc, M., Vyas, K.A., Dang, J., Schachner, M. and Schnaar, R.L. (2002). "Gangliosides are functional nerve cell ligands for myelin-associated glycoprotein (MAG), an inhibitor of nerve regeneration." Proc Natl Acad Sci U S A **99**(12): 8412-8417.

Wang, X., Gu, J., Ihara, H., Miyoshi, E., Honke, K. and Taniguchi, N. (2006). "Core fucosylation regulates epidermal growth factor receptor-mediated intracellular signaling." J Biol Chem **281**(5): 2572-2577.

Watkins, W.M. and Morgan, W.T. (1959). "Possible genetical pathways for the biosynthesis of blood group mucopolysaccharides." Vox Sang **4**(2): 97-119.

Westermark, P., Sletten, K., Johansson, B. and Cornwell, G.G., 3rd (1990). "Fibril in senile systemic amyloidosis is derived from normal transthyretin." Proc Natl Acad Sci U S A **87**(7): 2843-2845.

Willnow, T.E., Armstrong, S.A., Hammer, R.E. and Herz, J. (1995). "Functional expression of low density lipoprotein receptor-related protein is controlled by receptor-associated protein in vivo." Proc Natl Acad Sci U S A **92**(10): 4537-4541.

Wisniewski, T. and Goni, F. (2015). "Immunotherapeutic Approaches for Alzheimer's Disease." Neuron **85**(6): 1162-1176.

Wyss-Coray, T., Lin, C., Sanan, D.A., Mucke, L. and Masliah, E. (2000). "Chronic overproduction of transforming growth factor-beta1 by astrocytes promotes Alzheimer's disease-like microvascular degeneration in transgenic mice." Am J Pathol **156**(1): 139-150.

Wyss-Coray, T., Yan, F., Lin, A.H., Lambris, J.D., Alexander, J.J., Quigg, R.J. and Masliah, E. (2002). "Prominent neurodegeneration and increased plaque formation in complement-inhibited Alzheimer's mice." Proc Natl Acad Sci U S A **99**(16): 10837-10842.

Xia, M.Q. and Hyman, B.T. (1999). "Chemokines/chemokine receptors in the central nervous system and Alzheimer's disease." J Neurovirol **5**(1): 32-41.

Xia, M.Q., Qin, S.X., Wu, L.J., Mackay, C.R. and Hyman, B.T. (1998). "Immunohistochemical study of the beta-chemokine receptors CCR3 and CCR5 and their ligands in normal and Alzheimer's disease brains." Am J Pathol **153**(1): 31-37.

Xu JQ, M.S., Kochanek KD, Bastian BA. (2016). Deaths: Final data for 2013. National vital statistics reports, National Center for Health Statistics. **64**.

Yan, S.D., Stern, D., Kane, M.D., Kuo, Y.M., Lampert, H.C. and Roher, A.E. (1998). "RAGE-Abeta interactions in the pathophysiology of Alzheimer's disease." Restor Neurol Neurosci **12**(2-3): 167-173.

Yermakova, A.V., Rollins, J., Callahan, L.M., Rogers, J. and O'Banion, M.K. (1999). "Cyclooxygenase-1 in human Alzheimer and control brain: quantitative analysis of expression by microglia and CA3 hippocampal neurons." J Neuropathol Exp Neurol **58**(11): 1135-1146.

Zhang, Y., Chen, K., Sloan, S.A., Bennett, M.L., Scholze, A.R., O'Keeffe, S., Phatnani, H.P., Guarnieri, P., Caneda, C., Ruderisch, N., Deng, S., Liddelow, S.A., Zhang, C., Daneman, R., Maniatis, T., Barres, B.A. and Wu, J.Q. (2014). "An RNA-sequencing transcriptome and splicing database of glia, neurons, and vascular cells of the cerebral cortex." J Neurosci **34**(36): 11929-11947.

CHAPTER 2

GLYCOSYLATION AT THE CHOROID PLEXUS MODULATES INFLAMMATION STATUS IN ALZHEIMER'S DISEASE[1]

Nix, David B.[1], Rosenbalm, Katelyn E., Furgerson, Matthew, Furukawa, Ruth, Fechheimer, Marcus, Tiemeyer, Michael To be submitted to J. Neuroscience

Abstract

To assess the influence of glycomic changes in AD, we investigated protein and lipid glycosylation in a highly aggressive mouse model. Here we use the 5xFAD mouse model and detected broad changes in glycoprotein and glycolipid glycosylation. We also focused on changes in expression of glycan structures recognized by an anti-inflammatory SIGLEC (SIGLEC-F) to assess whether glycomic changes might contribute to neurodegenerative disease progression. Siglec-F is generally expressed on murine eosinophils and alveolar macrophages, inducible on microglia and T cells, and signals for apoptosis when engaged to its ligand in eosinophilic asthma models (Stevens et al. 2007; Zhang et al. 2007; Lunnon et al. 2011; Kiwamoto et al. 2015). Our results demonstrate significant changes in the glyco-terrain of the brain in aggressive AD. And, more significantly, we demonstrate the increased expression of anti-inflammatory glycans by epithelial cells of the Choroid Plexus (ChP), a CNS compartment positioned to mediate the trafficking and differentiation of innate immune cells (Meeker et al. 2012; Lehtinen et al. 2013). It is at this intersection that bone marrow derived M2 macrophages, or "Alternative" anti-inflammatory macrophages, can enter the brain (Shechter et al. 2013). Furthermore, alterations in expression and abundance of Low density Lipoprotein Receptor-Related Protein1 (LRP1) at the ChP are seen. We show that LRP1, a 600-kD protein that is cleaved by furin into a 515-kD α-chain that is non-covalently

attached to an 85-kD transmembrane β-chain (Bu 2009), is a glycoprotein that may interact with Siglec-F expressed on M2 macrophages from the blood. Therefore, we hypothesize that engagement of Siglec-F with its glycan ligand modulates the innate immune response through M2 macrophage activity via extravasation into the brain at the Choroid Plexus.

KEY WORDS Alzheimer's, glycosylation, innate immunity, choroid plexus, Siglecs, inflammation, leukocytes

Introduction

Aβ plauqes, derived from protease processing of the amyloid precursor protein (APP), cause inflammation in Alzheimer's Disease (AD) by their interaction with microglia and macrophages (Itagaki et al. 1989). Aβ plauqes are danger-associated molecular patterns (DAMPs) that are recognized by various receptor systems, including the receptor for advanced glycation end products (RAGE), which stimulates pro-inflammatory pathways (Yan et al. 1996; Yan et al. 1998). The interaction between Aβ and RAGE promotes transendothelial migration of T-cells into the brain, leading to enhanced immune surveillance of the brain (Li et al. 2009). Immune surveillance of neural tissue, whether by cellular components of the innate or adaptive immune systems, can significantly influence brain function though targeted cell interactions, cytokine release, and altered blood-brain barrier integrity (Ransohoff et al. 2003). Accordingly, the role

of inflammation in the pathophysiology of degenerative brain disorders is the subject of expanding attention.

Innate immune responses in the central nervous system (CNS) are mediated by microglia, the predominant tissue-resident immune cell type of the CNS, and by infiltrating leukocytes and macrophages derived from the bone marrow (Baruch et al. 2013; Cronk and Kipnis 2013). Each of these innate immune cells express various types of surface receptors that recognize complex carbohydrates (glycans) secreted into the local environment or expressed on cell surfaces. Among these glycan-binding proteins is a family of structurally related receptors known as SIGLECs (sialic-acid-binding immunoglobulin-like lectins) (Lunnon et al. 2011; Griciuc et al. 2013). SIGLECs are expressed on many cell types, but most highly on granulocytes, monocytes/macrophages, and lymphocytes. All SIGLECS bind sialylated glycans through their N-terminal V-set immunoglobulin-like domain. For some SIGLECs, glycan binding results in endocytosis without signaling (SIGLEC-1, sialoadhesin). But, for most SIGLECs, glycan binding results in the induction of signaling through the phosphorylation of immunoreceptor tyrosine-based inhibitory or activatory motifs (ITIM/ITAM domains) (Crocker et al. 2007). Cellular expression of SIGLEC receptors and subsequent engagement of their recognized glycan ligands imparts various cell-type specific consequences, including induction of apoptosis, sequestration of signaling molecules, or endocytosis of extracellular signals (Vyas et al. 2002; Tateno et al. 2007; Bochner 2009; Kawasaki et al. 2010; McMillan et al. 2014; Kiwamoto et al. 2015). This modulatory activity of SIGLEC receptors suggests

that the brain glycome, which includes glycan ligands that engage SIGLEC receptors, influences the inflammatory status of the tissue.

To comprehensively assess the glycomic changes in AD that might influence tissue inflammation, we have characterized protein and lipid glycosylation in a highly aggressive mouse model. The 5xFAD mouse model (AD), named for harboring 5 genetic mutations identified in familial Alzheimer's patients, has three mutations in APP and two in presenilin 1 (PS1). These mice have greatly accelerated neurodegenerative pathology, showing extraneuronal Aβ plaques at 2 months and significant neuron loss at 9 months (Oakley et al. 2006; Eimer and Vassar 2013). We queried glycomic changes in this extreme AD mouse model and detected broad changes in glycoprotein and glycolipid glycosylation. Additionally, we used MAA and SNA lectins to profile the distribution of sialyl-glycans in AD brains. These changes correlate with our MS data and predict unique trafficking of glycoproteins containing α2-3 sialic acid. We also investigated changes in expression of glycan structures recognized by SIGLEC-F, an anti-inflammatory SIGLEC, to assess whether glycomic changes might contribute to neurodegenerative disease progression. Our results demonstrate significant changes in the glyco-terrain of the brain in aggressive AD. We also demonstrate the increased expression of anti-inflammatory glycans on specific glycoproteins produced by epithelial cells of the choroid plexus (ChP), a CNS compartment positioned to mediate the trafficking and differentiation of immune cells. We propose that glycan binding to Siglec-F on extravasating macrophages at the ChP modulates their inflammatory status and provides a

mechanism for protecting the brain from excessive inflammation in aggressive AD.

Experimental Procedure

Reagents

All reagents are from Sigma Aldrich unless otherwise noted. All antibodies and blocking buffer [4% (w/v) BSA, 10% (v/v) Goat Serum, 0.12 mg/mL unconjugated goat anti-mouse IgG (Jackson Labs, 115-005-003)] were filtered through 0.2 μm SFCA filters (Corning, 431219) prior to Immunofluorescence (IF). Siglec-F-Fc (R&D systems, 1706SF050) at 1:500 for IHC/IF and 1:5000 for western blot (WB). Siglec-F-Fc was pre-complexed to Goat anti-Human HRP (Promega, W4038) at 1:2000 for Immunohistochemistry (IHC), Goat anti-Human Alexa 488 (Invitrogen, A11013) at 1:2000 for IF, and Goat anti-Human HRP at 1:10,000 for WB, Siglec-F (a generous gift from Dr. Bruce Bochner) at 1:200 for IF, LRP1 alpha-chain (Abcam, 8G1) at 1:1000 for IF, and 1:320 for WB using non-denaturing conditions, Versican (DSHB, 12C5) at 1:10 for IF, Iba1 (Wako, 019-19741) at 1:250 for IF, AQP1 (Santa Cruz, 32737) at 1:50 for IF, CD206 (Abcam, 15-2) at 1:50 for IF, Alexa 488 Goat anti-Rabbit (Invitrogen, A-11008) at 1:2000 for IF, Alexa 568 Goat anti-Rat (Invitrogen, A-11077) at 1:2000 for IF, Alexa 488 Goat anti-Mouse (Invitrogen, A-11001) at 1:2000 for IF, SNA (Vector, B-1305) at 1:250 with Streptavidin Alexa 568 (Invitrogen, S11226) at 1:2000 for IF, MAA (Roche, 11210238001) at 1:250 with DyLight 488 Anti-DIG (Vector, DI-7488) at 1:2000 for IF. Samples and slides were digested with 1μL of 44.5U/μL

Vibrio cholera Sialidase (a generous gift from Dr. Ronald Schnaar) in 0.1 M PIPES 4mM $CaCl_2$ pH 6.0 buffer prior to immunoassay, α2-3 specific sialidase (Prozyme, GK80020) was used according to manufacturer's recommendation. PNGase F (a generous gift from Dr. Kelly Moremen) digestion of samples and slides was performed in 0.1 M sodium phosphate pH 7.5 buffer for a minimum of 4 hrs.

Mice

B6SJLF1/J wild-type mice and 5xFAD transgenic mice (B6SJL-Tg(APPSwFlLon,PSEN1*M146L*L286V)6799Vas/J) were used for our experiments (https://www.jax.org/strain/006554). Mice were anesthetized with CO_2 and decapitated. Brains were harvested and washed with ice-cold 1x PBS; the olfactory bulb and cerebellum were removed prior to separating hemispheres. Eight to ten week-old mice were used for mass spectrometry, quantitative RT-PCR, and protein purification; each hemisphere was separately snap frozen in liquid nitrogen before storage at -80^{o}C. Sixteen week-old mice were used for IHC and incubated in formaldehyde overnight prior to mounting in wax or sucrose gradient incubation and storage at 4^{o}C.

Glycan analysis

Hemispheres were crushed in a ceramic mortar using liquid nitrogen and a pestle prior to immediate addition of 50% methanol and transfer into a glass

dounce homogenizer for additional homogenization. The homogenate was adjusted to a final concentration of Water:Chloroform:Methanol 4:8:3 (v/v/v) and extracted three times with additional 4:8:3 and once with ice-cold 80% acetone (v/v, aqueous to precipitate proteins. All supernatants generated during the extraction procedure were combined and dried under nitrogen for analysis of GSL, LLO and FOS. Protein content of the powder was determined by BCA assay (Pierce, 23235). Generally, 2 mg of protein powder (dry weight) was used for both, N- and O-glycan analysis. N-linked glycans were harvested from the protein powder as previously described (Aoki et al. 2007). Briefly, glycopeptides were generated by digestion of protein powder with trypsin/chymotrypsin (Sigma Aldrich) prior to enrichment by Sep-Pak C18 cartridge chromatography (Waters, WAT023590) and subjected to digestion with PNGaseF for 18 h at 37^{o}C. Released oligosaccharides were separated from residual peptides by Sep-Pak C18 clean up and permethylated prior to mass spectrometric analysis. O-linked glycans were released by reductive β-elimination, desalted on AG-50W-X8 resin (Sigma, 217506) (H^+ form) and enriched by Sep-Pak C18 cartridge chromatography (Aoki et al. 2008). GSLs prepared from dried supernatant were saponified for 18 h at 37^{o}C before enrichment and desalting by Sep-Pak tC18 cartridge chromatography. Free fatty acids were removed using Hexanes before suspension in Chloroform: Methanol: Water, 2:2:0.1 for HPTLC analysis (Boccuto et al. 2014). LLO and FOS were retrieved from the dried supernatant after brain homogenization. Briefly, supernatant was suspended in 50% aqueous methanol and loaded onto a double-jointed tC18/QMA (Waters, WAT036805/WAT023525)

strong anion-exchange column. FOS were collected in the flow through and water washes while LLO were eluted using 10:10:3 containing 450 mM ammonium acetate (NH_4OAc). LLO were then desalted and recovered by phase partition prior to mild acid hydrolysis using 0.1 N HCl in 50% 2-PrOH. Butanol saturated water was used for phase partition prior to a final desalting over Dowex (AG50W-8X) before purification using C18 column.

Permethylated N-glycans, O-glycans, GSL, FOS and LLO glycans were analysed by nanoelectrospray ionization mass spectrometry using an ion trap instrument (NSI-LTQ Orbitrap Discovery, Thermo-Fisher). N-glycans, O-glycans, FOS, and LLO were dissolved in 1 mM NaOH in 50% aqueous methanol (v/v) while GSLs were dissolved in 1 mM NaOH in Methanol:2-Propanol:1-Propanol, 16:3:3 by volume before direct infusion into the instrument at a syringe flow rate of 0.40–0.60 μL min^{-}1 and a capillary temperature set to 210^{o}C. For fragmentation by collision-induced dissociation (CID) in MS/MS and MS^n modes, 40% collision energy was applied. The total ion mapping functionality of the XCalibur software package (version 2.0) was utilized to detect and quantify the prevalence of individual glycans in the total glycan profile. Structural assignments were done using GRITS Toolbox (CCRC freeware); all structures were validated by manual inspection. Total ion mapping peaks for all charge states of a given ion with m/z ≤ 2000 were summed together for quantification. Glycan quantification was performed relative to a known quantity of external standards (maltotriose and maltotetraose, Supelco), which were permethylated with heavy

methyliodide ($^{13}CH_3I$) and spiked into the sample matrix prior to analysis (Mehta et al. 2016).

Immunohistochemistry

Brains stored in 30% sucrose (w/v) were frozen in Optimal Cutting Temperature compound (Tissue-Tek, 27050) prior to sectioning on a microtome-cryostat. The 20-µm sections were adhered onto SuperFrost Gold Plus (Fisher Scientific) and placed at -20^{o}C overnight before use. For immunofluorescent staining, slides were placed at RT for 30 min prior to post-fixation in acetone. Sections were hydrated in 1x PBS and permeabilized in PBS containing 0.1% Triton X-100 (v/v). Prolong Diamond mounting medium (Invitrogen, P36970) was allowed to cure overnight in the dark before sealing coverslips. Brains mounted in wax were sectioned at 5µm into ribbons and floated in a water bath to adhere onto SuperFrost Gold Plus (Fisher, 15-188-48) slides and kept at RT overnight before use. For IHC sections were hydrated in Xylene (3x), 100% EtOH, 95% EtOH (v/v), and 70% EtOH (v/v). Antigen retrieval was performed using 10 mM sodium citrate buffer pH 6.0 for 20 min at 100^{o}C. Sections were washed in 1x PBS and permeabilized in PBS containing 0.1% Triton X-100 prior to incubation with Dual Endogenous Enzyme Blocker (DAKO, S2003) for 10 min at RT. Sections were stained with 3,3'-Diaminobenzidine (DAB) and mounted in 70% Glycerol (v/v).

Immunoprecipitation and LC-MS/MS

100 µg of whole brain lysate was incubated with 20 µL of 50% slurry of protein A/G beads (Pierce, 20421) for 1hr at 4^{o}C to remove all non-specific interactions. For LRP1 immunoprecipitation (IP), cleared lysate was added to an Amicon 10K spin filter (Millipore, UFC501024) and buffer exchanged to 50 mM ammonium bicarbonate prior to overnight incubation with PNGase F at 37^{o}C. Digested lysate was washed with PBS and collected by inversion. Lysate was incubated with 5µg of antibody or fusion protein overnight at 4^{o}C before combining with fresh protein A/G beads and incubated for 1hr at room temperature. After incubation, beads were washed with PBS and boiled in Laemmli buffer to release bound protein. For fusion protein overlays samples were separated using SDS-PAGE prior to transfer to PVDF. For proteomic identification, eluted protein was separated using SDS-PAGE and visualized using G250-CBB prior to excision. Excised protein bands were then reduced, carbamidomethylated, and digested with modified trypsin (Promega, V5111) overnight at 37^{o}C. Peptides were purified using Sep-Pak C18 cartridge chromatography and dried in a SpeedVac prior. LC-MS/MS analysis was performed on an LTQ-Orbitrap Discovery equipped with a nanospray ion source by a data-dependent scan. Alternatively, samples were analyzed using Orbitrap Fusion or Orbitrap Fusion Lumos (Thermo Fisher). Obtained data were analyzed with Proteome Discoverer (Thermo Fisher) 1.4 using Sequest and a false discovery rate of 0.1% or Byonic (Protein Metrics). Post processing was performed using ProteoIQ (Premier Biosoft).

Western Blotting

Whole brains were weighed and homogenized in 10 volumes of 0.32 M sucrose using a Potter-Elvehjem pestle. Homogenate was centrifuged at 1,000 x g, 4^{o}C for 10 min. Supernatant was transferred into a separate tube and centrifuged again at 20,000 x g, 4^{o}C for 30 min. Resulting pellet was suspended in 1 volume of 0.32 M sucrose and homogenized a second time using the Potter-Elvehjem pestle before adding 10 volumes of 5 mM sodium phosphate buffer and centrifuging at 20,000 x g, 4^{o}C for 30 min. Pellet was resuspended in 2 volumes of 0.32 M sucrose and placed at -80^{o}C. Protein concentration was determined by BCA assay.

LRP1 Enrichment

Whole brains were weighed and homogenized in 5 volumes of 5 M Guadinium HCl in 50 mM Tris pH 8.0 using a Potter-Elvehjem pestle. Homogenate was centrifuged at 18,000g for 30 min. Supernatant was transferred and filtered using 5-µm PVDF spin filters followed by an additional 0.2-µm PVDF spin filter. The cleared homogenate was injected onto a Supelco 16/600 pg column and eluted using 5 M Guadinium HCl in 50 mM Tris pH 8.0 into 2 mL fractions. Fractions positive for Siglec-F-Fc binding were pooled and desalted and the buffer exchanged to 0.25 M Tris pH 8.2.

Results

Protein glycosylation is altered in the forebrain of 5xFAD mice

Using mass spectrometry we found broad changes in many categories of N-linked glycans between AD and control mice (**Figure 2.1A**). Grouping the identified glycans using common structures or epitopes we see significant changes in hybrid, tri-antennary, and quatra-antennary glycans along with those containing terminal fucose, N-glycolylneuraminic acid (NeuGc), and the Lewis X epitope. This decrease in N-glycans was mirrored by an increase in Free Oligosaccharides (FOS), an indicator of inefficient protein glycosylation or increased degradation of misfolded proteins (**Figure 2.1B**). Unlike N-glycans, O-glycans were not significantly changed in the 5xFAD model. Many mucin type O-glycans were detected but upon grouping based on their linkages or composition (i.e. Core 1, fucosylated, sialylated) no striking differences emerged (**Figure 2.2**). The glycosphingolipid profile was dominated by the ganglio series and showed specific changes in lactosylceramide (LacCer) and the ganglioside GD1 (**Figure 2.3**). No other GSL was affected in its expression. To understand the mechanism behind the changes in glycan abundance, we surveyed glycosyltransferase mRNA expression using qRT-PCR. Across many categories of glycosyltransferases - N-glycan extension, capping, initiating, etc. – no changes were observed in expression of the enzymes (**Figure 5.1-5.2**). The lack of variation in glycosyltransferases indicates that the glycomic changes we detected were unrelated to transcriptional regulation and, most likely, reflected altered secretory pathway function. To obtain greater perspective on the scope of the

glycomic changes in the 5xFAD model, we decided to look at the staining patterns for sialic acid binding lectins in these brains since sialoglycan abundance was particularly impacted in the affected brains.

Figure 2.1: N-glycosylation is decreased in Alzheimer's disease

Whole brains with the olfactory bulb and cerebellum removed were used for N-glycan analysis by nanoelectrospray mass spectrometry. In (A) many classes of N-glycans are decreased. These categories are broad and contain many different structures, some of which are overlapping with other categories. These decreases are mirrored by an increase in free oligosaccharides (FOS) in (B). FOS are generated through the misfolded protein response (ERAD) or cleavage of LLO precursors, indicating there is a global N-glycosylation defect.

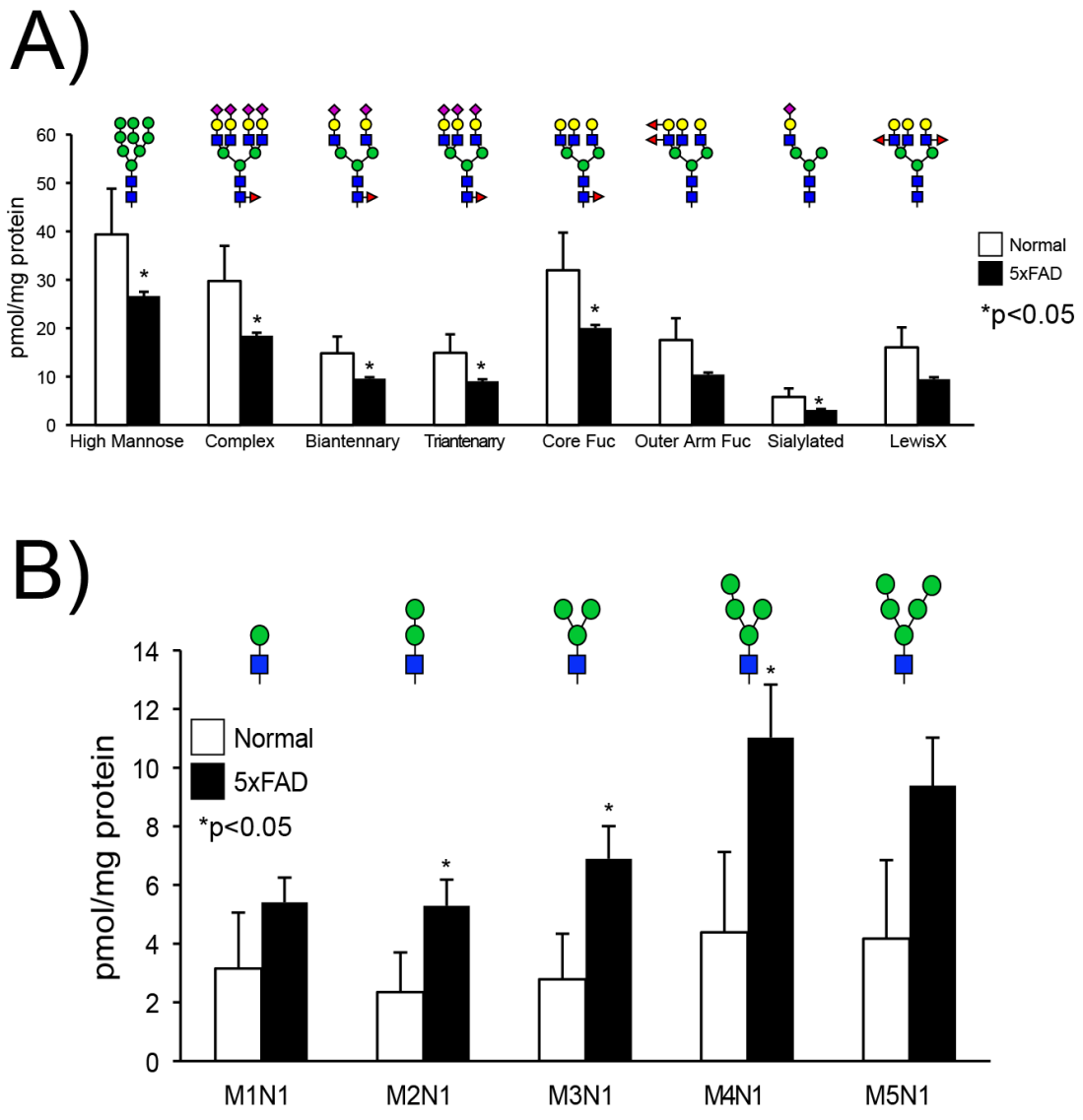

Figure 2.2: O-glycosylation is unaffected in Alzheimer's disease

Broad characterization of the O-glycome in AD brains revealed no changes from control brains. The lack of differences here further implicates ER dysfunction since the majority of O-glycans are initiated in the *cis*-Golgi.

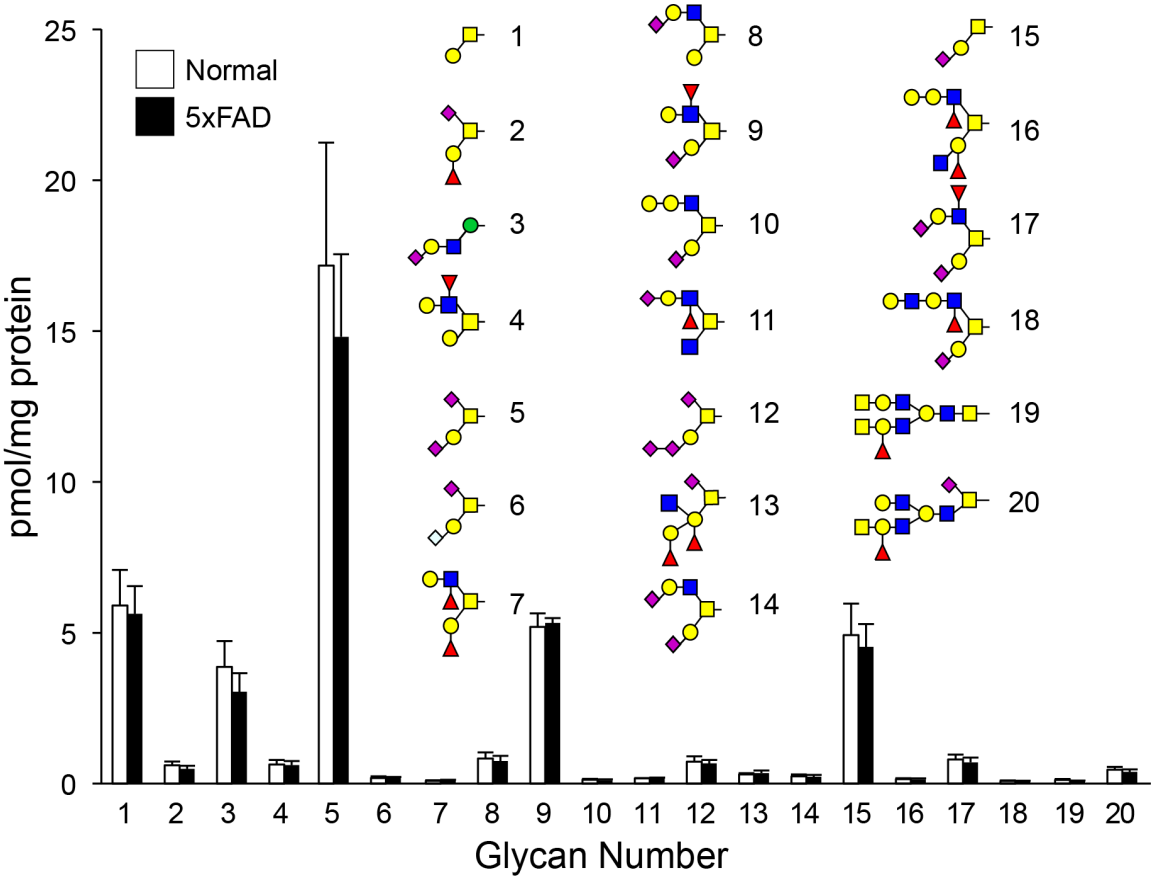

Figure 2.3: GSLs trend towards change in Alzheimer's disease

The glycosphingolipid profile shows distinct changes in lactosylceramide (LacCer) and GD1. Increased abundance of LacCer has been associated with higher levels of inflammation while GD1 is a ligand for Siglec-F making these differences substantial since no deficits in glycosyltransferases were found.

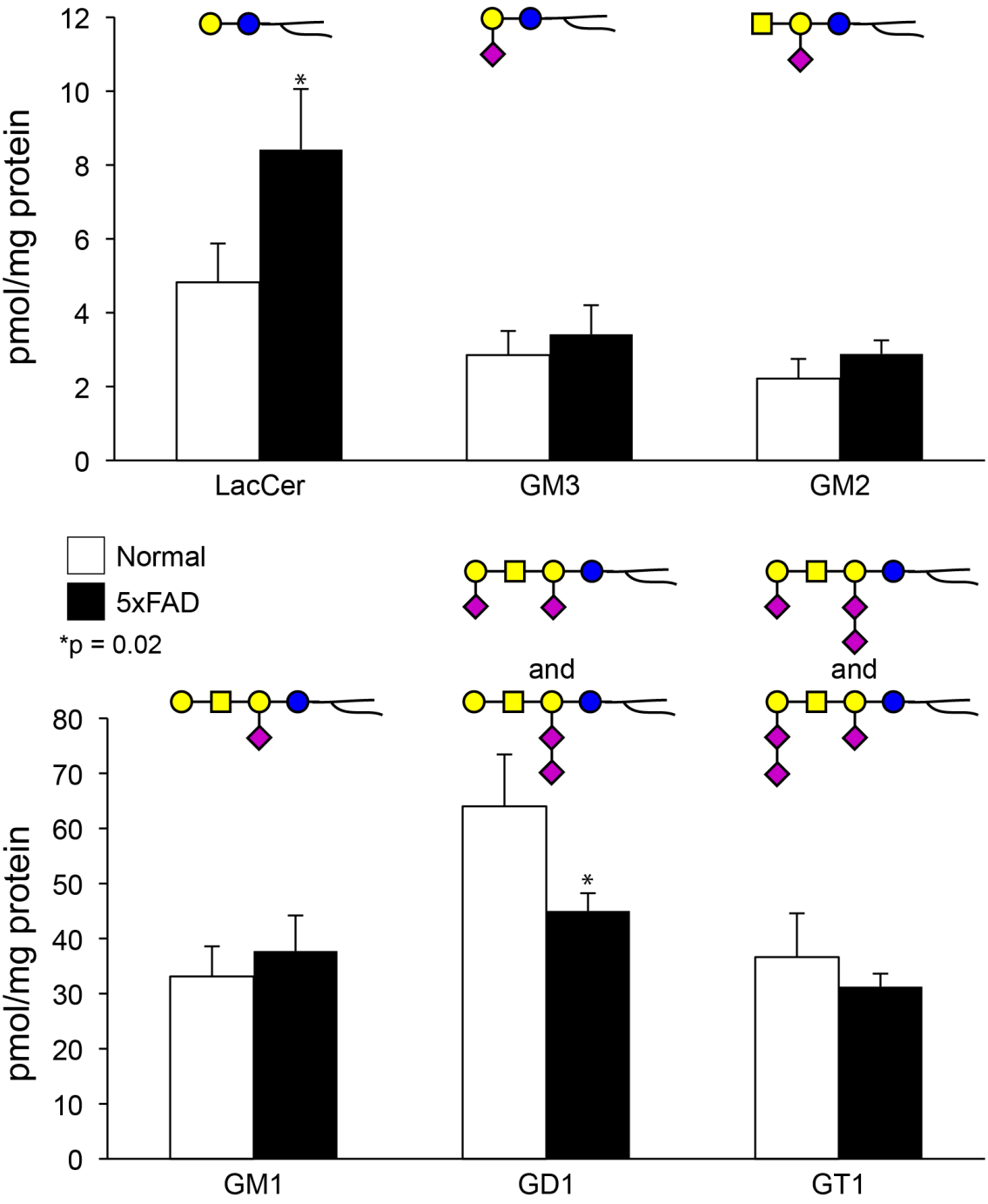

Profiling AD brains using MAA and SNA lectins

MAA lectin binds α2-3 sialylated glycoconjugates and SNA binds α2-6 sialylated glycoconjugates. We used these two lectins to compare and contrast changes in glycoprotein glycosylation in the 5xFAD mouse model. The most striking changes detected in 5xFAD mouse brain compared to wildtype were at the choroid plexus (ChP) within the lateral ventricles of the brain. In control brains, MAA staining revealed a diffuse vesicular distribution throughout the epithelial cell cytoplasm (**Figure 2.4**). In addition, heterogeneity across the ChP epithelium was detected in wildtype brains, such that some epithelial cells exhibited strong surface staining at the apical surface and others exhibited very little. In the 5xFAD brains, MAA revealed a reduced level of intracellular vesicular staining and substantially increased abundance of epithelial cells with strong apical surface staining. By 3D reconstruction, the altered distribution of MAA staining becomes more apparent (**Figure 2.5**). Here, a large increase in the number of apical patches that brightly fluoresce in AD was observed (arrows). Additionally, intracellular foci of strong punctate fluorescence are detected. These puncta appear similar to the fragmented Golgi previously reported in AD neurons (arrow heads) (Joshi et al. 2014). SNA lectin appears unchanged in 5xFAD ChP compared to wildtype (**Figure 2.4**). The differential staining patterns detected with MAA and SNA indicate that glycoconjugates with α2-3 sialic acid are preferentailly retained, or recycled, to the Golgi in the 5xFAD ChP, while those containing α2-6 sialic acid are properly trafficked to the apical surface. This differential trafficking deficit indicates that the secretory pathway is altered in its

structure and function in the neurodegenerative brain, a finding that can be substantiated by investigating the integrity of various Golgi markers, like trans-Golgi marker TGN38 and others.

Figure 2.4: Lectin staining patterns at the Choroid Plexus

The whole choroid plexus structure is labeled by MAA in control brains, most of which is likely vesicular. The overall intensity is lessened in AD brains along with increases in apical patches. The apical pattern of SNA in control brains is retained in AD brains with no changes observed.

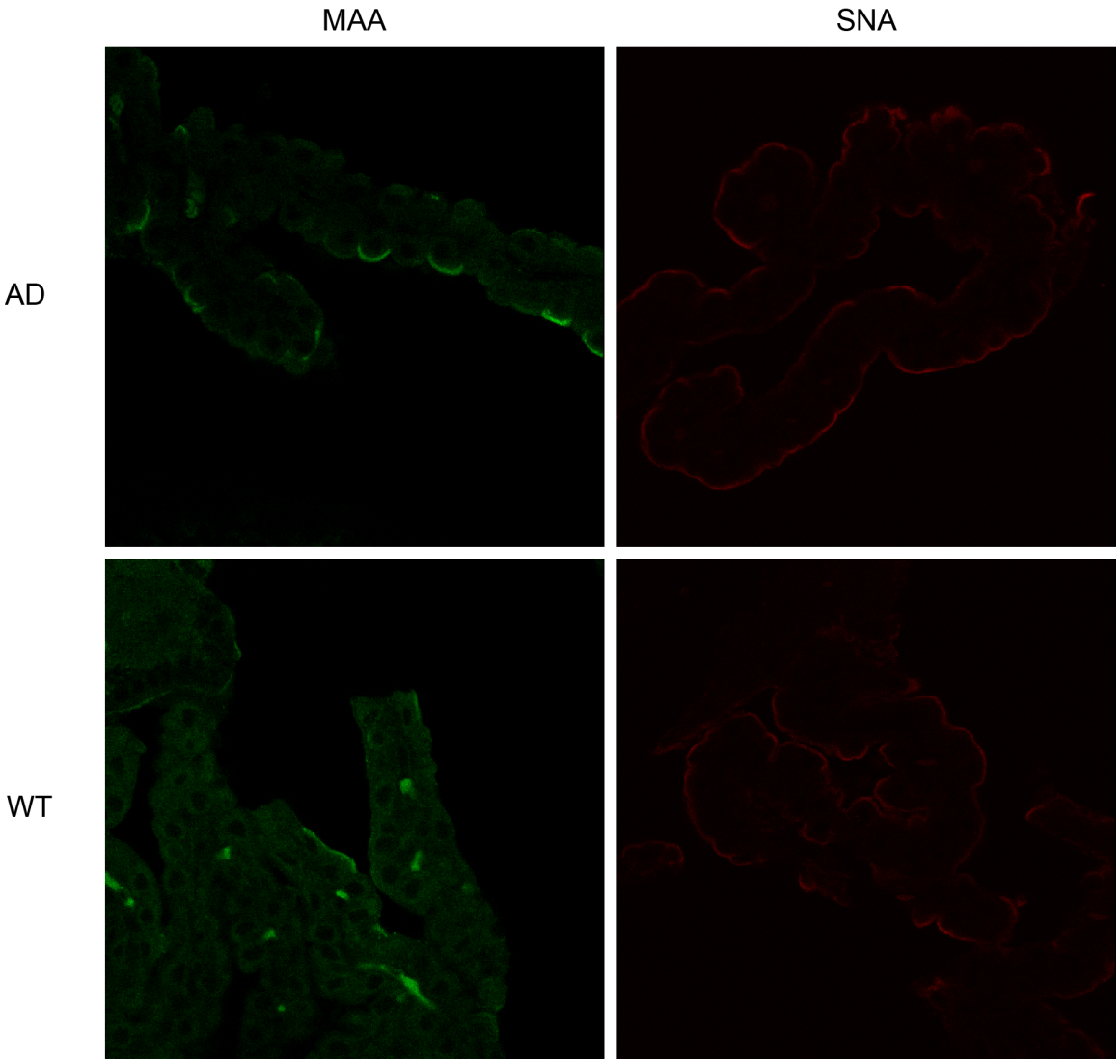

Figure 2.5: 3D rendering of MAA staining at the Choroid Plexus

Apical staining shows increased intensity for discrete patches in AD that are less frequently found in control brains. The overall appearance of these patches is that of individual epithelial cells expressing different glycoproteins at their apical surface (marked by arrows). Not all cells are activated in this way. Additionally, there are sub-cellular groups of punctate structures that have the appearance of fragmented Golgi in AD brains (marked by arrow heads). Curiously, these punctate structures are enriched in glycoproteins modified with α2-3 sialic acid.

MAA

AD

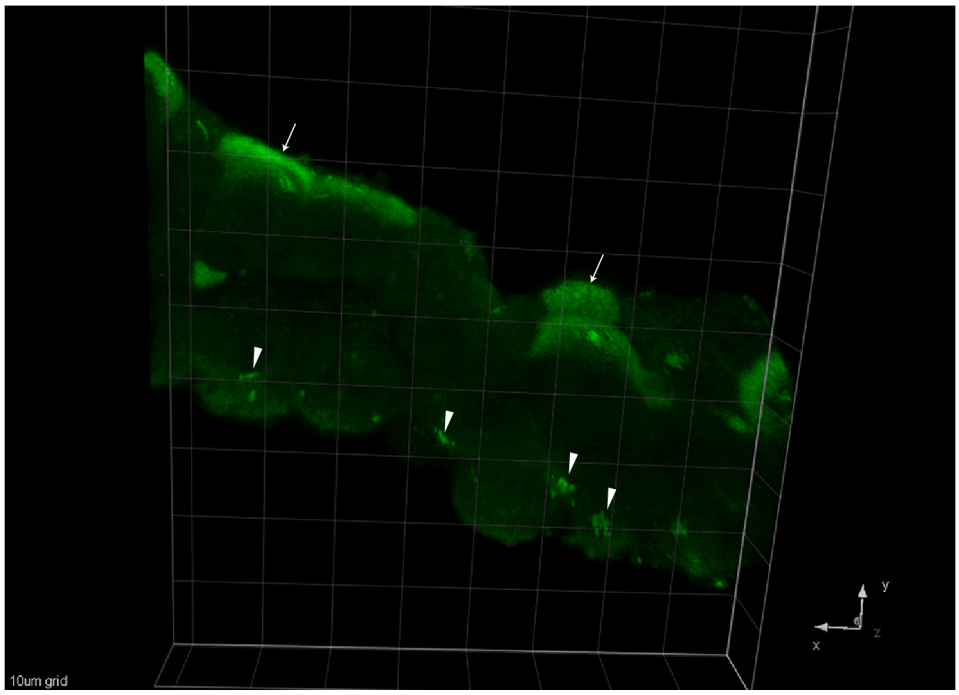

WT

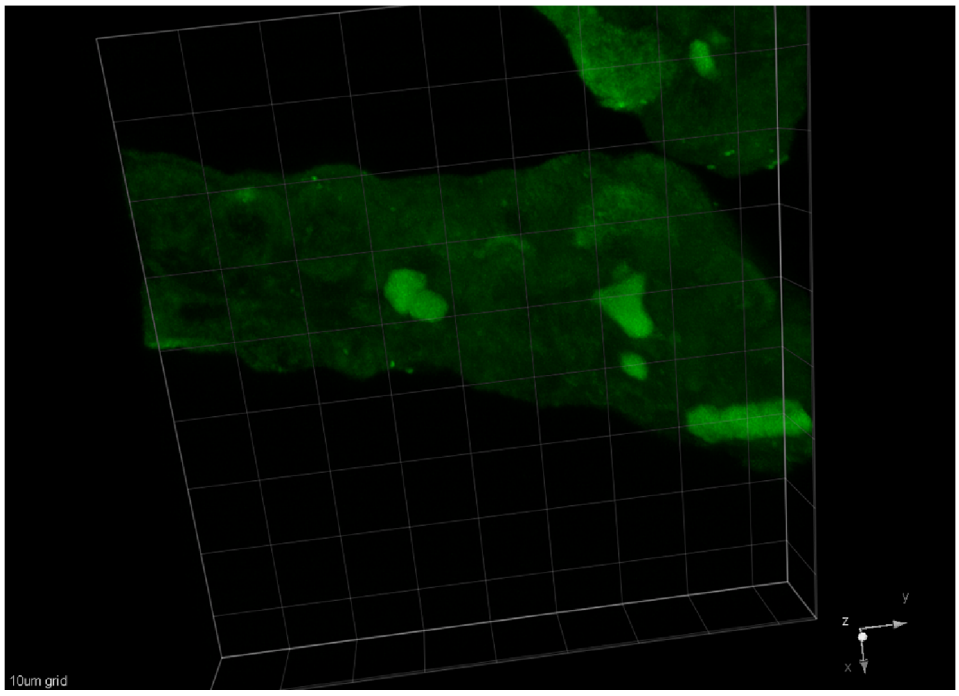

SIGLEC-F ligand is enriched at the Choroid Plexus

In addition to probing changes in glycan expression patterns using plant lectins, we also investigated the distribution of glycans that interact with endogenous mouse glycan binding proteins. We used chimeric constructs where the ectodomain of a subset of the members of a family of mouse sialic acid binding lectins, known as Siglecs, were fused to the Fc domain of an IgG antibody (Kelm et al. 1994). Using these chimeric constructs for Siglec-3, -E, and –F, we probed AD and control brains for their glycans ligands and were unable to find reproducible changes for either Siglec-3 or –E between AD and control brains. However, we did find substantial changes in ligands for Siglec-F at the apical surface of the choroid plexus and more broadly distributed throughout the brain parenchyma compared to WT (**Figure 2.6AB**). To test whether the Siglec-F binding that we detected was sialic acid sensitive we treated the sections with sialidase, which resulted in a complete loss of staining. We also treated sections with PNGaseF to remove N-glycans since our glycomic analysis showed broad changes in many categories of N-glycans. After treatment with PNGaseF, we detected a substantial but not complete decrease in staining, indicating that a portion of the ligand is presumably directed toward sialylated N-linked glycans (**Figure 2.7**). Siglec-F staining was also found on the ependymal surface of the ventricle, which is spatially continuous with the ChP epithelium.

To further characterize the localization and abundance of the endogenous Siglec-F ligand in brain, we used fluorescent confocal microscopy on frozen sections. Apical expression of the ligand is increased ~2 fold ($p=0.001$) in AD

when normalized to Aquaporin 1 (APQ1) expression (**Figure 2.6CD**). The appearance of the Siglec-F ligand by confocal is punctate and appears to be in vesicular structures that are outside the epithelial cells but located in close proximity to the apical surface of the epithelium, just extending into the ventricle. The extracellular structures that carry Siglec-F ligand closely resemble the extracellular vesicles seen to be secreted into the CSF by standard histochemical stains (**Figure 2.6A**).

Figure 2.6: Siglec-F ligand is increased at the Choroid Plexus

The Siglec family of lectins binds many different sialic acid containing epitopes, some of which were decreased in AD. Of the well-characterized Siglecs that have been predicted to be present in the brain, Siglec-F was a top candidate. Panel (A) shows the ChP stained with H&E. The apical surface is in contact with the cerebral spinal fluid and is ciliated. A fenestrated capillary bed is found below the basal surface. Using confocal microscopy we noticed a dramatic increase in the ligand for Siglec-F at the ChP in AD (C). When normalized to aquaporin 1 (AQP1) staining intensity, a ~2 fold increase ($p=0.001$) in the ligand is seen in AD (D). This increase is also seen in panel (B) where formalin fixed paraffin embedded brains were stained for Siglec-F-Fc and imaged using DAB. When sections are subjected to Sialidase or PNGase F treatment prior to staining, there is a total loss of staining or reduction, respectively.

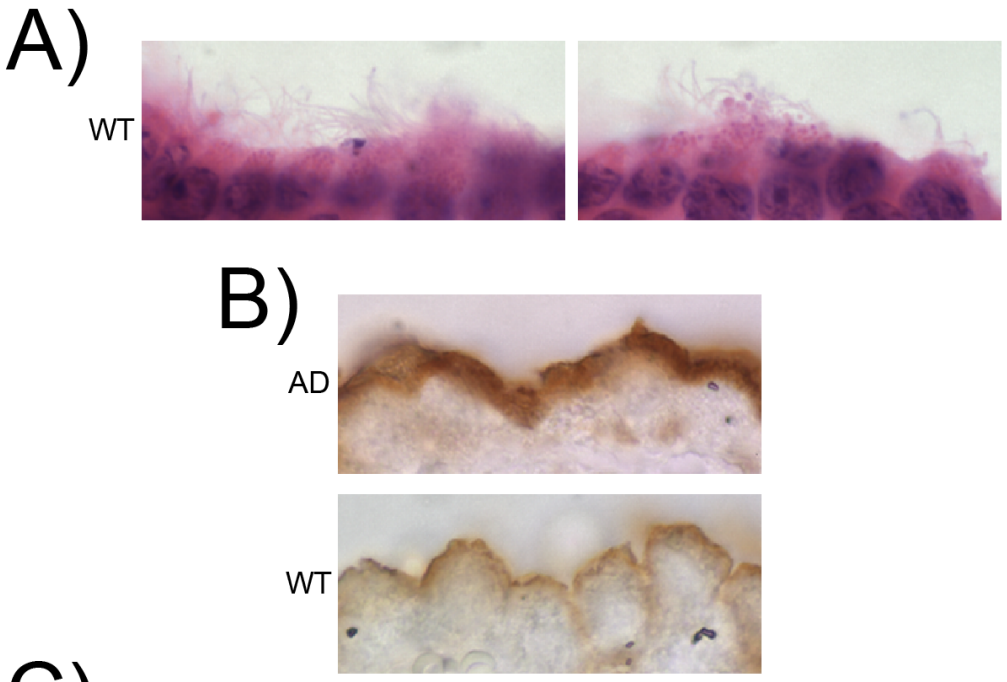
A)
WT
B)
AD
WT
C)
Siglec-F-Fc
AQP1
Merge
AD
WT
D)
Siglec-F : AQP1
Average Intensity
0.15
0.10
0.05
0.00
p=0.001
*
WT
AD

Figure 2.7: Siglec-F-Fc staining is sialidase sensitive

The intense staining pattern observed for Siglec-F-Fc in 5xFAD brains was completely lost when sections were previously treated with sialidase. This obligate requirement of sialic acid is a hallmark of Siglec glycan ligands. When sections are treated with PNGaseF prior to staining there is a large reduction in staining. This highlights that a portion on the ligand is N-linked.

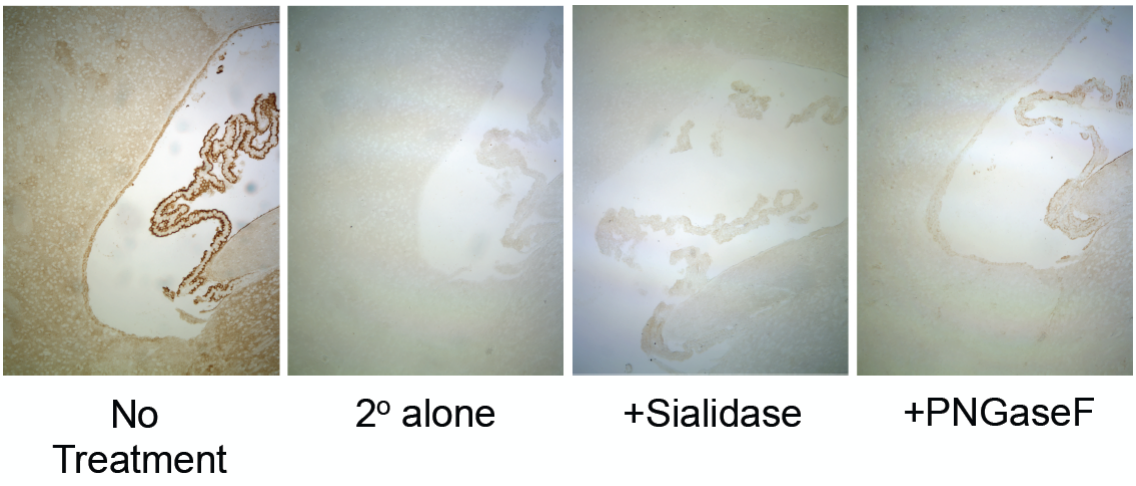

Validation of the identified Siglec-F ligand

The endogenous glycan ligands for Siglec-F in any tissue have been resistant to complete structural characterization, but are clearly distinct from the targets identified by various in vitro approaches, such as glycan binding arrays (Tateno et al. 2005; Patnode et al. 2013). Proposed epitopes for Siglec-F recognition are sialylated, sulfated glycans. However, recent reports show bi-, tri-, and quatra-antennary N-glycans that are not sulfated to be efficient ligands (Yu et al. 2017). To further define the endogenous ligand in this murine model, whole brain lysates were used for western blot analysis. Binding above the 250-kD marker covers a large area with a smeared appearance commonly associated with glycosylated proteins (**Figure 2.8A**). There doesn't appear to be any difference in band intensity between AD and control whole brain lysates, indicating that the differences detected at the ChP epithelium reflect cell type specific changes in glycan expression. PNGaseF treatment of whole brain lysates suggests that a larger portion of the ligand is N-linked in AD brains than in wildtype (**Figure 2.8B**). To further elucidate the sialic acid linkage, whole brain lysates were either treated with pan- or α2-3 specific sialidase prior to western blot analysis. Siglec-F binding was abolished following pan-sialidase treatment, whereas binding was partially lost after treatment with α2-3 specific sialidase indicating the ligand is mostly comprised of α2-3 linked sialic acid residues (**Figure 2.8B**). For validation purposes, we used the lectins MAA and SNA based on their preferences to recognize α2-3 and α2-6 linked sialic acid residues respectively (**Figure 4.4**). The linkage analysis is consistent with previous work

showing St3gal3 is required for ligand production in mouse lung tissue (Guo et al. 2011). To elucidate if sulfation has an impact on Siglec-F binding, solvolysis was performed on whole brain lysates. Upon solvolysis, a reduction in the dispersed smear appearance and a more discrete band was observed suggesting that sulfation isn't a requirement but does produce additional ligands (**Figure 2.8B**).

Identification of counter-receptors for Siglec-F

Epitopes that are ligands for an innate immune receptor, Siglec-F, are increased on the apical surface of the choroid plexus. Identification of the glycoprotein counter-receptors that carry these glycans would provide novel targets for regulating interactions between inflammatory cells and the ChP. Immunoprecipitation of cognate proteins bearing these epitopes was done using Siglec-F-Fc prior to in-gel proteomic identification via LC-MS/MS. Two proteins within the mass range of >250-kD were identified: low-density lipoprotein receptor-related protein 1 (LRP1) and Versican (VC) (**Figure 2.8E**). Initial work was limited to LRP1 since there is a known role in Alzheimer's disease, however, future work will focus on VC. To verify that LRP1 carries the glycan ligand for Siglec-F, we digested whole brain lysate using PNGaseF prior to immunoprecipitation using α-chain LRP1 antibody and visualized by Siglec-F-Fc overlay (**Figure 2.8C**). For both AD and control brains, LRP1 is shown to have 2 major glycoforms above the 250-kD marker. Additionally, whole brain lysate digested with PNGaseF prior to non-reducing PAGE separation and immunoblotting with anti-LRP1 shows two bands for AD while control brains only

show a single band (**Figure 2.8D**). These data indicate that LRP1 is modified with the glycan ligand for Siglec-F and that glycosylation of LRP1 in AD brains is altered. This differential glycosylation is likely the result of altered microheterogeneity and site occupancy and should be verified by site mapping.

Figure 2.8: LRP1 is modified with the ligand for Siglec-F

We used whole brain lysate to investigate the molecular nature of the Siglec-F ligand. Panel (A) shows the presence of Siglec-F binding glycoproteins in whole brain. The major binding component runs as a broad well above the 250-kD marker. Panel (B) demonstrates that PNGaseF treatment reduces Siglec-F recognition of the faster migrating material in AD. Sialidase completely abolishes all binding in both WT & AD while α2-3 Sialidase removes a large amount. Removal of sulfate via solvolysis appears to collapse the smear into a tighter band of higher intensity, demonstrating that sulfate isn't required for binding. To identify the protein(s) modified with this ligand we applied LC-MS/MS to in-gel digested material following Siglec-F-Fc immunoprecipitation (D). LRP1 was identified as a high priority candidate. Panel (C) presents the results of immunoprecipitation with anti-LRP antibody and western blot with Siglec-F-Fc, demonstrating that LRP1 carries ligands for Siglec-F.

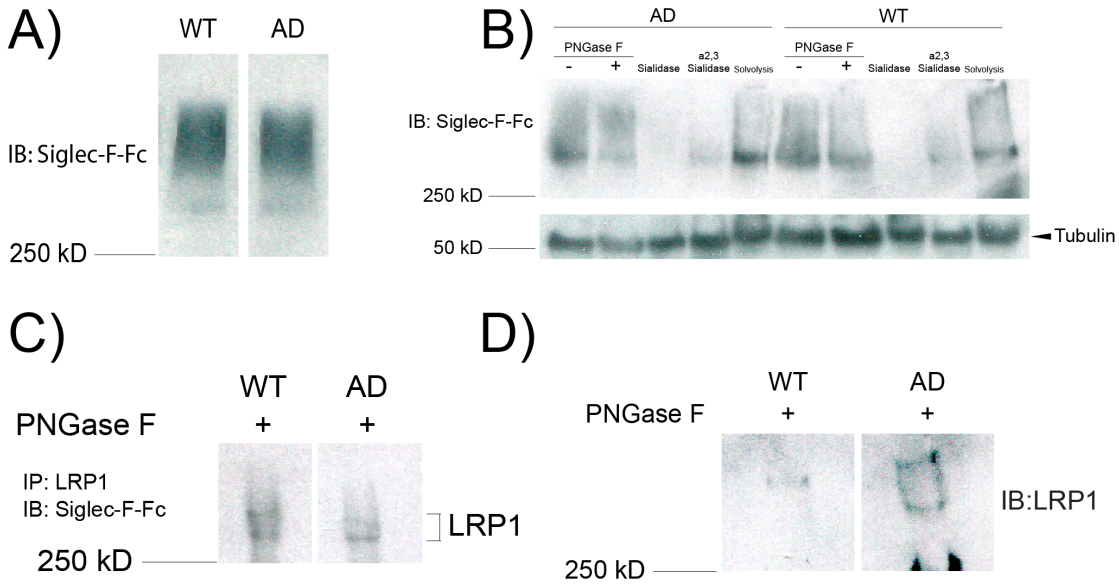

E)

Accession	Description	Score	Coverage	# Proteins	# Unique Peptides	# Peptides	MW [kDa]
A2ASS6	Titin OS=Mus musculus GN=Ttn PE=1 SV=1 - [TITIN_MOUSE]	23.34	9.97	3	1	252	3904.1
Q9QXZ0	Microtubule-actin cross-linking factor 1 OS=Mus musculus GN=Ma	26.04	8.28	4	2	46	831.4
E9Q401	Ryanodine receptor 2 OS=Mus musculus GN=Ryr2 PE=1 SV=1 - [	5.64	11.22	2	1	34	564.5
Q9QYX7	Protein piccolo OS=Mus musculus GN=Pclo PE=1 SV=4 - [PCLO_M	23.13	11.21	1	1	39	550.5
Q9QXS1	Plectin OS=Mus musculus GN=Plec PE=1 SV=3 - [PLEC_MOUSE]	558.13	22.13	2	34	101	533.9
Q9JHU4	Cytoplasmic dynein 1 heavy chain 1 OS=Mus musculus GN=Dync	318.03	17.66	1	19	73	531.7
Q91ZX7	Prolow-density lipoprotein receptor-related protein 1 OS=Mus mus	32.51	27.26	1	4	85	504.4
O88737	Protein bassoon OS=Mus musculus GN=Bsn PE=1 SV=4 - [BSN_M	142.05	11.54	1	8	38	418.6
V9GX34	Protein Csmd2 (Fragment) OS=Mus musculus GN=Csmd2 PE=1 S	40.46	4.82	1	1	9	372.4
Q62059	Versican core protein OS=Mus musculus GN=Vcan PE=1 SV=2 - [	55.16	6.20	6	5	19	366.6

LRP1 and VC expression at the Choroid Plexus

Identification of both LRP1 and VC proteins was done using whole brain lysate, not choroid plexus lysate. Therefore, we used immunofluorescence to determine if they are expressed at the choroid plexus. LRP1 and VC have a similar expression pattern at the interface between the basal surface of the ChP epithelial cells and the endothelial cells of the fenestrated capillaries of the choroid plexus (**Figure 2.9**). Additionally, both proteins show fluorescence throughout the epithelium that is most likely vesicular. This patterning is expected for LRP1 since it is primarily an endocytic receptor. Versican, however, is found in the extracellular matrix and does not have any described role or path in the retrograde pathway.

Figure 2.9: Expression of LRP1 and VC at the Choroid Plexus

Immunofluorescence of both proteins is primarily seen at the basal surface, or endothelial surface of capillaries, of the choroid plexus. Diffuse signal is also seen throughout the cytoplasm of the epithelial cells that is most likely vesicular.

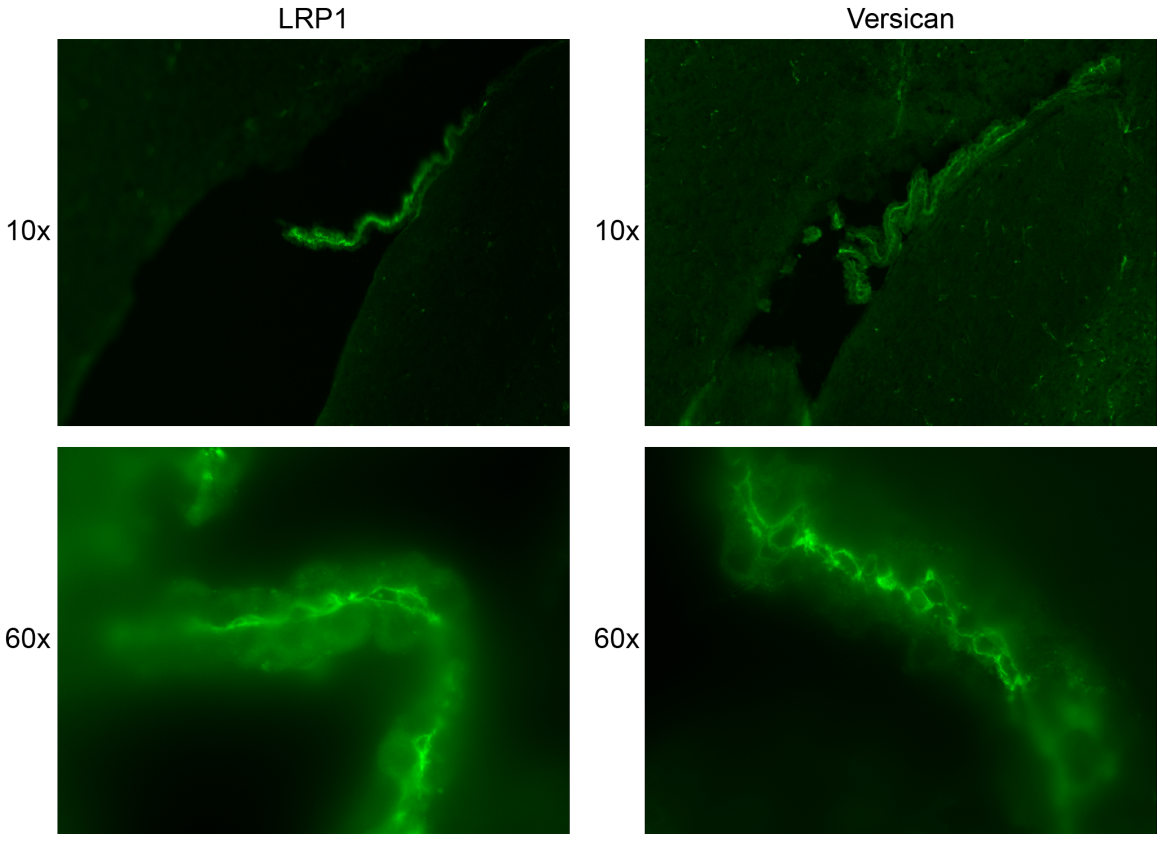

LRP1 expression and localization is altered in AD brains

Confocal analysis of fluorescently labeled LRP1 revealed low levels of expression at the choroid plexus in control brains. In contrast, choroid from AD sections demonstrated a significant increase in LRP1 expression when compared to control brains. The increased expression was almost exclusively on the basal membrane (**Figure 2.10A**); a staining pattern which has been previously reported in rat brain (Kounnas et al. 1994). When AD sections were digested with PNGaseF prior to probing with anti-LRP1 antibody, the expression pattern was augmented; two new pools of protein were detected – one at the apical membrane and a second vesicular pool scattered throughout the cytoplasm. The expression pattern didn't change in the wildtype brain following PNGaseF treatment (**Figure 2.10A**). The total fluorescence observed after PNGaseF treatment in AD sections did slightly increase. Interestingly, the amount of LRP1 at the apical surface after PNGaseF treatment in AD appears to more closely resemble that of untreated WT (**Figure 2.10A**). This doesn't correlate to the changes seen for whole brain lysate where ligands for Siglec-F are reduced in AD brains following PNGaseF treatment (**Figure 2.8B**), and supports the theory of cell type specific glycosylation that is tightly regulated and cell type specific.

To determine if the overall amount of LRP1 is equal between WT and AD we used a second antibody for LRP1 directed towards the 85-kD β-chain and found \differences in fluorescence (**Figure 2.10B**). The clustering of protein at the cytoplasmic surface of the apical membrane in AD is not found in control brains.

We suspect that a larger portion of the protein in the endosomal network is tethered near the apical membrane; however, future work will aim to understand this observation. Overall, our data show that LRP1 is specifically increased at the basal surface of ChP in AD along with an increase of a differentially glycosylated form in vesicles and at the apical surface. This suggests that LRP1 may have different functions at the apical and basal surfaces of ChP.

Figure 2.10: LRP1 expression and localization is altered in AD brains

In wild type sections, but not AD sections, LRP1 is detected at the apical surface of the ChP epithelial cells as small, intense puncta. In AD sections, an intense pool of LRP1 is detected at the basal surface. Very little apical LRP1 is detected in AD unless the section is first treated with PNGaseF, suggesting that the anti-LRP1 epitope is sensitive to glycosylation and, therefore, that LRP1 is alternatively glycosylated in AD. In AD, this shift in the staining pattern indicates the detection of a new pool of LRP1 (marked by white arrows) (A). The expression of LRP1 when probed for the β-chain is more concentrated at the apical surface in AD (B). This result is not fully understood, however, this may be a pool of rapidly endocytosed LRP1 during a signaling event.

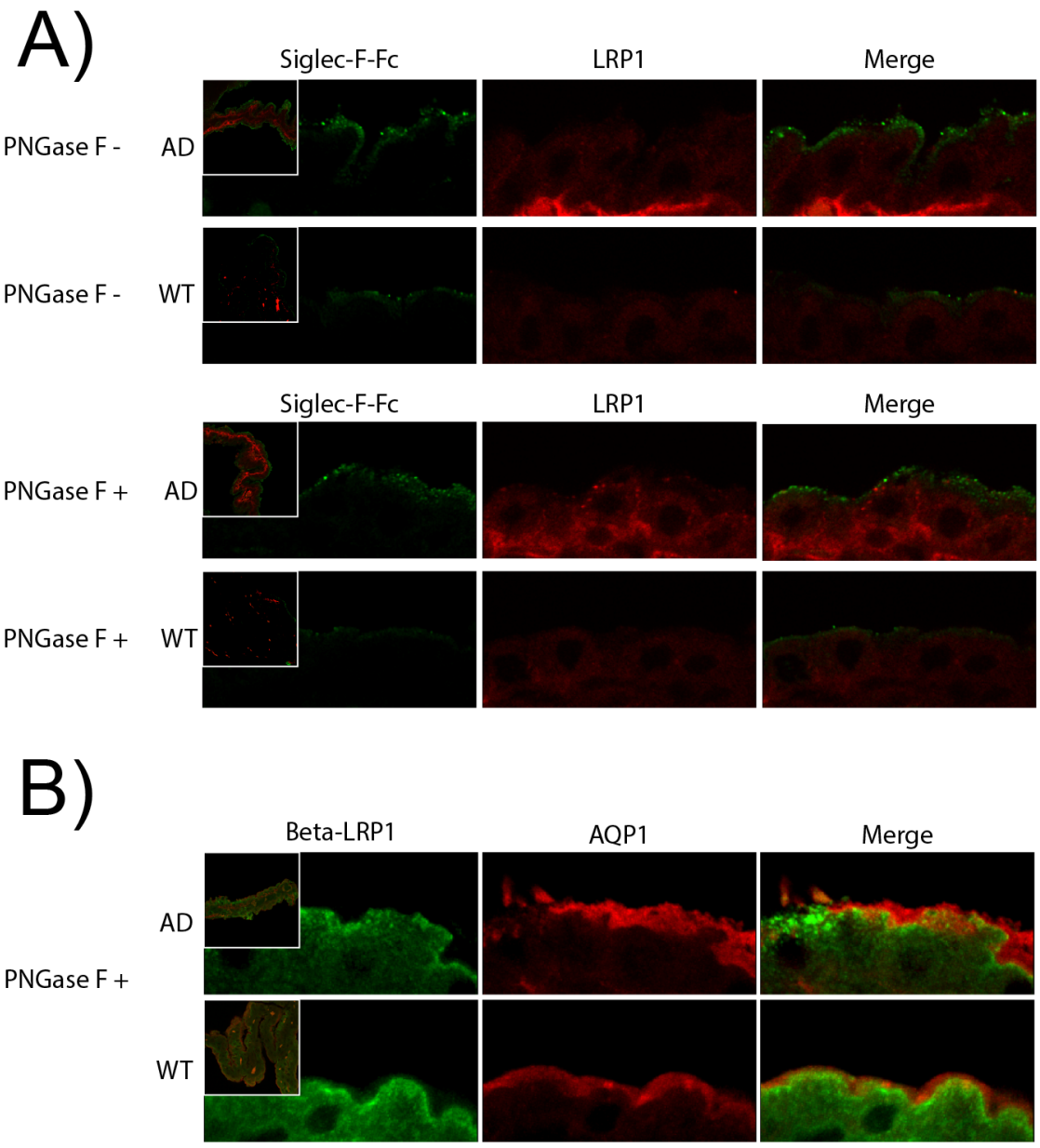
A)
Siglec-F-Fc
LRP1
Merge
PNGase F -
AD
PNGase F -
WT
Siglec-F-Fc
LRP1
Merge
PNGase F +
AD
PNGase F +
WT
B)
Beta-LRP1
AQP1
Merge
AD
PNGase F +
WT

Siglec-F expression on microglia and macrophages

Increased expression of the glycan ligand for Siglec-F at the ChP suggests a potential role for Siglecs in AD. Previous reports of induced Siglec-F expression on microglia due to protein aggregation, induced by injection of a prion forming agent (ME7), suggests a potential role for Siglec-F on microglia in neurodegenerative disease (Lunnon et al. 2011). We first suspected that microglia activated by Aβ plaques would interact with the differentially glycosylated form of LRP1 at the apical surface of ChP. To test this, the microglial marker Iba1 was used to probe WT and AD sections to assess microglia accumulation at the ChP. Iba1 staining demonstrated no change in microglial abundance at the ChP in AD compared to WT. Furthermore, when co-stained for the Siglec-F receptor there wasn't substantial colocalization, suggesting a different cell type is likely to express Siglec-F. Recent reports have demonstrated M2 macrophage migration into the brain through the ChP in response to spinal cord injury (Shechter et al. 2013). To determine if macrophage migration was increased in AD brains we used CD206 as a M2 macrophage specific marker and again inspected the ChP of both WT and AD mice. The ChP of AD mice showed a marked increase in M2 macrophages, which are distinct from brain resident microglia, when compared to WT (**Figure 2.11AB**). The infiltrating M2 macrophages expressing the Siglec-F receptor in the 5xFAD mouse. In both WT and AD brains, occassional puncta are detected at the apical surface of the ChP that are positive for both CD206 and Siglec-F. Additionally, Siglec-F-Fc is co-localized with infiltrating macrophages in AD suggesting that

the Siglec-F glycan ligand could be bound during macrophage migration and provide a gradient of interaction. Our data show that circulating macrophages enter the brain at the ChP in AD mice and express Siglec-F on their surface.

Figure 2.11: Siglec-F expression on macrophages and microglia

We wanted to identify the cell type that bears the receptor, Siglec-F, and is capable of binding the ligand. Panel (A) shows a significant increase in the number of extravasating M2 macrophages (CD206) in AD at the basal surface. These cells also appear to migrate to the apical surface. In WT, Siglec-F is also seen but doesn't appear to be highly expressed by blood derived macrophages. An arrow marks apparent colocalization between Siglec-F and it's glycan ligand. Panel (B) shows that microglia (Iba1) can be distinguished from macrophages.

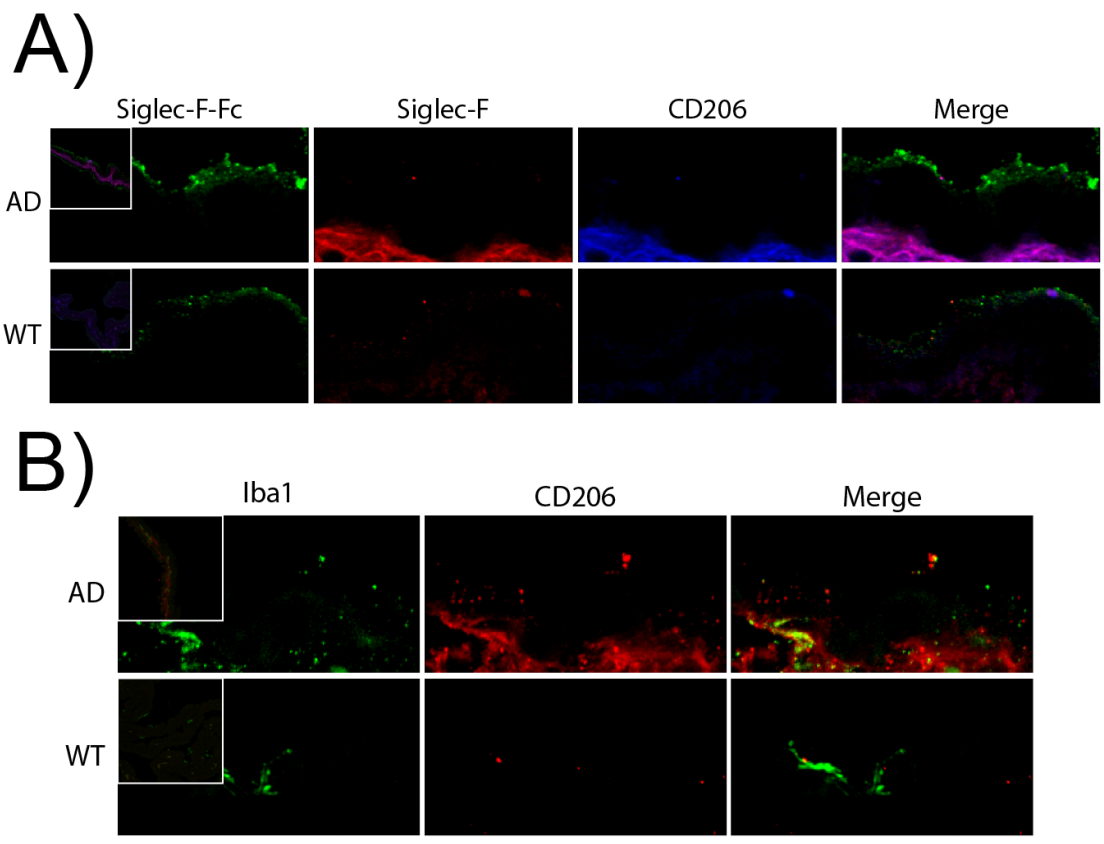

Figure 2.12: Glycosylation at the Choroid Plexus Modulates the Inflammatory Response

We hypothesize that the increase of LRP1 in AD is pleiotropic. First, at the basal surface of the ChP epithelial layer, LRP1 may influence extravasation of macrophages through an interaction with Integrin αmβ2 (Ranganathan et al. 2011). Second, LRP1 has been shown to influence and promote the M2 phenotype (May et al. 2013). Therefore, LRP1 interactions with Siglec-F may influence macrophage phenotype at the ChP, thereby influencing the secretion of anti-inflammatory cytokines into the CSF. In AD tissue, the presentation of altered LRP1 glycoforms on ChP epithelial cells is positioned to influence the survival and behavior of macrophages or other trafficking immune cell types.

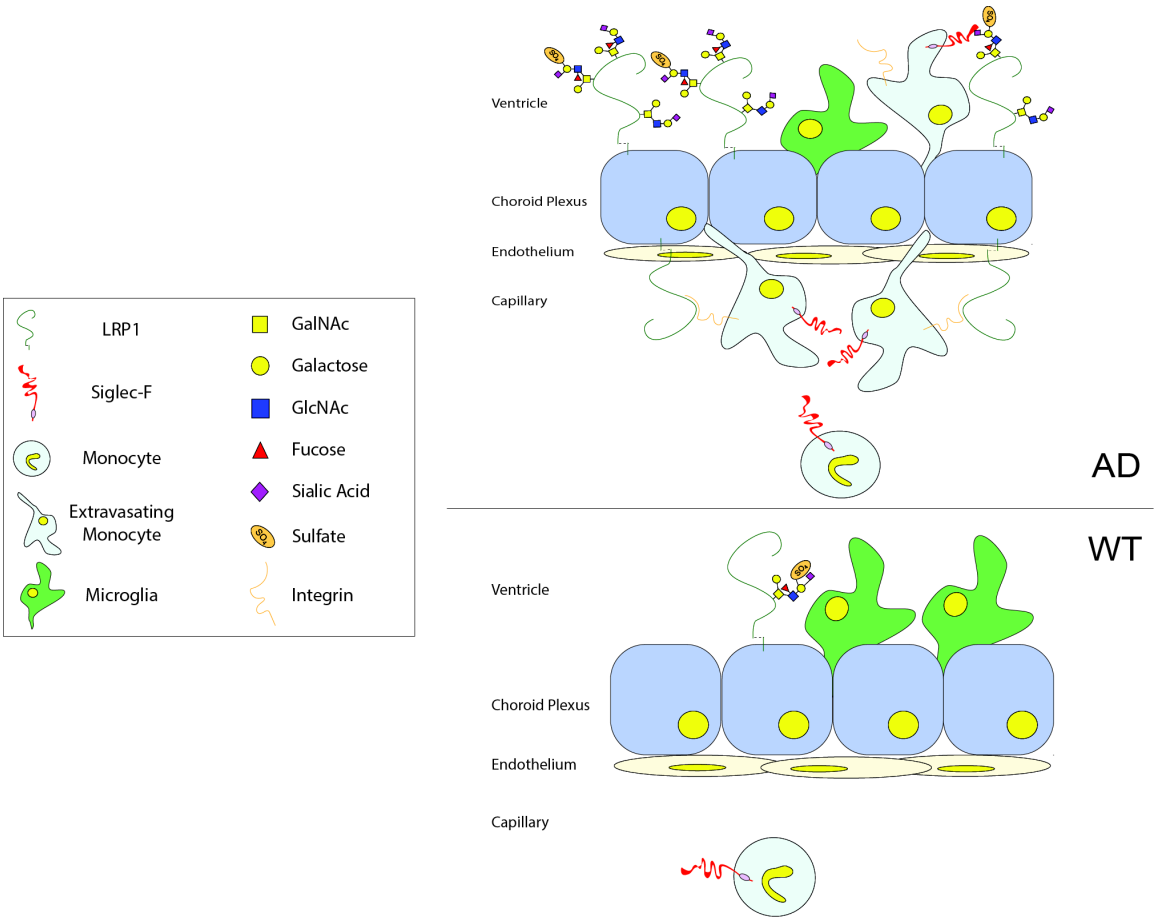

Discussion

A role for SIGLECs in the pathobiochemistry of AD is indicated by the previously published identification of a protective, single nucleotide polymorphism (SNP) in the human gene encoding SIGLEC-3 (CD33) (Griciuc et al. 2013). This SNP reduces expression of SIGLEC-3 on microglia and lowers the levels of insoluble Aβ peptide in the brain, suggesting that SIGLEC-3 normally functions to negatively modulate the Aβ endocytic activity of microglia (Griciuc et al. 2013). Thus, SIGLEC-3 is not the endocytic receptor for Aβ since its reduced expression enhances clearance. But, SIGLEC-3 activation by its own sialoglycan ligand must modulate the capacity of microglial cells to interact with Ab resulting in altered clearance and altered microglial release of neurotoxic cytokines (Kim and de Vellis 2005; Walker and Lue 2005; Heneka et al. 2015). This modulatory activity of SIGLEC-3 implies that the brain glycome, which includes many glycan ligands capable of engaging SIGLEC-3 and various other SIGLEC receptors, influences the inflammatory status of the tissue.

Relatively little data is available to evaluate the extent to which protein and lipid glycosylation may be affected in AD and may, as a consequence, impact the engagement of pro- and anti-inflammatory glycan binding proteins such as SIGLECs (Liu et al. 2004; Robertson et al. 2004; Yuzwa et al. 2012; Palmigiano et al. 2016). Here, we have demonstrated decreased global protein N-linked glycosylation and a concomitant increase in the production of FOS, suggesting decreased efficiency in co-translational glycoprotein glycosylation at the level of the oligosaccharyltransferase in the endoplasmic reticulum. An identical

glycosylation phenotype was reported previously in cells with disrupted Golgi stacking (Xiang et al. 2013). Similar Golgi fragmentation defects have also been reported following exposure of cultured primary neurons to Ab and in CNS neurons of AD mouse models (Joshi et al. 2014). Thus, glycoprotein glycosylation and secretory pathway integrity are both impacted in AD models, leading to cell surface glyco-terrain alterations that can impact tissue homeostasis.

Our glycomic characterization of AD and control mouse brains identified several glycan topologies that are recognized by SIGLEC proteins (Macauley et al. 2014). Thus, the significant increase of sialidase-sensitive, SIGLEC-F ligands at the choroid plexus was likely undetected in our whole brain glycomics due to dilution by the greater abundance of non-choroid glycans. Targeted choroid plexus glycomics is technically challenging, especially in mouse, but will be required to achieve informative insights into the exact structural nature of the recognized epitopes. Nonetheless, some structural features of the SIGLEC-F glycan ligands can be inferred from the data available currently. The recognized glycans are found as both N-linked and O-linked structures. In both cases, sialic acid is required and is predominantly in α2-3 linkage. Sulfation is not essential for SIGLEC-F recognition, as has also been shown in other tissues (Kiwamoto et al. 2015). While glycan structural topologies capable of interacting with SIGLEC-F may be presented on many different proteins, the most potent ligands may be restricted to a subset of cell types or proteins. These data are supported by lectin binding profiles for MAA and SNA. While no differences are detected for SNA

binding at the apical surface of the ChP, MAA lectin staining is quite different in wildtype and 5xFAD ChP. First, larger and more frequent patches of MAA binding are detected at the apical surface of ChP epithelial cells in AD brains compared to control brains. Second, the ChP epithelial cells in the 5xFAD are characterized by increased intracellular staining of apparently aberrant Golgi-like structures. Similar changes in the Golgi apparatus have been previously reported (Xiang et al. 2013; Joshi et al. 2014).

To identify the relevant protein counter-receptors that carry SIGLEC-F glycan ligands, we used SIGLEC-F-Fc chimeric probes to immunoprecipitate candidate counter-receptors from brain extracts. Proteomic characterization by LC-MS/MS of the precipitated proteins identified Versican and LRP1 as counter-receptor proteins that carry glycan ligands for SIGLEC-F. Based on its previous characterization as a clearance receptor that moves Ab–APOE complexes across the blood-brain and CSF-blood barriers and on its ability to modulate signaling pathways, we chose to focus on LRP1, but also investigated the expression of VC in the 5xFAD mouse (Fujiyoshi et al. 2011; Kanekiyo and Bu 2014). LRP1 is broadly expressed in many tissues but is highest in lung, liver, and brain (Kanekiyo and Bu 2014). LRP1 expression is altered in AD and may exhibit differential changes in specific cell types and brain regions (Businaro et al. 1997; Kang et al. 2000; Arelin et al. 2002; Hartz et al. 2010; Kanekiyo and Bu 2014; Gonzalez-Marrero et al. 2015).

LRP1 is synthesized as a 600-kD protein that is cleaved by furin into a 515-kD α-chain and a non-covalently associated 85-kD transmembrane β-chain

(Bu 2009). The extracellular domain of LRP1 is highly glycosylated, containing 52 consensus sites for N-linked glycosylation and multiple O-glycan additions (Van Leuven et al. 1993). Our initial attempts to immunoprecipitate SIGLEC-F-Fc binding activity with an anti-LRP antibody (8G1) were unsuccessful, most likely due to epitope shielding by one or more N-linked glycans near the amino terminus of the protein, the polypeptide region against which the antibody was raised (Strickland et al. 1990). Consistent with glycan-based epitope shielding, pre-treatment of brain extract with PNGaseF allowed the anti-LRP antibody to immunoprecipitate proteins that were subseqeuntly recognized by immunoblot with SIGLEC-F-Fc. Thus, in both wildtype and AD brain extracts, SIGLEC-F-Fc immunoprecipitated high molecular weight material that was identified as LRP1 by LC-MS/MS and anti-LRP1 antibody immunoprecipitated high molecular weight material that was recognized by SIGLEC-F-Fc.

Two results presented here indicate that LRP1 is structurally different in AD compared to wildtype brain. First, the SDS-PAGE migration of the PNGaseF digested material is different for material from AD than from wildtype brain by anti-LRP1, indicating altered protein modification in AD. Second, immunodetection of LRP1 in the AD mouse brain revealed a dominant pool of LRP1 located at the basal surface of the ChP epithelial cells that was not detected in wildtype. In wildtype, anti-LRP1 immunoreactivity was primarily detected in apical punctae at the ChP, similar in appearance and occassionally overlapping with SIGLEC-F-Fc binding activity. This apical pool was not detected in the ChP cells of AD brains. However, PNGaseF treatment of AD tissue

sections revealed a latent pool of apically localized LRP1, indicating the existence of an alternative glycoform of LRP1 at the ChP in AD brain. Thus, differently localized and alternatively glycosylated LRP1 is a characteristic of ChP epithelial cells in AD.

While our data supports designating LRP1 as a SIGLEC-F counter receptor in the mouse brain, it also indicates LRP1 is not the only protein capable of interacting with SIGLEC-F. Further attention should be focused on versican, for instance, and SIGLEC-F-Fc pull-downs directly from ChP extracts would be extremely valuable in understanding the diversity of glycoproteins that may serve as SIGLEC-F counter receptors in AD and control brains. However, the substantial accumulation of LRP1 on the basal surface of ChP epithelial cells in the AD mice implies a disease-specific alteration in LRP1 function. Furthermore, that this pool of LRP1 is not recognized by SIGLEC-F indicates different glycoforms of LRP1 subserve specific functions within specific epithelial domains at the ChP.

At the basal surface, the ChP epithelial layer comprises a major point of intersection between the immune system and the brain (Meeker et al. 2012; Lehtinen et al. 2013). It is at this intersection that bone marrow derived macrophages extravasate from the circulation to enter the CSF (Shechter et al. 2013). At the basal surface, where SIGLEC-F ligands are not detected in AD or control ChP, the localized increase in LRP1 glycoforms in AD may support the recruitment of circulating macrophages. This activity for LRP1 has been reported previously and takes advantage of interactions with integrin $\alpha_M\beta_2$ and promotes

the differentiation of M2, anti-inflammatory macrophage phenotypes (Ranganathan et al. 2011; May et al. 2013). Here we show that macrophage infiltration of the ChP is upregulated in AD. These cells have the capacity to become either pro- or anti-inflammatory depending on the signals they receive along the migration route they undertake. The migration of monocytes through the ChP involves a unique set of homing proteins including integrin VLA-4-VCAM1 and potentially CCR6-CCL20 (Shechter et al. 2013). Migration mediated by these receptors appears to prime monocytes towards M2 differentiation (May et al. 2013). The macrophages that we detect accumulating in the ChP of AD brains are of the M2, anti-inflammatory phenotype and express SIGLEC-F, although SIGLEC-F glycans are not detected at the basal surface of the ChP epithelial cells.

We detect significant increases in SIGLEC-F ligand expression at the apical surface of ChP epithelial cells in AD. The apical surface of ChP cells secrete cerebral spinal fluid (CSF) as well as growth factors, morphogens, and essential metabolites that modulate neural function and neural stem cell niche activity. To this list of important modulatory activities, we now add the expression of glycan ligands that are capable of modulating inflammatory cell activation. In particular, increased SIGLEC-F ligand expression on ChP epithelial cells provides a mechanism for influencing extravasating macrophage activation. Siglec-F is generally expressed on murine eosinophils and alveolar macrophages, inducible on microglia and T cells, and signals for apoptosis when engaged to its ligand in eosinophilic asthma models but also provides other anti-

inflammatory signals, such as secretion of anti-inflammatory cytokines, and internalization of *Neisseria meningitides* (Stevens et al. 2007; Tateno et al. 2007; Zhang et al. 2007; Lunnon et al. 2011; Suzukawa et al. 2013; Kiwamoto et al. 2015).

Based on our experimental observations, we propose that LRP1 glycoforms at the basal surface of ChP epithelial cells facilitate the recruitment of macrophages into the ChP stroma and promote anti-inflammatory M2 differentiation. Furthermore, we propose that apical glycoforms of LRP1 carrying SIGLEC-F ligands reinforce this anti-inflammatory phenotype by enhancing the secretion of anti-inflammatory cytokines and other yet-to-be-identified factors from the recruited M2 macrophages into the CSF (**Figure 2.12**). Therefore, in the aggressive 5xFAD mouse model, we propose that upregulation of SIGLEC-F ligand expression is a compensatory mechanism by which ChP epithelial cells attempt to enhance anti-inflammatory responses, albeit with insufficient efficacy in regards to limiting the progression of neuropathology in the face of massive Ab deposition. The 5xFAD model has highlighted previoulsy unappreciated plasticity in brain glycan expression and unexpected dynamics in anti-inflammatory glycan expression at the ChP in an extreme degenerative neural disorder.

References

Aoki, K., Perlman, M., Lim, J.M., Cantu, R., Wells, L. and Tiemeyer, M. (2007). "Dynamic developmental elaboration of N-linked glycan complexity in the Drosophila melanogaster embryo." J Biol Chem **282**(12): 9127-9142.

Aoki, K., Porterfield, M., Lee, S.S., Dong, B., Nguyen, K., McGlamry, K.H. and Tiemeyer, M. (2008). "The diversity of O-linked glycans expressed during Drosophila melanogaster development reflects stage- and tissue-specific requirements for cell signaling." J Biol Chem **283**(44): 30385-30400.

Arelin, K., Kinoshita, A., Whelan, C.M., Irizarry, M.C., Rebeck, G.W., Strickland, D.K. and Hyman, B.T. (2002). "LRP and senile plaques in Alzheimer's disease: colocalization with apolipoprotein E and with activated astrocytes." Brain Res Mol Brain Res **104**(1): 38-46.

Baruch, K., Ron-Harel, N., Gal, H., Deczkowska, A., Shifrut, E., Ndifon, W., Mirlas-Neisberg, N., Cardon, M., Vaknin, I., Cahalon, L., Berkutzki, T., Mattson, M.P., Gomez-Pinilla, F., Friedman, N. and Schwartz, M. (2013). "CNS-specific immunity at the choroid plexus shifts toward destructive Th2 inflammation in brain aging." Proc Natl Acad Sci U S A **110**(6): 2264-2269.

Boccuto, L., Aoki, K., Flanagan-Steet, H., Chen, C.F., Fan, X., Bartel, F., Petukh, M., Pittman, A., Saul, R., Chaubey, A., Alexov, E., Tiemeyer, M., Steet, R. and Schwartz, C.E. (2014). "A mutation in a ganglioside biosynthetic enzyme, ST3GAL5, results in salt & pepper syndrome, a neurocutaneous disorder with altered glycolipid and glycoprotein glycosylation." Hum Mol Genet **23**(2): 418-433.

Bochner, B.S. (2009). "Siglec-8 on human eosinophils and mast cells, and Siglec-F on murine eosinophils, are functionally related inhibitory receptors." Clin Exp Allergy **39**: 317-324.

Bu, G. (2009). "Apolipoprotein E and its receptors in Alzheimer's disease: pathways, pathogenesis and therapy." Nat Rev Neurosci **10**(5): 333-344.

Businaro, R., Fabrizi, C., Persichini, T., Starace, G., Ennas, M.G., Fumagalli, L. and Lauro, G.M. (1997). "Modulation of the alpha 2 macroglobulin receptor/low density lipoprotein receptor related protein by interferon-gamma in human astroglial cells." J Neuroimmunol **72**(1): 75-81.

Crocker, P.R., Paulson, J.C. and Varki, A. (2007). "Siglecs and their roles in the immune system." Nat Rev Immunol **7**(4): 255-266.

Cronk, J.C. and Kipnis, J. (2013). "Microglia - the brain's busy bees." F1000Prime Rep **5**: 53.

Eimer, W.A. and Vassar, R. (2013). "Neuron loss in the 5XFAD mouse model of Alzheimer's disease correlates with intraneuronal Abeta42 accumulation and Caspase-3 activation." Mol Neurodegener **8**: 2.

Fujiyoshi, M., Tachikawa, M., Ohtsuki, S., Ito, S., Uchida, Y., Akanuma, S., Kamiie, J., Hashimoto, T., Hosoya, K., Iwatsubo, T. and Terasaki, T. (2011). "Amyloid-beta peptide(1-40) elimination from cerebrospinal fluid involves low-density lipoprotein receptor-related protein 1 at the blood-cerebrospinal fluid barrier." J Neurochem **118**(3): 407-415.

Gonzalez-Marrero, I., Gimenez-Llort, L., Johanson, C.E., Carmona-Calero, E.M., Castaneyra-Ruiz, L., Brito-Armas, J.M., Castaneyra-Perdomo, A. and Castro-Fuentes, R. (2015). "Choroid plexus dysfunction impairs beta-amyloid clearance in a triple transgenic mouse model of Alzheimer's disease." Front Cell Neurosci **9**: 17.

Griciuc, A., Serrano-Pozo, A., Parrado, A.R., Lesinski, A.N., Asselin, C.N., Mullin, K., Hooli, B., Choi, S.H., Hyman, B.T. and Tanzi, R.E. (2013). "Alzheimer's Disease Risk Gene CD33 Inhibits Microglial Uptake of Amyloid Beta." Neuron.

Guo, J.P., Brummet, M.E., Myers, A.C., Na, H.J., Rowland, E., Schnaar, R.L., Zheng, T., Zhu, Z. and Bochner, B.S. (2011). "Characterization of Expression of Gylcan Ligands for Siglec-F in Normal Mouse Lungs." Am J Respir Cell and Molec Biol **44**: 238-243.

Hartz, A.M., Miller, D.S. and Bauer, B. (2010). "Restoring blood-brain barrier P-glycoprotein reduces brain amyloid-beta in a mouse model of Alzheimer's disease." Mol Pharmacol **77**(5): 715-723.

Heneka, M.T., Carson, M.J., El Khoury, J., Landreth, G.E., Brosseron, F., Feinstein, D.L., Jacobs, A.H., Wyss-Coray, T., Vitorica, J., Ransohoff, R.M., Herrup, K., Frautschy, S.A., Finsen, B., Brown, G.C., Verkhratsky, A., Yamanaka, K., Koistinaho, J., Latz, E., Halle, A., Petzold, G.C., Town, T., Morgan, D., Shinohara, M.L., Perry, V.H., Holmes, C., Bazan, N.G., Brooks, D.J., Hunot, S., Joseph, B., Deigendesch, N., Garaschuk, O., Boddeke, E., Dinarello, C.A., Breitner, J.C., Cole, G.M., Golenbock, D.T. and Kummer, M.P. (2015). "Neuroinflammation in Alzheimer's disease." Lancet Neurol **14**(4): 388-405.

Itagaki, S., McGeer, P.L., Akiyama, H., Zhu, S. and Selkoe, D. (1989). "Relationship of microglia and astrocytes to amyloid deposits of Alzheimer disease." J Neuroimmunol **24**(3): 173-182.

Joshi, G., Chi, Y., Huang, Z. and Wang, Y. (2014). "Abeta-induced Golgi fragmentation in Alzheimer's disease enhances Abeta production." Proc Natl Acad Sci U S A **111**(13): E1230-1239.

Kanekiyo, T. and Bu, G. (2014). "The low-density lipoprotein receptor-related protein 1 and amyloid-beta clearance in Alzheimer's disease." Front Aging Neurosci **6**: 93.

Kang, D.E., Pietrzik, C.U., Baum, L., Chevallier, N., Merriam, D.E., Kounnas, M.Z., Wagner, S.L., Troncoso, J.C., Kawas, C.H., Katzman, R. and Koo, E.H. (2000). "Modulation of amyloid beta-protein clearance and Alzheimer's disease susceptibility by the LDL receptor-related protein pathway." J Clin Invest **106**(9): 1159-1166.

Kawasaki, N., Rademacher, C. and Paulson, J.C. (2010). "CD22 regulates adaptive and innate immune responses of B cells." J Innate Immun **3**(4): 411-419.

Kelm, S., Pelz, A., Schauer, R., Filbin, M.T., Tang, S., de Bellard, M.E., Schnaar, R.L., Mahoney, J.A., Hartnell, A., Bradfield, P. and et al. (1994). "Sialoadhesin, myelin-associated glycoprotein and CD22 define a new family of sialic acid-dependent adhesion molecules of the immunoglobulin superfamily." Curr Biol **4**(11): 965-972.

Kim, S.U. and de Vellis, J. (2005). "Microglia in health and disease." J Neurosci Res **81**(3): 302-313.

Kiwamoto, T., Katoh, T., Evans, C.M., Janssen, W.J., Brummet, M.E., Hudson, S.A., Zhu, Z., Tiemeyer, M. and Bochner, B.S. (2015). "Endogenous airway mucins carry glycans that bind Siglec-F and induce eosinophil apoptosis." J Allergy Clin Immunol **135**(5): 1329-1340 e1321-1329.

Kounnas, M.Z., Haudenschild, C.C., Strickland, D.K. and Argraves, W.S. (1994). "Immunological localization of glycoprotein 330, low density lipoprotein receptor related protein and 39 kDa receptor associated protein in embryonic mouse tissues." In Vivo **8**(3): 343-351.

Lehtinen, M.K., Bjornsson, C.S., Dymecki, S.M., Gilbertson, R.J., Holtzman, D.M. and Monuki, E.S. (2013). "The choroid plexus and cerebrospinal fluid: emerging roles in development, disease, and therapy." J Neurosci **33**(45): 17553-17559.

Li, M., Shang, D.S., Zhao, W.D., Tian, L., Li, B., Fang, W.G., Zhu, L., Man, S.M. and Chen, Y.H. (2009). "Amyloid beta interaction with receptor for advanced glycation end products up-regulates brain endothelial CCR5 expression and promotes T cells crossing the blood-brain barrier." J Immunol **182**(9): 5778-5788.

Liu, F., Iqbal, K., Grundke-Iqbal, I., Hart, G.W. and Gong, C.X. (2004). "O-GlcNAcylation regulates phosphorylation of tau: a mechanism involved in Alzheimer's disease." Proc Natl Acad Sci U S A **101**(29): 10804-10809.

Lunnon, K., Teeling, J.L., Tutt, A.L., Cragg, M.S., Glennie, M.J. and Perry, V.H. (2011). "Systemic inflammation modulates Fc receptor expression on microglia during chronic neurodegeneration." J Immunol **186**(12): 7215-7224.

Macauley, M.S., Crocker, P.R. and Paulson, J.C. (2014). "Siglec-mediated regulation of immune cell function in disease." Nat Rev Immunol **14**(10): 653-666.

May, P., Bock, H.H. and Nofer, J.R. (2013). "Low density receptor-related protein 1 (LRP1) promotes anti-inflammatory phenotype in murine macrophages." Cell Tissue Res **354**(3): 887-889.

McMillan, S.J., Sharma, R.S., Richards, H.E., Hegde, V. and Crocker, P.R. (2014). "Siglec-E Promotes beta2-Integrin-dependent NADPH Oxidase

Activation to Suppress Neutrophil Recruitment to the Lung." J Biol Chem **289**(29): 20370-20376.

Meeker, R.B., Williams, K., Killebrew, D.A. and Hudson, L.C. (2012). "Cell trafficking through the choroid plexus." Cell Adh Migr **6**(5): 390-396.

Mehta, N., Porterfield, M., Struwe, W.B., Heiss, C., Azadi, P., Rudd, P.M., Tiemeyer, M. and Aoki, K. (2016). "Mass Spectrometric Quantification of N-Linked Glycans by Reference to Exogenous Standards." J Proteome Res **15**(9): 2969-2980.

Oakley, H., Cole, S.L., Logan, S., Maus, E., Shao, P., Craft, J., Guillozet-Bongaarts, A., Ohno, M., Disterhoft, J., Van Eldik, L., Berry, R. and Vassar, R. (2006). "Intraneuronal beta-amyloid aggregates, neurodegeneration, and neuron loss in transgenic mice with five familial Alzheimer's disease mutations: potential factors in amyloid plaque formation." J Neurosci **26**(40): 10129-10140.

Palmigiano, A., Barone, R., Sturiale, L., Sanfilippo, C., Bua, R.O., Romeo, D.A., Messina, A., Capuana, M.L., Maci, T., Le Pira, F., Zappia, M. and Garozzo, D. (2016). "CSF N-glycoproteomics for early diagnosis in Alzheimer's disease." J Proteomics **131**: 29-37.

Patnode, M.L., Cheng, C.W., Chou, C.C., Singer, M.S., Elin, M.S., Uchimura, K., Crocker, P.R., Khoo, K.H. and Rosen, S.D. (2013). "Galactose 6-o-sulfotransferases are not required for the generation of siglec-f ligands in leukocytes or lung tissue." J Biol Chem **288**(37): 26533-26545.

Ranganathan, S., Cao, C., Catania, J., Migliorini, M., Zhang, L. and Strickland, D.K. (2011). "Molecular basis for the interaction of low density lipoprotein receptor-related protein 1 (LRP1) with integrin alphaMbeta2: identification of binding sites within alphaMbeta2 for LRP1." J Biol Chem **286**(35): 30535-30541.

Ransohoff, R.M., Kivisakk, P. and Kidd, G. (2003). "Three or more routes for leukocyte migration into the central nervous system." Nat Rev Immunol **3**(7): 569-581.

Robertson, L.A., Moya, K.L. and Breen, K.C. (2004). "The potential role of tau protein O-glycosylation in Alzheimer's disease." J Alzheimers Dis **6**(5): 489-495.

Shechter, R., Miller, O., Yovel, G., Rosenzweig, N., London, A., Ruckh, J., Kim, K.W., Klein, E., Kalchenko, V., Bendel, P., Lira, S.A., Jung, S. and Schwartz, M. (2013). "Recruitment of beneficial M2 macrophages to injured spinal cord is orchestrated by remote brain choroid plexus." Immunity **38**(3): 555-569.

Stevens, W.W., Kim, T.S., Pujanauski, L.M., Hao, X. and Braciale, T.J. (2007). "Detection and quantitation of eosinophils in the murine respiratory tract by flow cytometry." J Immunol Methods **327**(1-2): 63-74.

Strickland, D.K., Ashcom, J.D., Williams, S., Burgess, W.H., Migliorini, M. and Argraves, W.S. (1990). "Sequence identity between the alpha 2-macroglobulin receptor and low density lipoprotein receptor-related protein suggests that this molecule is a multifunctional receptor." J Biol Chem **265**(29): 17401-17404.

Suzukawa, M., Miller, M., Rosenthal, P., Cho, J.Y., Doherty, T.A., Varki, A. and Broide, D. (2013). "Sialyltransferase ST3Gal-III regulates Siglec-F ligand formation and eosinophilic lung inflammation in mice." J Immunol **190**(12): 5939-5948.

Tateno, H., Crocker, P.R. and Paulson, J.C. (2005). "Mouse Siglec-F and human Siglec-8 are functionally convergent paralogs that are selectively expressed on eosinophils and recognize 6-sulfo-sialyl Lewis X as a preferred glycan ligand." Glycobiology **15**: 1125-1135.

Tateno, H., Li, H., Schur, M.J., Bovin, N., Crocker, P.R., Wakarchuk, W.W. and Paulson, J.C. (2007). "Distinct endocytic mechanisms of CD22 (Siglec-2) and Siglec-F reflect roles in cell signaling and innate immunity." Mol Cell Biol **27**(16): 5699-5710.

Van Leuven, F., Stas, L., Raymakers, L., Overbergh, L., De Strooper, B., Hilliker, C., Lorent, K., Fias, E., Umans, L., Torrekens, S. and et al. (1993). "Molecular cloning and sequencing of the murine alpha-2-macroglobulin receptor cDNA." Biochim Biophys Acta **1173**(1): 71-74.

Vyas, A.A., Patel, H.V., Fromholt, S.E., Heffer-Lauc, M., Vyas, K.A., Dang, J., Schachner, M. and Schnaar, R.L. (2002). "Gangliosides are functional nerve cell ligands for myelin-associated glycoprotein (MAG), an inhibitor of nerve regeneration." Proc Natl Acad Sci U S A **99**(12): 8412-8417.

Walker, D.G. and Lue, L.F. (2005). "Investigations with cultured human microglia on pathogenic mechanisms of Alzheimer's disease and other neurodegenerative diseases." J Neurosci Res **81**(3): 412-425.

Xiang, Y., Zhang, X., Nix, D.B., Katoh, T., Aoki, K., Tiemeyer, M. and Wang, Y. (2013). "Regulation of protein glycosylation and sorting by the Golgi matrix proteins GRASP55/65." Nat Commun **4**: 1659.

Yan, S.D., Chen, X., Fu, J., Chen, M., Zhu, H., Roher, A., Slattery, T., Zhao, L., Nagashima, M., Morser, J., Migheli, A., Nawroth, P., Stern, D. and Schmidt, A.M. (1996). "RAGE and amyloid-beta peptide neurotoxicity in Alzheimer's disease." Nature **382**(6593): 685-691.

Yan, S.D., Stern, D., Kane, M.D., Kuo, Y.M., Lampert, H.C. and Roher, A.E. (1998). "RAGE-Abeta interactions in the pathophysiology of Alzheimer's disease." Restor Neurol Neurosci **12**(2-3): 167-173.

Yu, H., Gonzalez-Gil, A., Wei, Y., Fernandes, S.M., Porell, R.N., Vajn, K., Paulson, J.C., Nycholat, C.M. and Schnaar, R.L. (2017). "Siglec-8 and Siglec-9 binding specificities and endogenous airway ligand distributions and properties." Glycobiology.

Yuzwa, S.A., Shan, X., Macauley, M.S., Clark, T., Skorobogatko, Y., Vosseller, K. and Vocadlo, D.J. (2012). "Increasing O-GlcNAc slows neurodegeneration and stabilizes tau against aggregation." Nat Chem Biol **8**(4): 393-399.

Zhang, M., Angata, T., Cho, J.Y., Miller, M., Broide, D.H. and Varki, A. (2007). "Defining the in vivo function of Siglec-F, a CD33-related Siglec expressed on mouse eosinophils." Blood **109**(10): 4280-4287.

CHAPTER 3

GLYCOSYLATION OF DIFFERENTIATING NHBE CELLS IN ALI CULTURE[1]

Nix, David B.[1], Krunkosky, Thomas, Krause, Duncan, Tiemeyer, Michael To be submitted to J. Biol. Sci

Abstract

Human bronchial epithelium is subject to constant assault by pathogens and allergens. These challenges can be assessed directly using an Air-Liquid Interface (ALI) culture method for normal human bronchial epithelium (NHBE). NHBE cells are generated from bronchial explants through enzymatic digestion of the tissue followed by removal of fibroblasts. The resulting cells can be seeded onto a coated well insert and monitored for morphological changes and response to challenges. This culture method for airway tissue has been used to describe changes in electrical resistance and the associated transcellular molecule transport, response to pathogens, and ability to heal following wounding. Using this method we determined the changes in glycosylation over a 43-day differentiation of NHBE cells using nanoelectrospray mass spectrometry. We observed an increase in glycoprotein glycosylation as the cells differentiate showing a general trend for most categories of N- and O-glycans. Sulfation of O-glycans is detectable after 10 days ALI that increases in abundance and diversity by day 43. Glycosphingolipid (GSL) profile is dominated by the neutral Globo series with a decrease in the ganglio series over time. Additionally, we see a dramatic increase at day 43 for anti-inflammatory glycan epitopes capable of binding innate immune receptors that are a mixture of α2-3 and α2-6 linked sialic acids.

KEY WORDS: NHBE, glycosylation, airway, bronchus

Introduction

Normal human bronchial epithelia (NHBE) are primary cells grown using an Air-Liquid Interface (ALI) method that mimics the airway (Lin et al. 2007). These cells are a primary means of evaluating changes in airway epithelium when challenged with a pathogen or allergen. Differentiated NHBE show variable expression of α2-3 sialic acid on their apical surface and are susceptible to human influenza A infection through abundant α2-6 sialic acid, thereby accurately mirroring intact tissue (Viswanathan et al. 2010; Davis et al. 2015). Similarly, previous reports indicate *M. pneumoniae* binds sulfated glycosphingolipids (GSL) and NeuAcα2-3LacNAc containing glycoproteins (Krivan et al. 1989; Nagai and Miyata 2006; Kasai et al. 2013). This binding preference for α2-3 sialic acid isn't consistant with known glycosylation patterns of the upper airway where infections are most common. While much is known about NHBE cells and how they respond to stimuli and pollutants in culture, very little is known about their glycosylation during differentiation and the impact these changes have on inflammation and immunity.

Glycans are found on every cell throughout the body and are involved in many biological processes and diseases, such as leukocyte rolling and extravasation into damaged tissues, juxtacrine signaling in neurons, identification and clearance of non-self, and cancer growth and metastasis (Varki 1994; Baas et al. 2011; Maverakis et al. 2015; Taniguchi and Kizuka 2015). In the airway,

glycans are involved in the clearance of immune cells by inducing apoptosis of eosinophils to limit inflammation during an allergic response (Kiwamoto et al. 2015). The airway is also covered in a densely glycosylated mucosal layer that protects the epithelium from allergens and assists in removing pathogens. Interestingly, this mucosal barrier isn't sufficient in preventing *M. pneumoniae's* gliding movement or infection as the bacterium was found to be at the base of cilia 2 minutes post infection of NHBE cells (Krause and Balish 2004; Krunkosky et al. 2007).

Here, we investigate how NHBE alter their glycosylation profile over the course of a 43-day differentiation in ALI culture. To do this we used nanoelectrospray mass spectrometry to analyze the structural variability and abundance of N-glycans, O-glycans, and glycosphingolipids of cells in culture for 0, 2, 10, and 43 days. Additionally, we probed protein extracts at the four time periods for alterations in specific glycosylation epitopes that are ligands for various anti-inflammatory receptors. These data indicate the variability of the developing airway and may provide insight towards directed therapeutics.

Experimental Procedure

Reagents

Siglec-F-Fc (R&D systems, 1706SF050) was diluted 1:5000 and pre-complexed to Goat anti-Human HRP (Invitrogen, A11013) at 1:10,000. Samples were digested with 1μL of 44.5U/μL *Vibrio cholera* Sialidase (a generous gift from

Dr. Ronald Schnaar) in 0.1M PIPES 4mM $CaCl_2$ pH6.0 buffer prior to immunoassay. PNGase F (a generous gift from Dr. Kelly Moremen) digestion of samples and slides was performed in 0.1M sodium phosphate pH 7.5 buffer for a minimum of 4 hrs.

Cell culture

Expansion, cryopreservation and culturing of NHBE cells in an air–liquid interface system were performed as previously described (Krunkosky et al. 2000). Briefly, NHBE cells (Cambrex, San Diego, CA) were seeded into vented T75 tissue culture flasks (500 cells/cm^2) until cells reached 75–80% confluence. Cultures were dissociated with trypsin/EDTA and cultured in an ALI system initiated by seeding NHBE cells (passage-2, 2 **x**10^4 cells/cm^2) onto Transwell-clear culture inserts (24.5, 0.45mm pore size; Costar, Cambridge, MA) that were thin-coated with rat tail collagen, type I (Collaborative Res., Bedford, MA). Cells were cultured submerged for the first 5–7 days. At that time, removing the apical medium and feeding cells with medium on their basal surface only created the ALI. The apical surface of the cells was exposed to a humidified 95% air/5% CO_2 environment. Medium beneath the cells was changed daily thereafter (Krunkosky et al. 2000). Cells were cultured for an additional 43 days in ALI.

Glycan analysis

Cells were lysed in 50% methanol by mechanical pestle on ice and homogenate was transferred to a clean glass tube. The homogenate was adjusted to a final concentration of Water: Chloroform: Methanol 4:8:3 (v/v/v) before removal from ice. After 18 h of end-over-end agitation (Nutator), the insoluble proteinacious material was collected by centrifugation. Following re-extraction of the pellet three times with 4:8:3 and once with ice-cold 80% acetone (v/v, aqueous), the final pellet was dried under a gentle stream of nitrogen and stored as protein powder at -20^{o}C. All supernatants generated during the extraction procedure were combined and dried under nitrogen for analysis of GSL. Protein content of the powder was determined by BCA assay (Pierce). Generally, 2mg of protein powder (dry weight) was used for both, N- and O-glycan analysis. N-linked glycans were harvested from the protein powder as previously described (Aoki et al. 2007). Briefly, glycopeptides were generated by digestion of protein powder with trypsin/chymotrypsin prior to enrichment by Sep-Pak C18 cartridge chromatography (Waters) and subjected to digestion with PNGase F for 18 h at 37^{o}C. Released oligosaccharides were separated from residual peptides by Sep-Pak C18 cleanup and permethylated prior to mass spectrometric analysis. O-linked glycans were released by reductive β-elimination, desalted on AG-50W-X8 resin (H^{+} form) and enriched by Sep-Pak C18 cartridge chromatography (Aoki et al. 2008). GSLs prepared from dried supernatant were saponified for 18 h at 37^{o}C before enrichment and desalting by Sep-Pak tC18 cartridge chromatography. Free fatty acids were removed using

Hexanes before suspension in Chloroform: Methanol: Water, 2:2:0.1 for HPTLC analysis (Boccuto et al. 2014).

Permethylated N-glycans, O-glycans, and GSL were analysed by nanoelectrospray ionization mass spectrometry using an ion trap instrument (NSI-LTQ Orbitrap Discovery, Thermo-Fisher). N-glycans, O-glycans were dissolved in 1mM NaOH in 50% aqueous methanol (v/v) while GSLs were dissolved in 1mM NaOH in Methanol: 2-Propanol: 1-Propanol, 16:3:3 by volume before direct infusion into the instrument at a syringe flow rate of 0.40–0.60 μL $min^{-}1$ and a capillary temperature set to 210^{o}C. For fragmentation by collision-induced dissociation (CID) in MS/MS and MS^{n} modes, 40% collision energy was applied. The total ion mapping functionality of the XCalibur software package (version 2.0) was utilized to detect and quantify the prevalence of individual glycans in the total glycan profile. Structural assignments were done using GRITS Toolbox (CCRC freeware); all structures were validated by manual inspection. Total ion mapping peaks for all charge states of a given ion with $m/z \leq 2000$ were summed together for quantification. Glycan quantification was performed relative to a known quantity of external standards (maltotriose and maltotetraose, Supelco), which were permethylated with heavy methyliodide ($^{13}CH_3I$) and spiked into the sample matrix prior to analysis (Mehta et al. 2016).

Western Blots

Acetone washed protein powder was suspended in 900µL H_2O, 100µL of 1% Triton X-100, 50µL of 1M β-mercaptoethanol, 1mL of 8M Urea and incubated at 56^{o}C for 24 hours with intermittent vortexing. SDS-PAGE gels were loaded with 100ng per lane based on BCA.

Results and Discussion

Protein glycosylation is increased with differentiation

The N- and O-glycans were profiled for the 10 most abundant glycans present in the MS^1 for NHBE cells at 0, 2, 10, and 43 days ALI culture. No changes in glycan composition were observed as the cells differentiate but changes in abundance were easily noted. N-glycans were released by PNGase F from trypsin-digested glycoproteins prior to permethylation. NSI-MS^n identified the major N-glycan as $Man_5GlcNAc_2$ (*m/z* 1783.89) with nearly 30% profile abundance by day 43. High mannose glycans dominate the profile with sialylated fucosylated complex structures at second most abundant. Significant changes are seen for $Man_5GlcNAc_2$, $Man_6GlcNAc_2$, $Man_8GlcNAc_2$, and $NeuAc_1Deoxyhexose_1Hex_1HexNAc_1$ + $Man3GlcNAc_2$.

These differences are dependent upon which comparative analysis is used to visualize the data. When a glycan is compared by relative abundance to the other nine glycans in the profile, providing a percent of the *total* profile, the result is very different from a quantification of each glycan against an external standard that is normalized to protein. For example, the dominant structure $Man_5GlcNAc_2$ increases by less than 2% when observed as a percent of the total profile but shows an ~8 fold increase when quantified for differences between days 0 and 43 (**Figure 3.1**). It is important to utilize both measurements since they represent different aspects of the cell surface. When using percent total profile, a glycan is shown to have a ratio to other glycans allowing an overview of

diversity. This is different from absolute quantification since a glycan can be very abundant but not be the most prevalent for a cell type. Consider the glycan $NeuAc_1Deoxyhexose_1Hex_1HexNAc_1$ + $Man3GlcNAc_2$, there is no difference in the percent total profile between any time point yet there is a dramatic increase for day 43. These changes between time points can easily been seen by viewing a total ion chromatograph (TIC) for each time point (**Figure 3.2**). Here, each peak represents the relative abundance for the fragmentation of a single mass. All time points share a similar signature of an initial peak around 6.06 minutes that represents $Man_5GlcNAc_2$ but changes over the remaining time course. The changes in TIC easily show the differences between the time points without any data manipulation. Therefore, a clear change in N-glycosylation abundance with minor changes in heterogeneity is observed as NHBE cells differentiate.

O-glycans were released from glycoproteins by β-elimination prior to permethylation. The O-glycan profile is dominated by O-GalNAc structures at all time points with Core 1 $NeuAc_1Hex_1HexNAc_1$-*O*-S/T (*m/z* 895.47) reaching 40% abundance. Here there are significant changes for $NeuAc_1Hex_1HexNAc_1$-*O*- S/T, $NeuAc_2Hex_1HexNAc_1$-*O*-S/T, $NeuAc_1Hex_2HexNAc_2$-*O*- S/T, $NeuAc_2Hex_2HexNAc_2$-*O*- S/T, $Hex_2HexNAc_2$-*O*- S/T, and $Deoxyhexose_1Hex_2HexNAc_3$-*O*-S/T. Here, the difference between the percent of total profile and absolute quantification is even more exaggerated. Not a single glycan shows a change in percent total profile while nearly every glycan shows a large jump in abundance at day 43 (**Figure 3.3**). The relative abundance profile and the quantification profile look similar in general trend for each glycan but are

telling different stories. O-glycosylation of proteins in increased when NHBE cells are fully differentiated but do not alter the ratio of attachment.

Sulfated O-glycans are separated from neutral O-glycans following permethylation by phase partition (Kumagai et al. 2013; Nix et al. 2014) and are not detectable before 10 days in ALI culture. This appearance of sulfated O-glycans is punctuated by a sharp increase in abundance for Core 2 O-GalNAc structures at day 43 (**Figure 3.4**). The quantity and diversity of structures identified is quite striking and resembles what is found in saliva. Comparatively, six sialylated sulfated O-glycans were identified from human saliva (Kumagai et al. 2013) while the top ten identified here has four sialylated sulfated structures. The prevailing trend seen for N- and O-glycans of successive increases in abundance as the cells differentiate is observed here, making the appearance and expansion of sulfated structures quite remarkable (**Figure 3.5**). The manipulation of O-glycosylation appears to be reserved to sulfated structures, which may be more limited in their biological activity.

Glycosphingolipids are reduced in complexity

GSLs are enriched from homogenized cells using an organic extraction before removal of glyceraldehyde containing lipids by saponification. Analysis of permethylated GSLs was done by NSI-MS^n allowing identification of the carbohydrate in addition to the sphingosine and fatty acid tail length. The GSL profiles are more heterogeneous at 0 and 2 days ALI, with multiple gangliosides being detected at early stages but is reduced to GM3 at day 43. At the end of the

differentiation period the profile is much simpler and dominated by the globo series. The most abundant GSL is globotriaosylceramide with ~35% abundance on day 0 and increases to ~70% abundance by day 43 (**Figure 3.6**). The heterogeneity of the ceramide backbone is roughly split between the shortest and longest species in days 0 and 2. By day 10 this equitable distribution of lipid length shifts to being dominated by the shorter species. Structural analysis of the ceramide backbone is possible but would require a slightly different analytical approach. However, the gross morphological differences described here are informative since lipid length influences membrane fluidity and diffusion, both of which impact protein localization to specific domains, and, ultimately, protein function and signaling. Differences in lipid lengths have been described for glucosylceramide in several tissues from 12-week old mice (Ishibashi et al. 2013) yet I am unaware of any report detailing the differences in differentiating NHBE cells.

Changes in glycosylation have an unknown function

It is currently unknown why NHBE cells show a large increase for these particular glycans. It is also unknown why there is such a large increase in abundance for almost every O-glycan yet N-glycans gradually increase over the differentiation. The simplest hypothesis would be O-glycans play a distinct role in the growth and differentiation of NHBE cells that cannot be duplicated by N-glycans. To date, the main role for O-glycans in the airway is found in the mucin layer as a barrier to infection (Cohen et al. 2013). This raises the possibility that

O-glycans are playing a role on the cell surface that may or may not be distinct from the mucus layer.

Several of the changes seen are for glycans who have structural similarity to those involved in infection of various pathogens. For example, *M. pneumoniae* preferentially binds NeuAcα2-3LacNAc containing glycans in the airway while *influenza* is promiscuous and binds any α2-6 linked sialic acid. An increase in abundance for glycans containing these determinants are seen in fully differentiated cells, however, why there is an increase is not understood. The presence of common pathogens that bind these structures indicates the cells are purposfully expressing these epitopes, therefore, there must be some advantage for expressing a ligand that also increases the probability of infection.

NHBE cells increase expression of anti-inflammatory glycans during differentiation

Glycosylation is well documented in its ability to modulate the inflammatory response in the airway (Guo et al. 2011; Mao et al. 2013; Kiwamoto et al. 2015; Schleimer et al. 2016). Here, a specific cell surface receptor, Siglec-F, found on eosinophils induces apoptosis of the infiltrating leukocytes when a unique glycan ligand is bound. These glycans have been found in multiple places, attached to multiple proteins - including secreted Muc4ac and Muc5b and attached to the apical surface of trachea and bronchus (Yu et al. 2017). The end result of ligand binding is a reduction in localized inflammation. Identification of the glycans capable of binding Siglec receptors has produced many possibilities

that all have different structures (Blixt et al. 2004; Bochner et al. 2005; Tateno et al. 2005; Guo et al. 2011; Patnode et al. 2013; Macauley et al. 2014). Using a chimeric receptor-Fc (Siglec-F-Fc) construct (Kelm et al. 1994) we probed for epitopes in NHBE cell lysate. Minor banding was seen for day 0 above the 250-kD marker, which disappeared in day 2 and day 10, and reappeared with increased intensity, by day 43 (**Figure 3.7A**). To determine the linkage between sialic acid and the underlying monosaccharide in the ligand we used the lectins MAA, which binds α2-3, and SNA, which binds α2-6 sialic acid (**Figure 3.7B-C**). It appears that the ligand may have both linkages present, but if both contribute to binding is undetermined. Lysate was also treated with PNGaseF, sialidase, and underwent solvolysis to determine the characteristics of the ligand. Binding was retained following removal of N-glycans but was completely abolished after loss of sialic acid and sulfate (**Figure 3.7D**). This does not agree with the Siglec-F binding data for airway or cell lysate from mice, which shows sulfate is not required (Kiwamoto et al. 2015). Interestingly, Siglec-F binding on human tissues has a strict requirement for sulfate (**Figure 3.7D**). This is most likely due to differences in the glycans made by different species; murine Siglecs do not have the same binding pattern on human tissue as their human paralogs, making the argument for different ligands being present at the same approximate location. (Yu et al. 2017). Additionally, murine tracheal epithelial cells (mTEC) show two bands above 250-kD by Siglec-F-Fc overlay (Kiwamoto et al. 2015) while NHBE cells show a single band (**Figure 3.7A**). This could be the result of altered glycosylation in human tissues which limits the number of glycan structures,

effectively enhancing the focus on a very specific specific subset of O-glycans. The subset of O-glycans that is highly regulated and selectively expressed in human tissue is likely sulfated, and sialylated, with an underlying LacNAc backbone. More specifically, 6'-su-sLacNAc, which is increased at day 43 (**Figure 3.4, 3.5**). The human paralog of Siglec-F is Siglec-8 – which is extrememly limited in ligand recognition and binds 6'-su-sLacNAc (Bochner 2009; Yu et al. 2017). This increase in sulfated O-glycans may be an endogenous method of limiting immune system mediated inflammation in the airway.

Conclusions

The glyco-terrain of developing NHBE cells is characterized by successive increases in glycan abundance for N- and O-linked glycans and a consolidation in diversity of GSLs. These changes, in concert with changes in anti-inflammatory glycans, will provide the basis of knowledge for therapeutic design in the future.

Changes in the diversity and abundance of hybrid and complex N-glycans, alongside changes in high mannose, dominate the profile. No changes are observed in O-glycan diversity, but class wide increases in abundance, as differentiation proceeds is obvious. Sulfated O-glycans show an increase for highly regulated structures that are not found in mice. Finally, GSLs are reduced in complexity with globo series structures dominating the profile. Overall, these

changes in glycosylation during differentiation give new insights into the production of immunomodulatory epitopes.

Figure 3.1: N-glycosylation is altered as NHBE cells differentiate

Cells were cultured in ALI for 0, 2, 10, and 43 days before harvesting. N-glycans were analyzed from ~1 mg of crude protein extract. The percent of the total profile for each glycan is graphed for a relative change while the absolute quantification was determined by comparison with an external standard and normalized to protein amount by BCA. There are bidirectional alterations when each glycan is compared to others and displayed in percent total profile. However, most structures are increased at day 43 over previous time points when quantified by external standard.

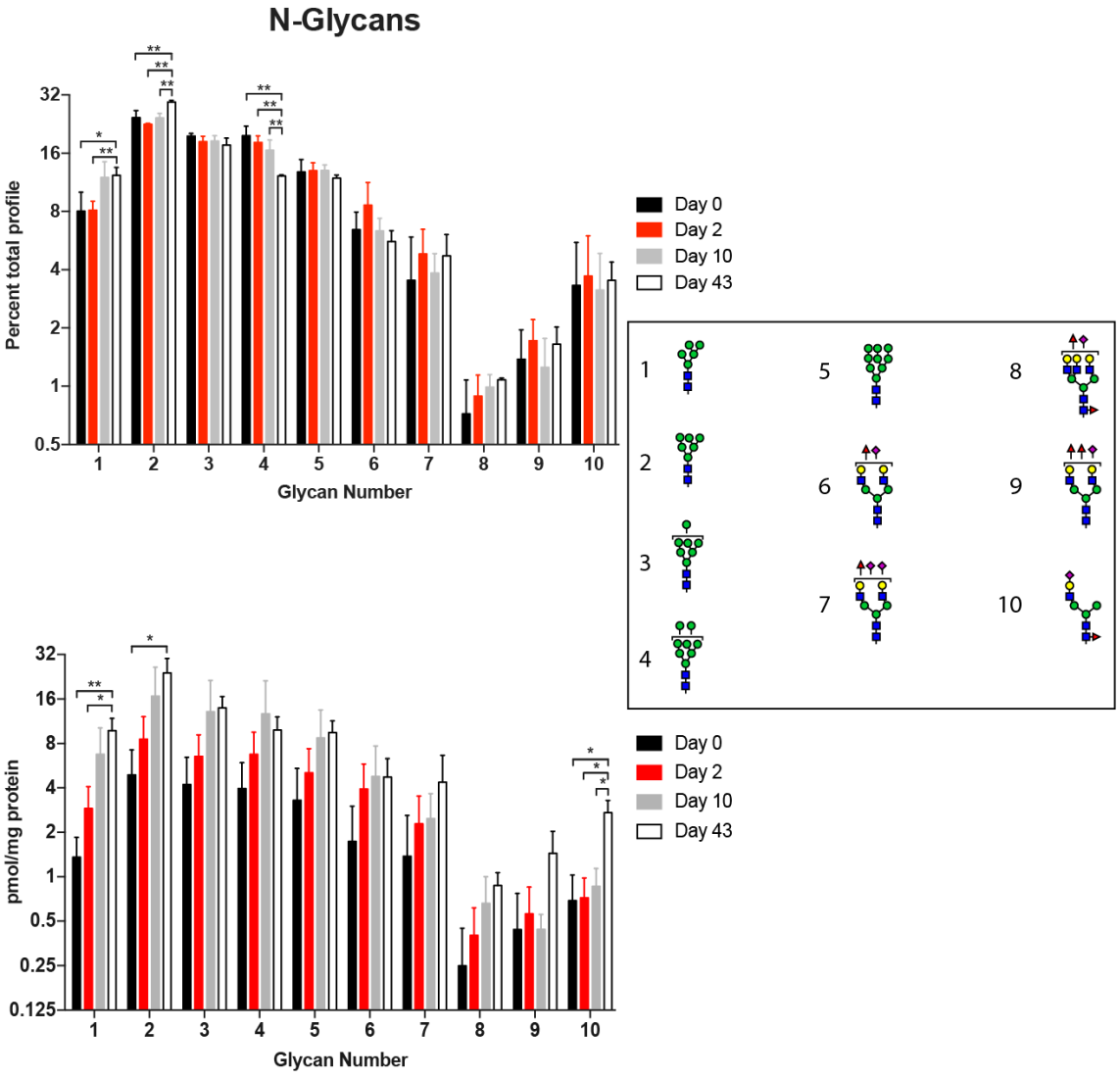

Figure 3.2: Total ion chromatogram of N-glycans during differentiation

Using the total ion mapping function of XCalibur 2.0, N-glycans were fragmented every 2 Daltons between 700-2000 *m/z*. The profiles look similar between the different time points with differences in relative intensity for several peaks.

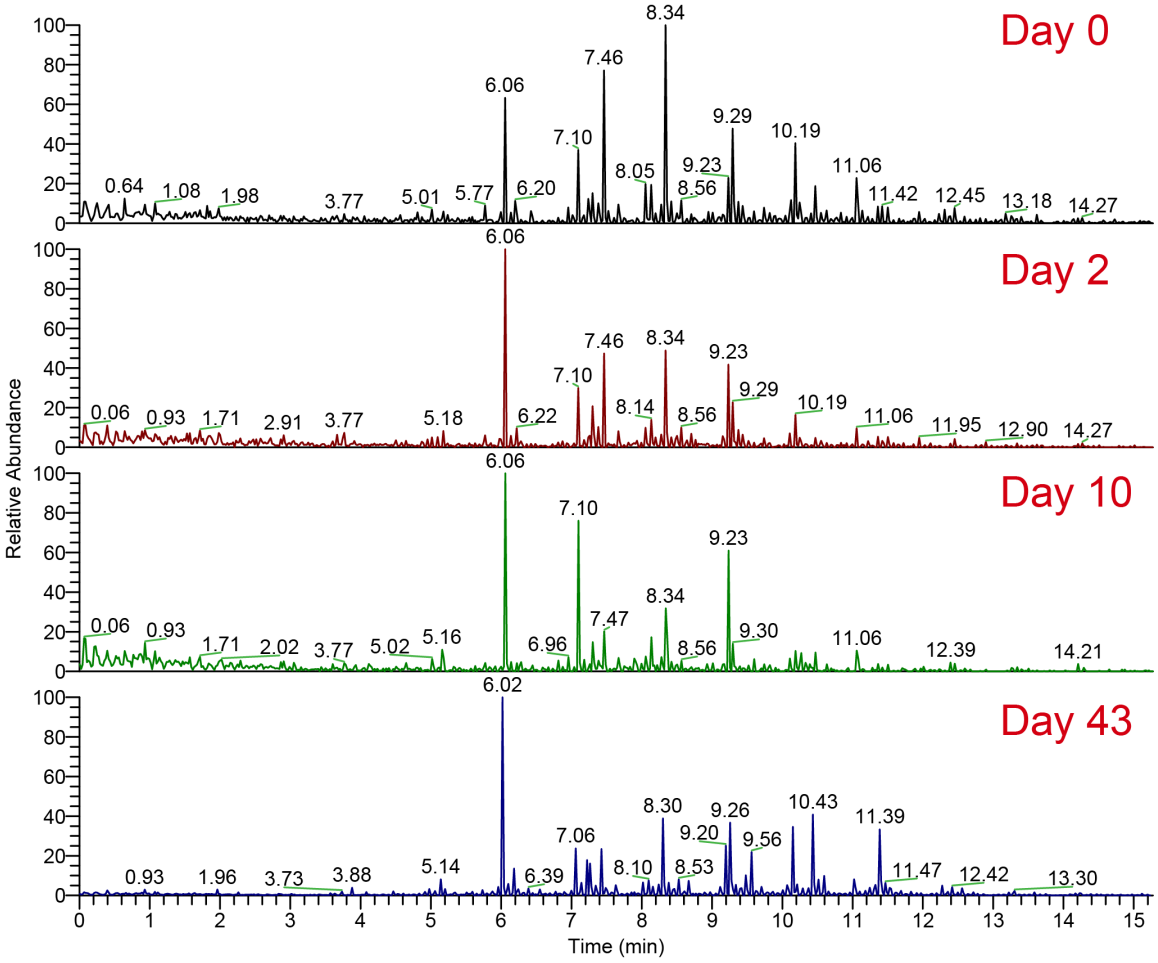

Figure 3.3: O-glycosylation is altered as NHBE cells differentiate

Cells were cultured in ALI for 0, 2, 10, and 43 days before harvesting. O-glycans were analyzed from ~1 mg of crude protein extract. The percent of the total profile for each glycan is graphed for a relative change while the absolute quantification was determined by comparison with an external standard and normalized to protein amount by BCA. There are bidirectional alterations when each glycan is compared to others and displayed in percent total profile. However, all structures are increased at day 43 over previous time points when quantified by external standard.

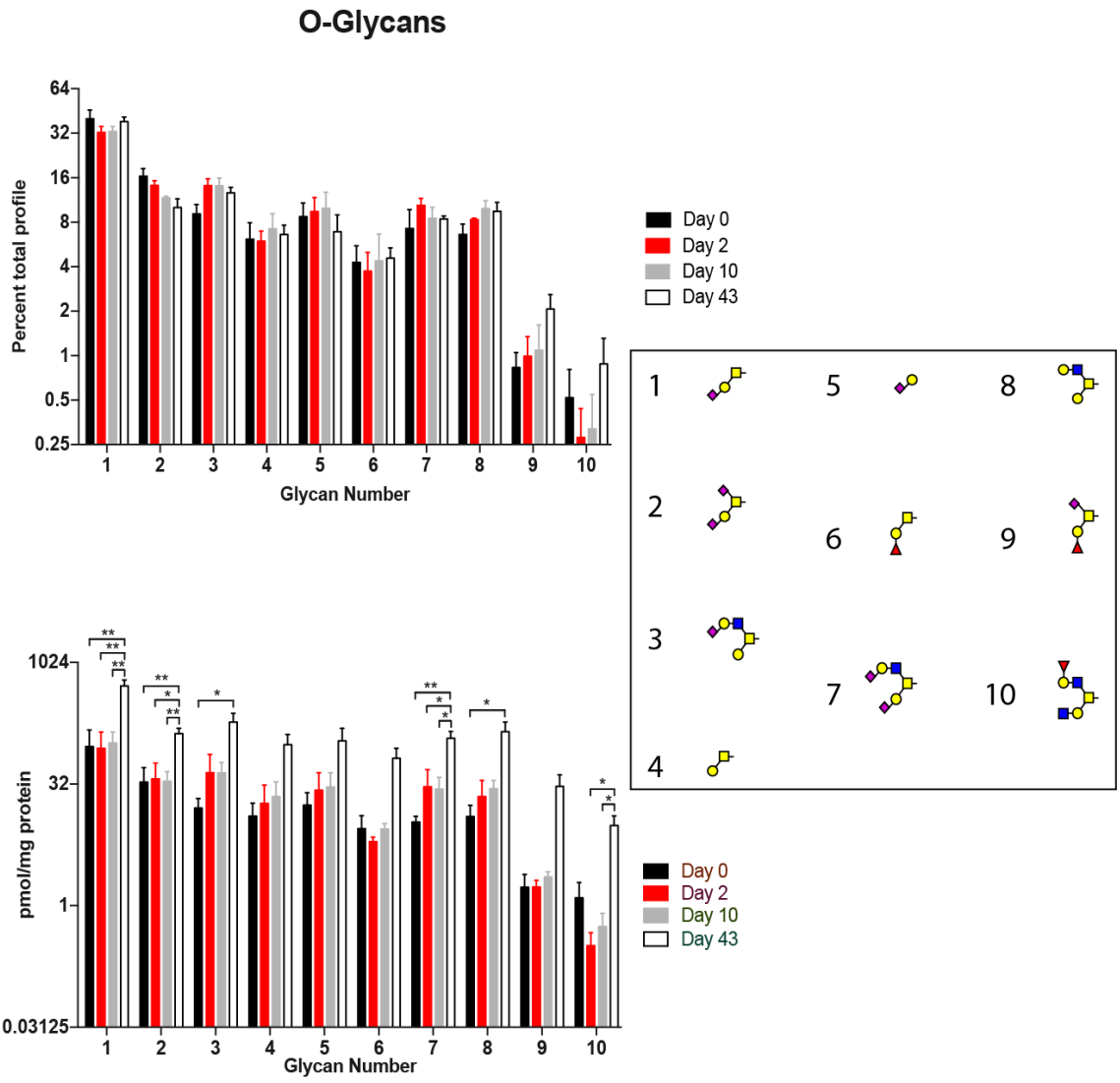

Figure 3.4: Sulfated O-glycans appear by day 10 and increase over time

Sulfated O-glycans were separated from neutral structures by phase partition using dichloromethane and water. All structures were analyzed in negative ion mode to ensure that each structure was sulfated. Sulfated structures are present by day 10 but increase in abundance and diversity by day 43. Structures are compared relative to all others and displayed in percent total profile.

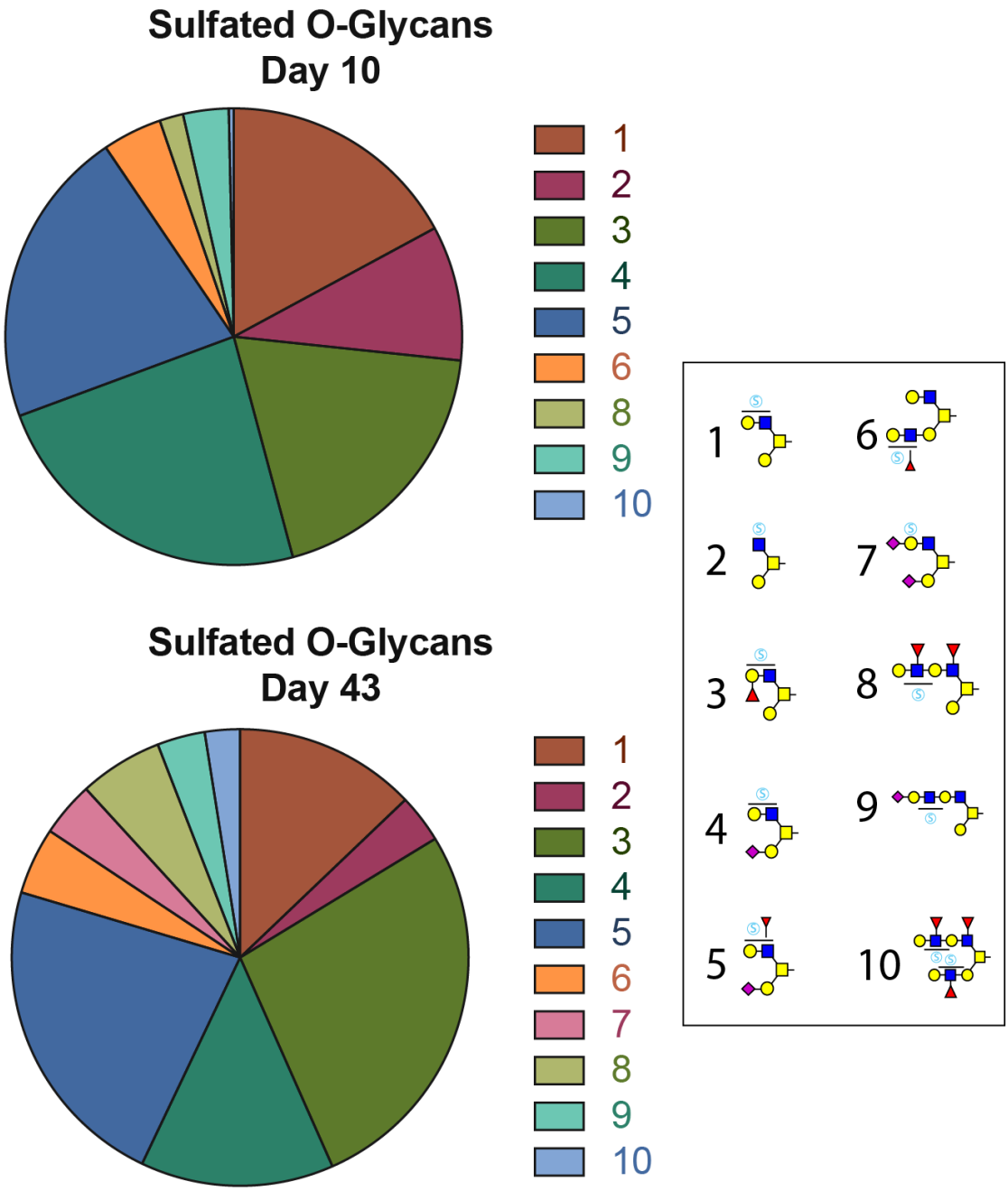

Figure 3.5: Sulfated O-glycans show a distinct increase over time.

Qualitative changes in sulfated O-glycans show distinct differences as NHBE cells differentiate. While detectable, sulfated glycans prior to 10 days ALI culture are very low in abundance. Fully differentiated and confluent cells are achieved by 43 days ALI culture and show significant increases in sulfated O-glycans.

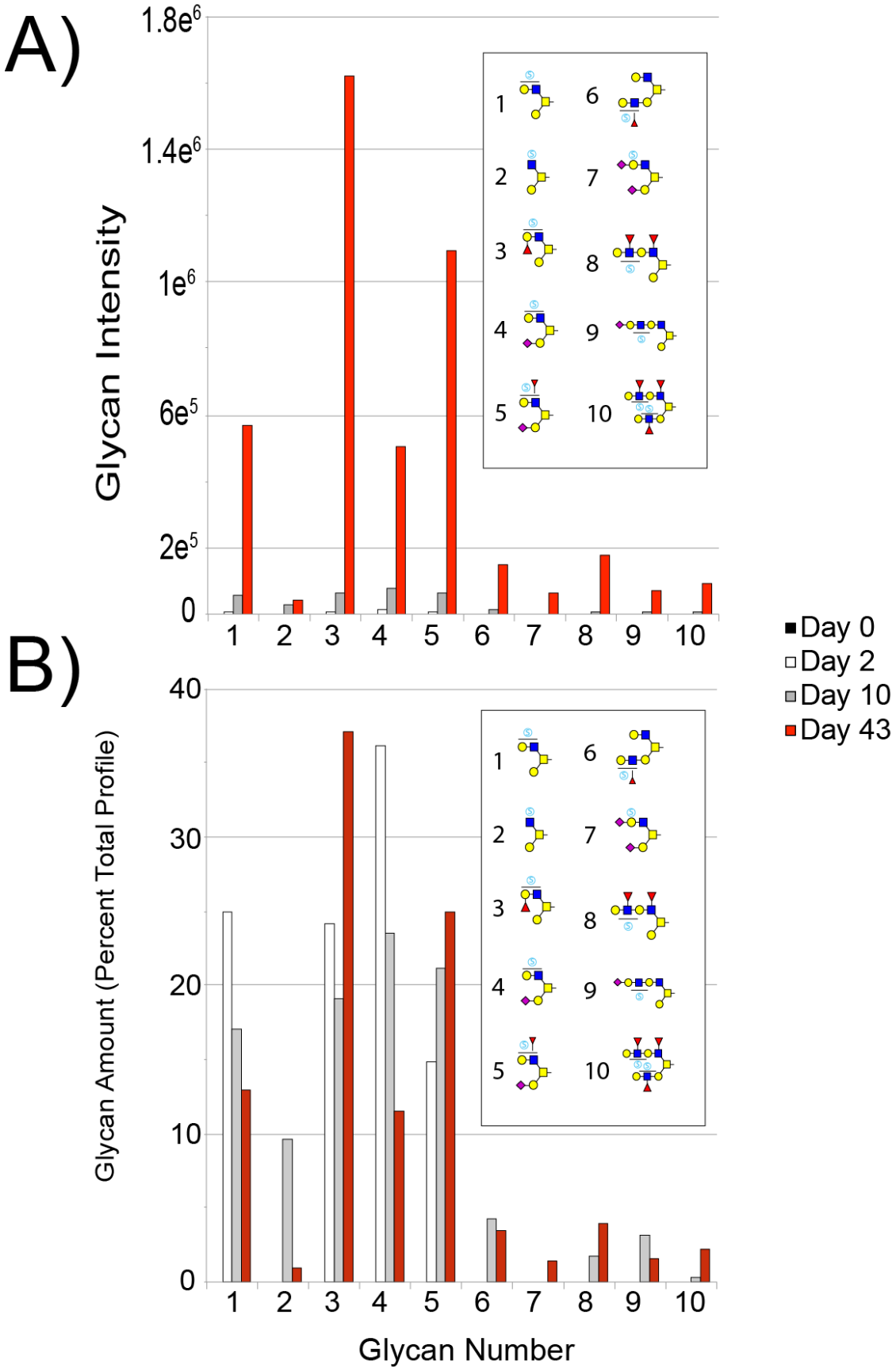
A)
1.8e6
1.4e6
1e6
6e5
2e5
0
Glycan Intensity
1 2 3 4 5 6 7 8 9 10
B)
40
30
20
10
0
Glycan Amount (Percent Total Profile)
1 2 3 4 5 6 7 8 9 10
Glycan Number
Day 0
Day 2
Day 10
Day 43

Figure 3.6: Glycosphingolipids are reduced in variation in fully differentiated NHBE cells.

Glycosphingolipids (GSL) are extracted from NHBE cells using C:M:W and separated from glycerol lipids through saponification. All structures are compared by raw relative intensity. GSLs are dominated by neutral globo series throughout the differentiation. A decrease in diversity is seen over the differentiation and an almost complete loss of ganglio series by day 43.

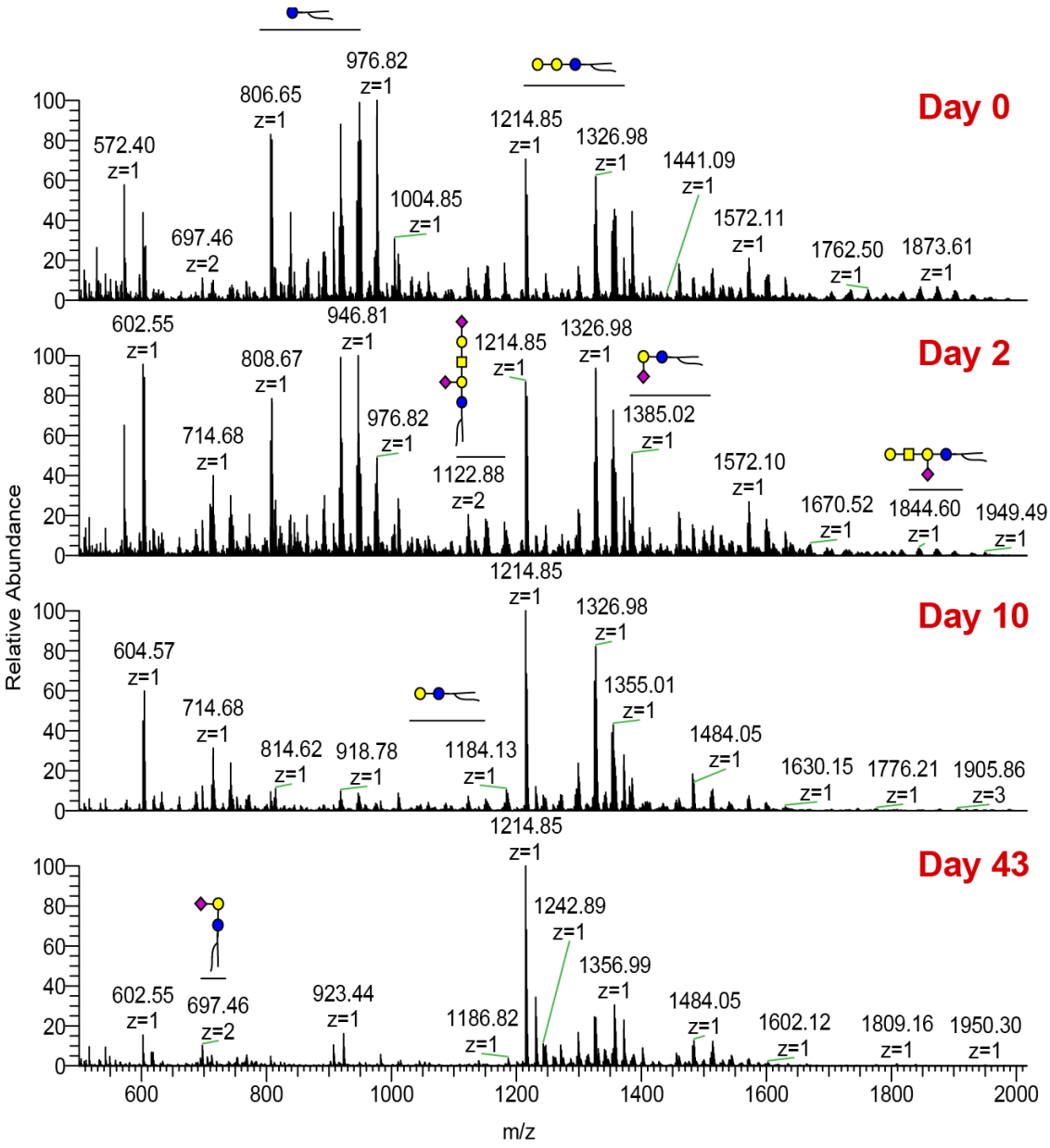

Figure 3.7: NHBE lectin blots

Whole protein prepared for glycomic analysis was solubilized in a reduced Tris buffer with detergent and urea at 56^{o}C for 48 hours. Protein from 0, 2, 10, and 43 days were probed for ligands of Siglec-F (A). Day 0 shows minimal banding that disappears until a strong resurgence at day 43. The band seen in Siglec-F-Fc overlay appears to match the banding for MAA (B) and SNA (C). Interestingly, there were three other bands observed that bind SNA. The observed Siglec-F ligand was also determined to be an O-linked glycan that requires sulfate and sialic acid (D).

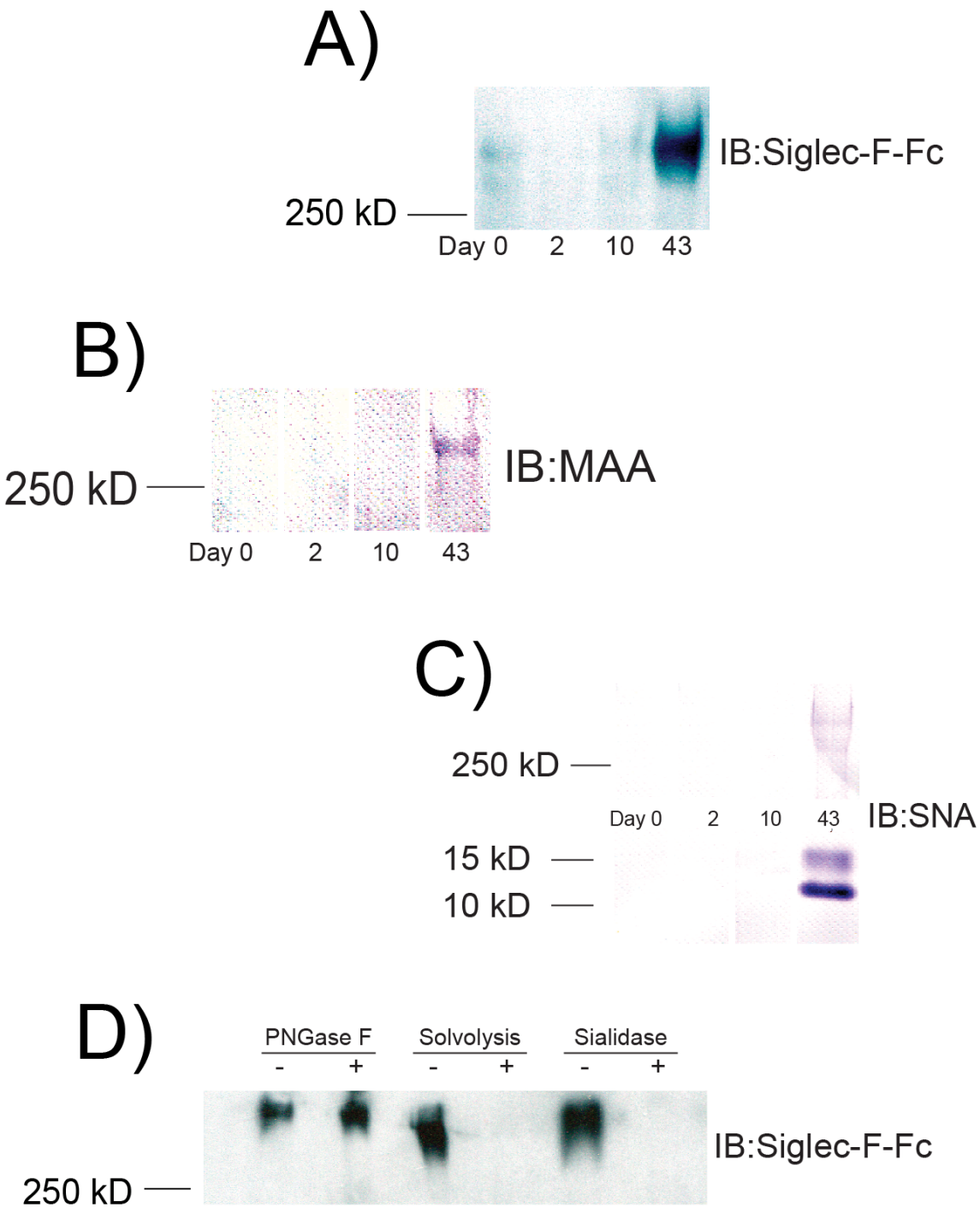
A)
IB:Siglec-F-Fc
250 kD
Day 0 2 10 43
B)
250 kD
IB:MAA
Day 0 2 10 43
C)
250 kD
Day 0 2 10 43
IB:SNA
15 kD
10 kD
D)
PNGase F
Solvolysis
Sialidase
- + - + - +
IB:Siglec-F-Fc
250 kD

References

Aoki, K., Perlman, M., Lim, J.M., Cantu, R., Wells, L. and Tiemeyer, M. (2007). "Dynamic developmental elaboration of N-linked glycan complexity in the Drosophila melanogaster embryo." J Biol Chem **282**(12): 9127-9142.

Aoki, K., Porterfield, M., Lee, S.S., Dong, B., Nguyen, K., McGlamry, K.H. and Tiemeyer, M. (2008). "The diversity of O-linked glycans expressed during Drosophila melanogaster development reflects stage- and tissue-specific requirements for cell signaling." J Biol Chem **283**(44): 30385-30400.

Baas, S., Sharrow, M., Kotu, V., Middleton, M., Nguyen, K., Flanagan-Steet, H., Aoki, K. and Tiemeyer, M. (2011). "Sugar-free frosting, a homolog of SAD kinase, drives neural-specific glycan expression in the Drosophila embryo." Development **138**(3): 553-563.

Blixt, O., Head, S., Mondala, T., Scanlan, C., Huflejt, M.E., Alvarez, R., Bryan, M.C., Fazio, F., Calarese, D., Stevens, J., Razi, N., Stevens, D.J., Skehel, J.J., van Die, I., Burton, D.R., Wilson, I.A., Cummings, R., Bovin, N., Wong, C.H. and Paulson, J.C. (2004). "Printed covalent glycan array for ligand profiling of diverse glycan binding proteins." Proc Natl Acad Sci U S A **101**(49): 17033-17038.

Boccuto, L., Aoki, K., Flanagan-Steet, H., Chen, C.F., Fan, X., Bartel, F., Petukh, M., Pittman, A., Saul, R., Chaubey, A., Alexov, E., Tiemeyer, M., Steet, R. and Schwartz, C.E. (2014). "A mutation in a ganglioside biosynthetic enzyme, ST3GAL5, results in salt & pepper syndrome, a neurocutaneous disorder with altered glycolipid and glycoprotein glycosylation." Hum Mol Genet **23**(2): 418-433.

Bochner, B.S. (2009). "Siglec-8 on human eosinophils and mast cells, and Siglec-F on murine eosinophils, are functionally related inhibitory receptors." Clin Exp Allergy **39**: 317-324.

Bochner, B.S., Alvarez, R.A., Mehta, P., Bovin, N.V., Blixt, O., White, J.R. and Schnaar, R.L. (2005). "Glycan array screening reveals a candidate ligand for Siglec-8." J Biol Chem **280**(6): 4307-4312.

Cohen, M., Zhang, X.Q., Senaati, H.P., Chen, H.W., Varki, N.M., Schooley, R.T. and Gagneux, P. (2013). "Influenza A penetrates host mucus by cleaving sialic acids with neuraminidase." Virol J **10**: 321.

Davis, A.S., Chertow, D.S., Moyer, J.E., Suzich, J., Sandouk, A., Dorward, D.W., Logun, C., Shelhamer, J.H. and Taubenberger, J.K. (2015). "Validation of normal human bronchial epithelial cells as a model for influenza A infections in human distal trachea." J Histochem Cytochem **63**(5): 312-328.

Guo, J.P., Brummet, M.E., Myers, A.C., Na, H.J., Rowland, E., Schnaar, R.L., Zheng, T., Zhu, Z. and Bochner, B.S. (2011). "Characterization of Expression of Gylcan Ligands for Siglec-F in Normal Mouse Lungs." Am J Respir Cell and Molec Biol **44**: 238-243.

Ishibashi, Y., Kohyama-Koganeya, A. and Hirabayashi, Y. (2013). "New insights on glucosylated lipids: metabolism and functions." Biochim Biophys Acta **1831**(9): 1475-1485.

Kasai, T., Nakane, D., Ishida, H., Ando, H., Kiso, M. and Miyata, M. (2013). "Role of binding in Mycoplasma mobile and Mycoplasma pneumoniae gliding analyzed through inhibition by synthesized sialylated compounds." J Bacteriol **195**(3): 429-435.

Kelm, S., Pelz, A., Schauer, R., Filbin, M.T., Tang, S., de Bellard, M.E., Schnaar, R.L., Mahoney, J.A., Hartnell, A., Bradfield, P. and et al. (1994). "Sialoadhesin, myelin-associated glycoprotein and CD22 define a new family of sialic acid-dependent adhesion molecules of the immunoglobulin superfamily." Curr Biol **4**(11): 965-972.

Kiwamoto, T., Katoh, T., Evans, C.M., Janssen, W.J., Brummet, M.E., Hudson, S.A., Zhu, Z., Tiemeyer, M. and Bochner, B.S. (2015). "Endogenous airway mucins carry glycans that bind Siglec-F and induce eosinophil apoptosis." J Allergy Clin Immunol **135**(5): 1329-1340 e1321-1329.

Krause, D.C. and Balish, M.F. (2004). "Cellular engineering in a minimal microbe: structure and assembly of the terminal organelle of Mycoplasma pneumoniae." Mol Microbiol **51**(4): 917-924.

Krivan, H.C., Olson, L.D., Barile, M.F., Ginsburg, V. and Roberts, D.D. (1989). "Adhesion of Mycoplasma pneumoniae to sulfated glycolipids and inhibition by dextran sulfate." J Biol Chem **264**(16): 9283-9288.

Krunkosky, T.M., Fischer, B.M., Martin, L.D., Jones, N., Akley, N.J. and Adler, K.B. (2000). "Effects of TNF-alpha on expression of ICAM-1 in human airway epithelial cells in vitro. Signaling pathways controlling surface and gene expression." Am J Respir Cell Mol Biol **22**(6): 685-692.

Krunkosky, T.M., Jordan, J.L., Chambers, E. and Krause, D.C. (2007). "Mycoplasma pneumoniae host-pathogen studies in an air-liquid culture of differentiated human airway epithelial cells." Microb Pathog **42**(2-3): 98-103.

Kumagai, T., Katoh, T., Nix, D.B., Tiemeyer, M. and Aoki, K. (2013). "In-gel beta-elimination and aqueous-organic partition for improved O- and sulfoglycomics." Anal Chem **85**(18): 8692-8699.

Lin, H., Li, H., Cho, H.J., Bian, S., Roh, H.J., Lee, M.K., Kim, J.S., Chung, S.J., Shim, C.K. and Kim, D.D. (2007). "Air-liquid interface (ALI) culture of human bronchial epithelial cell monolayers as an in vitro model for airway drug transport studies." J Pharm Sci **96**(2): 341-350.

Macauley, M.S., Crocker, P.R. and Paulson, J.C. (2014). "Siglec-mediated regulation of immune cell function in disease." Nat Rev Immunol **14**(10): 653-666.

Mao, H., Kano, G., Hudson, S.A., Brummet, M., Zimmermann, N., Zhu, Z. and Bochner, B.S. (2013). "Mechanisms of Siglec-F-induced eosinophil apoptosis: a role for caspases but not for SHP-1, Src kinases, NADPH oxidase or reactive oxygen." PLoS One **8**(6): e68143.

Maverakis, E., Kim, K., Shimoda, M., Gershwin, M.E., Patel, F., Wilken, R., Raychaudhuri, S., Ruhaak, L.R. and Lebrilla, C.B. (2015). "Glycans in the immune system and The Altered Glycan Theory of Autoimmunity: a critical review." J Autoimmun **57**: 1-13.

Mehta, N., Porterfield, M., Struwe, W.B., Heiss, C., Azadi, P., Rudd, P.M., Tiemeyer, M. and Aoki, K. (2016). "Mass Spectrometric Quantification of N-Linked Glycans by Reference to Exogenous Standards." J Proteome Res **15**(9): 2969-2980.

Nagai, R. and Miyata, M. (2006). "Gliding motility of Mycoplasma mobile can occur by repeated binding to N-acetylneuraminyllactose (sialyllactose) fixed on solid surfaces." J Bacteriol **188**(18): 6469-6475.

Nix, D.B., Kumagai, T., Katoh, T., Tiemeyer, M. and Aoki, K. (2014). "Improved in-gel reductive beta-elimination for comprehensive O-linked and sulfo-glycomics by mass spectrometry." J Vis Exp(93): e51840.

Patnode, M.L., Cheng, C.W., Chou, C.C., Singer, M.S., Elin, M.S., Uchimura, K., Crocker, P.R., Khoo, K.H. and Rosen, S.D. (2013). "Galactose 6-o-sulfotransferases are not required for the generation of siglec-f ligands in leukocytes or lung tissue." J Biol Chem **288**(37): 26533-26545.

Schleimer, R.P., Schnaar, R.L. and Bochner, B.S. (2016). "Regulation of airway inflammation by Siglec-8 and Siglec-9 sialoglycan ligand expression." Curr Opin Allergy Clin Immunol **16**(1): 24-30.

Taniguchi, N. and Kizuka, Y. (2015). "Glycans and cancer: role of N-glycans in cancer biomarker, progression and metastasis, and therapeutics." Adv Cancer Res **126**: 11-51.

Tateno, H., Crocker, P.R. and Paulson, J.C. (2005). "Mouse Siglec-F and human Siglec-8 are functionally convergent paralogs that are selectively expressed on eosinophils and recognize 6-sulfo-sialyl Lewis X as a preferred glycan ligand." Glycobiology **15**: 1125-1135.

Varki, A. (1994). "Selectin ligands." Proc Natl Acad Sci U S A **91**(16): 7390-7397.

Viswanathan, K., Chandrasekaran, A., Srinivasan, A., Raman, R., Sasisekharan, V. and Sasisekharan, R. (2010). "Glycans as receptors for influenza pathogenesis." Glycoconj J **27**(6): 561-570.

Yu, H., Gonzalez-Gil, A., Wei, Y., Fernandes, S.M., Porell, R.N., Vajn, K., Paulson, J.C., Nycholat, C.M. and Schnaar, R.L. (2017). "Siglec-8 and Siglec-9 binding specificities and endogenous airway ligand distributions and properties." Glycobiology.

CHAPTER 4

IMPROVED IN-GEL REDUCTIVE β-ELIMINATION FOR COMPREHENSIVE O-LINKED AND SULFO-GLYCOMICS BY MASS SPECTROMETRY[1]

Nix, David B.[1], Kumagai, Tadahiro, Katoh, Toshihiko, Tiemeyer, Michael, Aoki, Kazuhiro J. Vis. Exp.

Abstract

SDS-PAGE is a widely used and effective technique for protein separation and in-gel proteolytic digestion of resolved protein bands has opened the door for high-resolution proteomic analysis of biological samples. In an effort to augment this methodology and to expand the usefulness of SDS-PAGE for glycoproteomics, we describe methods to release and recover O-linked glycans from proteins resolved in SDS-PAGE gels for subsequent analysis by mass spectrometry (MS). The major aim of this study is to improve O-glycomic methodology in order to explore the composition of O-linked glycans released from glycoproteins separated on gels. To that end, we address a critical issue related to in-gel release and subsequent glycomic analysis: removal of gel-derived contaminants that interfere with glycan profiling. While previous reports relied on HPLC separations to achieve sample clean-up during LC-MS, we now present a robust, and efficient sample workflow that ends with shotgun MSn analysis and eliminates the need for in-line HPLC separation prior to MS. Gel pieces containing target proteins are washed in acetonitrile, water, and ethyl acetate to remove contaminants, including polymeric acrylamide fragments. O-linked glycans are released through reductive β-elimination by hydrating gel pieces in base and adding reductant. Following straightforward sample clean-up, this simple but effective treatment provides a material suitable for subsequent MS analysis. An additional advantage of our complete workflow is that it

improves sensitivity and detection of sulfated glycans. Our method provides an efficient separation of sulfated permethylated glycans from non-sulfated (sialylated and neutral) permethylated glycans with a rapid and efficient phase-partition prior to MS analysis, demonstrating the feasibility of in-depth sulfoglycomic analysis using SDS-PAGE resolved glycoproteins.

KEY WORDS: glycoprotein; glycosylation; in-gel β-elimination; O-linked glycan; sulfated glycan; mass spectrometry; protein ID; SDS-PAGE; glycomics; sulfoglycomics.

Introduction

Glycosylation is an essential protein post-translational modification, contributing to a variety of extracellular events that influence cellular physiology, pathology, and recognition (Varki 1993; Ohtsubo and Marth 2006; Moremen et al. 2012). Despite major advances in analytical glycoscience, identifying the complete diversity of glycans on a specific protein remains an extremely challenging task, especially on proteins isolated from biological tissues under physiologic condition. Nonetheless, the microheterogeneity of glycoprotein glycans frequently affects functional interactions with other proteins or biological targets. Therefore, characterizing glycan diversity is essential for understanding the physiological significance of glycosylation changes involved in normal tissue function and disease pathologies (Lowe and Marth 2003; Yan and Lennarz

2005). In order to understand the contribution of glycoprotein glycosylation to tissue physiology and pathophysiology, robust glycomic analytical techniques, that provides depth, breadth, and sensitivity, have become increasingly important. Complete glycoprotein characterization must include protein identification, determination of glycosylation site utilization, and profiling of glycan heterogeneity. These analyses are generally referred to as proteomics, glycoproteomics, and glycomics, respectively. Proteomic identifications are generally achieved by LC-MS/MS analysis of tryptic peptides (Washburn 2004). Protein digestion can be carried out using a purified protein or proteins resolved by SDS-PAGE following in-gel digestion with proteases such as trypsin (Rosenfeld et al. 1992; Hellman et al. 1995; Morelle et al. 2006). Pre-enrichment of the protein mixture by SDS-PAGE enhances the depth and accuracy of protein ID. The development of analogous strategies for glycomic analysis of glycoprotein glycosylation lies at the forefront of glycoscience.

The two major classes of glycans attached to protein backbones are N-linked and O-linked glycans. N-linked glycans are attached to asparagine (Asn) residues of the tripeptide sequon Asn-X-Ser/Thr/Cys (X is any amino acid except proline). The enzymatic release of N-linked glycans with peptide-*N*-glycanase (PNGaseF or A) is highly effective and has been successfully adapted for in-gel and on-blot use (Mortz et al. 1996; Kuster et al. 1997; Kuster and Mann 1999). O-linked glycans are mainly attached to serine (Ser) or threonine (Thr) residues. However, only one enzyme has been identified that is capable of releasing O-linked glycans from glycoprotein and it has extremely limited glycan specificity,

releasing only the simplest O-linked glycans. Chemical release strategies remain the method of choice for comprehensive release of O-linked glycans from glycoproteins. Reductive or non-reductive β-elimination, or hydrazinolysis are well-characterized chemical release techniques and are currently the most commonly used approaches for releasing O-linked glycans from glycoproteins (Aoki et al. 2008; Kozak et al. 2012). Although reductive β-elimination has been applied to release O-linked glycans from glycoproteins resolved in SDS-PAGE gels, (either in-gel or after blotting to PVDF), previous approaches required HPLC separation for subsequent analysis (Schulz et al. 2002; Thomsson et al. 2005; Taylor et al. 2006).

At present ESI-MS and MS^n analyses are widely applied for the structural characterization of glycans released from glycoproteins. Under most circumstances, underivatized glycans demonstrate poor ionization, which is highly influenced by the structural features, including common glycan modifications with anionic substituents. Permethylation of released glycans dramatically increases sensitivity in MS analysis and also tends to equalize the molar signal response across a broad range of glycan structures, enabling quantitative glycan analysis (Anumula and Taylor 1992; Aoki et al. 2007). Moreover, permethylation imparts unique masses to terminal and substituted monosaccharide moieties, which provides important clues for structural elucidation; MS or MS/MS-based analysis of native glycans is unable to unambiguously discern positional information (Domon and Costello 1988; Ashline et al. 2005; Lapadula et al. 2005; Ashline et al. 2007). For example, acidic

glycans, such as those containing sialic acid, are generally difficult to detect as non-permethylated species by MS. Although these acidic glycans can be detected in negative ion mode by MS, it is impossible to detect both charged acidic glycans and neutral glycans in the same ion mode. A major advantage of glycan permethylation is that all of the free hydroxyl groups (OH) on a glycan's monosaccharides will be capped with a methyl group (OCH_3 or OMe), thus the sialylated glycan's charges are neutralized, making them detectable at the same sensitivity as permethylated neutral (asialo) glycans in positive ion mode. However, the hydroxyls of sulfate moieties on sulfoglycans are resistant to permethylation, resulting in retention of anionic charge, which suppresses ionization and decreases sensitivity. This suppression currently prevents comprehensive glycomic analysis of very complex glycoproteins such as mucins, which carry a high abundance of sulfated glycans (Thomsson et al. 2002; Yu et al. 2009; Yu et al. 2013).

Recent reports on purifying sulfated glycans used charged, reverse-phase chromatography to purify and separate permethylated glycans prior to MALDI analysis. This method relies on complete separation of sulfated and non-sulfated glycans using different mobile phases for elution, which we have found to be less stringent than organic phase partitioning. Therefore, new techniques suitable for the detection and enrichment of sulfoglycans are presented here. These techniques allow for the quantitative recovery of sulfated glycans in the aqueous phase following water:DCM (dichloromethane) extraction, which is routinely performed at the end of glycan permethylation reactions (Kumagai et al. 2013).

Importantly, this robust separation of permethylated sulfoglycans from a mixture of permethylated non-sulfated glycans concomitantly enriches for charged species while also simplifying MS2 fragmentation patterns. A comprehensive protocol for improved in-gel O-linked glycan analysis is also presented. The improved protocol enhances glycan recovery, increases the structural information obtainable through MSn analysis of permethylated glycans, and improves the sensitivity of sulfoglycomic analyses applied to essential glycoproteins isolated from biological sources.

This protocol is intended for O-linked glycan analysis of whole glycoprotein extracts or of a specific glycoprotein of interest resolved by SDSPAGE and is composed of three experimental procedures; A) gel clean-up, B) in-gel reductive β-elimination, and C) glycan permethylation. The goal is to obtain comprehensive O-linked glycomic data for glycoproteins harvested from primary sources of biological interest (Figure 1). Glycoproteins separated by SDS-PAGE are visualized by staining and bands of interest are excised and the resulting gel band is sliced into small pieces. The gel pieces are destained and subjected to ethyl acetate washes to remove gel contaminants (Figure 2A). Glycan release is achieved by in-gel reductive β-elimination (Figure 2B) and the released glycans are permethylated. Aqueous-organic extraction following permethylation quantitatively partitions the anionic sulfated glycans away from non-sulfated neutral glycans (Figure 2C). In-gel reductive β-elimination coupled to aqueous-organic extraction enables the characterization of O-linked glycans and sulfoglycans released from small amounts of glycoprotein separated by

SDS-PAGE. The strategic overview is summarized in Figure 1 and the details are shown in Figure 2. In addition, a portion of the destained and washed gel pieces can be used for protein ID by standard LC-MS/MS proteomic techniques.

Protocol Text

Lab Safety Concerns

All organic solvents must be stored in appropriate locations.

All waste materials must be kept in chemical waste containers with clear labeling of chemical compositions.

Several reagents used are potential carcinogens. These reagents must be handled in a fume hood with ventilation.

Personal protective equipment such as gloves, lab coat, and eye protection should be worn when working with organic solvents.

Strategic Overview

This protocol is intended for O-linked glycan analysis of whole glycoprotein extracts or of a specific glycoprotein of interest resolved by SDS-PAGE and is composed of three experimental procedures; A) gel clean-up, B) in-gel β-elimination, and C) glycan permethylation. The strategy is designed to

obtain glycomic data for glycoproteins of interest harvested from biological material (**Figure 4.1**). Target glycoproteins separated and visualized by either Coomassie or silver staining on SDS-PAGE are then excised and the resulting gel band is sliced into small pieces. Following destaining and ethyl acetate wash (**Figure 4.2A**), O-linked glycans are released from the gel pieces by in-gel β-elimination (**Figure 4.2B**). Released glycans are permethylated and aqueous-organic extraction at the end of the permethylation reaction results in quantitative partition of sulfated and non-sulfated neutral glycans into the aqueous and organic phases, respectively (**Figure 4.2C**). The in-gel β-elimination and aqueous-organic extraction strategy enabled characterization of O-linked glycans with and without sulfate group harvested from small amounts of glycoprotein separated by SDS-PAGE. The strategic overview is summarized in **Figure 4.1** and the details are shown in **Figure 4.2**. In addition, a portion of the destained and washed gel pieces can be used for protein ID by standard LC-MS/MS proteomic techniques.

Figure 4.1: Procedure for in-gel O-glycomics.

(A) Proteins of interest are resolved by SDS-PAGE, detected by appropriate staining procedures (Coomassie or silver), and excised. Excised gel pieces are sliced into small cubes, destained, and washed with ethyl acetate to reduce contaminants that interfere with subsequent MS analysis. A portion of the gel slice can be reserved for in-gel tryptic digestion and subsequent proteomic characterization by LC-MS/MS. (B) O-linked glycans are released from resolved glycoproteins by in-gel reductive β-elimination. Essential steps include desalting and borate removal by azeotrope with methanol. (C) O-linked glycans released by reductive β-elimination are permethylated and subsequently partitioned into aqueous and organic phases. Sulfoglycans are quantitatively recovered in the upper (aqueous) phase while neutral and sialylated glycans partition into the lower (DCM) layer.

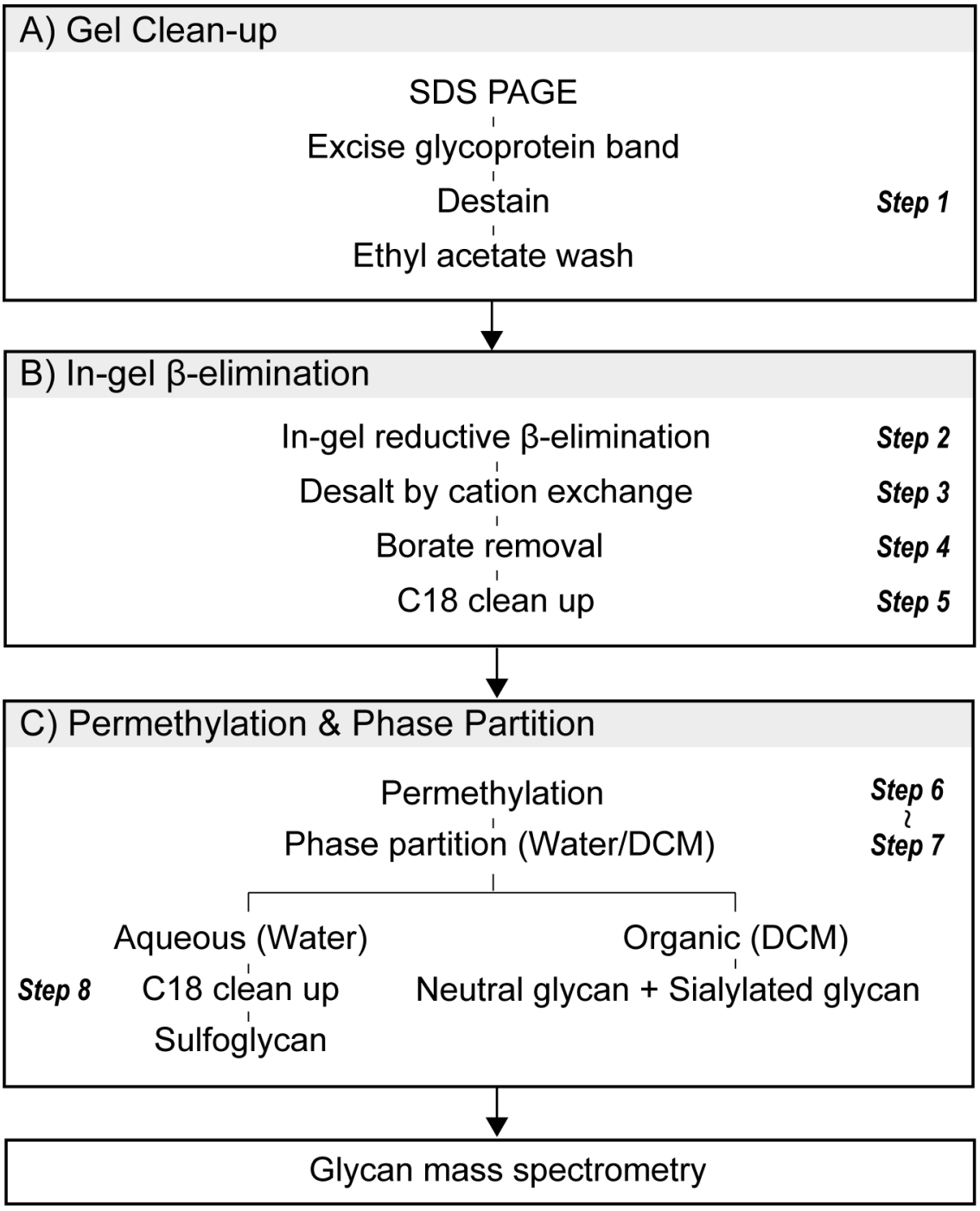
A) Gel Clean-up
SDS PAGE
Excise glycoprotein band
Destain
Ethyl acetate wash
Step 1
B) In-gel β-elimination
In-gel reductive β-elimination
Step 2
Desalt by cation exchange
Step 3
Borate removal
Step 4
C18 clean up
Step 5
C) Permethylation & Phase Partition
Permethylation
Step 6
Phase partition (Water/DCM)
Step 7
Aqueous (Water)
Organic (DCM)
Step 8
C18 clean up
Neutral glycan + Sialylated glycan
Sulfoglycan
Glycan mass spectrometry

Figure 4.2: Detail flow chart for in-gel glycomics.

Each experimental step shown in Figure 1 is individually illustrated. (A) gel destaining and EtOAc extraction, (B) direct in-gel reductive β-elimination for O-linked glycan release, and (C) permethylation and phase partition.

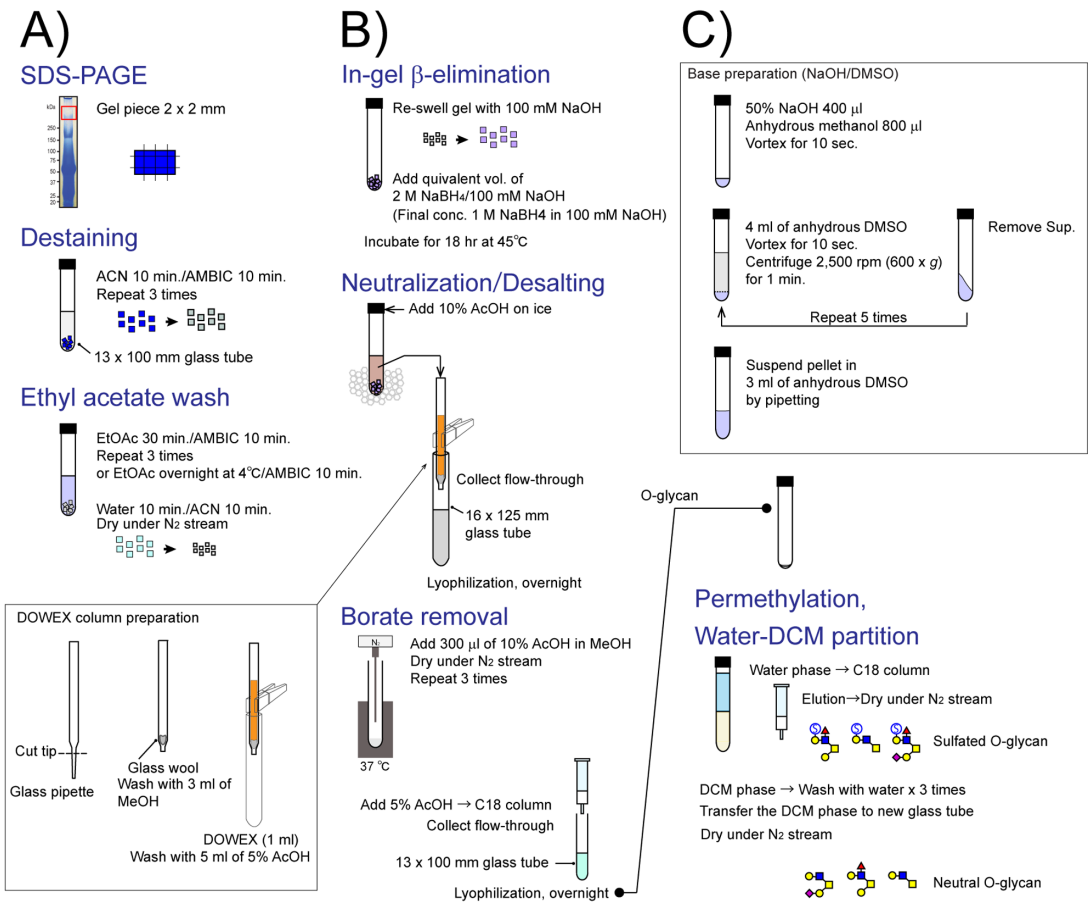

The following protocol describes a method to remove gel-derived contaminants by a simple washing process (**Figure 4.2A**).

1. Gel Excision and Removal of Gel-Derived Contaminants

1.1) Before starting the procedure, prepare chemicals and reagents listed in Table 1.

1.2) Resolve protein on SDS-PAGE gel and stain with either Coomassie Brilliant Blue (Bio-Rad) or Silver Stain (Pierce).

1.3) After electrophoresis, place the gel on a glass plate and excise the region of interest using a clean scalpel or razor blade.

1.4) To increase yield of O-glycans, transfer the gel band of interest onto another glass plate and cut the excised gel piece into approximately 2 mm cubes. Avoid making gel pieces smaller than 1 mm cubes because glycan recovery is reduced. Transfer the small gel pieces into a screw top glass tube (13 x 100 mm) with a stainless steel microspatula.

1.5) Add 1 ml of 25 mM ammonium bicarbonate (AMBIC, NH_4HCO_3) to the sample tube, cap the glass tube with a Teflon-lined screw top cap, and gently mix by flicking the tube before letting stand for 10 min. Do not employ vigorous agitation in order to avoid ripping the gel piece.

1.6) Carefully remove AMBIC from the glass tube using either a Pasteur glass pipette or a pipette equipped with an extra long plastic tip. Avoid smashing and transferring the small gel pieces while removing the AMBIC solution.

1.7) Add 1 ml of acetonitrile (ACN) to the glass tube, cap, and gently mix by flicking tube before letting stand for 10 min. The gel pieces should become dehydrated and may stick to the glass tube.

1.8) Pipette off ACN from the glass tube and repeat steps 1.5 - 1.7 until the bright blue color is eliminated; a minimum of five sequential AMBIC/ACN washes may be required. For silver stained gels, use destain kit (Pierce). Proceed to the next step when the gel piece turns uniformly white while in ACN.

1.9) Pipette off any liquid from the glass tube, recap the tube, add 1ml AMBIC and let stand for 5 min.

1.10) Remove AMBIC and add 2 ml of ethyl acetate (EtOAc) to the glass tube. Recap tube with Teflon-lined cap and place at 4 °C overnight with end-over-end agitation or alternatively perform three EtOAc washes at room temperature for 30 min each. The longer the EtOAc wash, the more efficient the removal of contaminants.

1.11) Remove the final EtOAc wash and perform three washes each with 2 ml of H_2O. Complete EtOAc removal will ensure a robust reductive β-elimination reaction.

1.12) Pipette off H_2O and dehydrate the gel by washing once with 1 ml of ACN. After drying, the dehydrated gels are ready for in-gel β-elimination. Dehydrated gel pieces can be stored at -20 °C until use.

The washing process can be stopped at any step and the gel pieces can be stored at 4 °C overnight, regardless of which buffer or solution is applied to the gel (AMBIC, ACN, H_2O). Sample preparation can be re-started anytime within the next 2 days.

Note: A portion of the destained and dehydrated gel pieces can be used for protein ID by standard proteomic approaches.

The following protocol describes a method for releasing O-linked glycoprotein glycans by in-gel reductive β-elimination (**Figure 4.2B**). After allowing the β-elimination reaction to proceed for 18hr, the desalting process must be performed within the same day.

2. In-Gel O-glycan Release by Reductive β-Elimination

2.1) Prepare a stock solution of 1 M sodium hydroxide (NaOH) using 50% NaOH (Fisher Scientific) or solid NaOH and store at 4 °C until use. Take 5.2 ml of

50% NaOH (or 4 g of solid NaOH) and adjust volume to 100 ml to make 1 M NaOH solution. Dilute the 1 M NaOH stock solution to 100 mM NaOH, which can be stored at 4 °C up to 6 months without loss of efficiency in reductive β-elimination reactions.

2.2) Make 2 M sodium borohydride ($NaBH_4$) in 100 mM NaOH. Dissolve 38 mg of $NaBH_4$ in 0.5 ml of 100 mM NaOH. Generally, 0.5 – 1.0 ml of the borohydride solution will be used for each sample. The volume of the reaction solution depends on the amount of dried gel pieces prepared in step 1. Expect to use 0.5 ml of borohydride solution for 1 - 2 excised gel pieces (step 1.3).

2.3) Add 500 µL of 100 mM NaOH to the dehydrated gel pieces and let stand for 3 - 5 min on ice in order to equilibrate the gel to the basic conditions that enhance glycan recovery.

2.4) Add 500 µL of 2 M $NaBH_4$ in 100 mM NaOH, resulting in final concentrations of 1 M $NaBH_4$ in 100 mM NaOH. Gently mix the tube and incubate at 45 °C for 18 hr. During the first hour of incubation, gently mix the tube every 15 min. Avoid strong agitation, because it may rip the gel pieces. The reaction can be performed in a well-equilibrated incubator/oven or in a heating block. The gel pieces must be covered with reaction solution.

2.5) Stop the reaction by removing the sample tube from the incubator or heating block and placing it on ice.

3. Desalting on Cation-Exchange Chromatography

3.1) While maintaining the sample tube on ice to prevent excessive heat formation, slowly add 10% acetic acid (AcOH) dropwise to neutralize. Gently vortex the sample tubes between additions of AcOH. The addition of acid will produce a “volcano” of bubbles so be careful to add acid slowly and dropwise. It may be necessary to centrifuge the tube to eliminate bubbles and prevent spillover.

3.2) In order to remove the large amount of sodium in the reaction mixture, the reaction mixture is passed through a small cation-exchange column (Dowex or AG-50W-X8 resin, H^+ form). The cation exchange resin should be washed with 1 M NaOH and 1 M HCl prior to column chromatography in order to remove contaminants that interfere with MS analysis, even if the resin is of analytical grade. Briefly, soak the resin in 1 M NaOH and remove solution by decantation. Add de-ionized water, remove water, and then add 1 M HCl. Repeat these steps until the solution above the resin is colorless. Wash the cleaned resin with deionized water and store in 5% AcOH at 4 °C.

3.3) To make a small glass column, scratch and break the tip of a Pasteur glass pipette using a ceramic cutter (Alltech Fused Silica Cutter, AT3194) so that the taper of the pipette tip is approximately 1 cm long. Tease apart a plug of glass wool and push towards the tip forming a support for the resin

bed. Secure the pipette column with a clamp or wood spring clothespin and place over a culture tube.

3.4) Wash the empty pipette with 1 ml of methanol (MeOH) and 3 ml of 5% AcOH. Swirl H^+ Dowex or AG50 cation exchange resin slurry stored in 5% AcOH and transfer enough of the slurry to produce a 1 ml bed volume in the Pasteur pipette column.

3.5) Rinse the column using five volumes of 5% AcOH. Check flow through for the appearance of resin particles and do not use the column if resin is detected.

3.6) Place column over a new screw top glass tube (16 x 125 mm) and load sample. Collect the flow through and elute glycans with at least 3 volumes of 5% AcOH into the same tube.

3.7) Cover the tube with parafilm and make tiny holes with a needle. Place the sample tube at -80 °C or on dry ice. Once frozen, dry the sample by lyophilization. The dried material can be stored at -20 °C until use.

4. Borate Removal

4.1) Prepare 10% AcOH in MeOH. Take 10 ml of glacial acetic acid and adjust volume to 100 ml with methanol. This reagent can be stored in a glass bottle with Teflon-lined cap for up to 6 months.

4.2) Add 300 µL of 10% AcOH in MeOH to the dried, lyophilized sample tube and vortex. Mixing borate salts with methanol under acidic conditions produces trimethyl borate, which is a volatile compound and can be readily removed by evaporation under a N_2 stream.

4.3) Dry under N_2 stream at 37 °C. After drying, add another aliquot of AcOH in MeOH as described in step 4.2. The liquid can be dried in 5 min under nitrogen (N_2) stream at 37 °C. Repeat suspension and drying at least 3 times. The dried material can be stored at -20 °C until use.

The dried material contains contaminating amino acids and small peptides produced from glycoprotein by chemical side-reactions that potentially interfere with MS analysis. The following C18 clean-up step will improve the quality of the MS analysis.

5. C18 Clean-Up

5.1) Equilibrate a C18 cartridge column (Bakerbond C18, size 1 ml, 100 mg or comparable) using three volumes of ACN and five volumes of 5% AcOH. Passage of the equilibrating solutions can be accelerated by application of mild positive pressure using airflow.

5.2) Add 500 µL of 5% AcOH to the desalted and borate-free sample tube and dissolve by vortex.

5.3) Load resuspended sample onto the equilibrated C18 column and collect the flow through into a glass screw cap tube (13 x 100 mm). Elute O-glycans with 3 ml of 5% AcOH into the same tube.

5.4) Parafilm the tube, make small holes with a small needle, and freeze the sample at -80 °C or on dry ice. Remove solvent by lyophilization.

The dried sample is ready for permethylation and can be stored at -20 °C until use.

The following procedures describe small-scale permethylation reactions prior to MS analysis (**Figure 4.2C**). In order to achieve robust permethylation, NaOH slurry must be freshly prepared and all glassware must be scrupulously cleaned.

6. Base Preparation for Permethylation

6.1) To prepare the base reagent for permethylation, add 400 µL of 50% NaOH to a clean glass screw-top tube (13 x 100 mm). Add 800 µL of anhydrous MeOH and vortex.

6.2) Add 4 ml of anhydrous dimethyl sulfoxide (DMSO) and vortex. A white precipitate will be generated.

6.3) Centrifuge at 2,500 rpm (600 x *g*) for 1 min to pellet the basic slurry. Pipette off supernatant and the non-pelleted white material.

6.4) Repeat step 6.2 and 6.3 a minimum of three more times or until no white precipitate forms.

6.5) Dissolve the pelleted base in 3 ml anhydrous DMSO and gently mix by pipetting up-and-down with a clean Pasteur pipette.

The base should be used immediately for the following permethylation reaction and cannot be stored.

7. Permethylation of Released Glycans

7.1) Add 200 µL of anhydrous DMSO to the C18-purified sample and vortex. Make sure all clumps are broken up and suspended before proceeding further.

7.2) Add 300 µL of the resuspended base slurry to the sample and immediately add 100 µL of iodomethane (MeI). Seal tube with Teflon-lined cap and vigorously mix for 5 min by vortex.

7.3) To stop the permethylation reaction, add 2 ml of 5% AcOH on ice and vortex. To remove excess MeI, bubble off the solution by pipetting. The AcOH neutralizes the solution and removal of MeI increases the extraction efficiency of sulfated glycans into the water phase during the phase-partition.

7.4) Add 2 ml of dichloromethane (DCM) and vortex. Centrifuge at 2,500 rpm (600 x *g*) for 1 min at room temperature to separate the aqueous and organic phases.

7.5) Transfer the top layer (aqueous phase) into a new glass tube (13 x 100 mm). This phase contains the majority of permethylated sulfated glycans.

7.6) Add 2 ml of H_2O to the organic phase and vortex. Centrifuge at 2,500 rpm (600 x *g*) for 1 min to separate the aqueous and organic phases and combine this second aqueous phase with the first aqueous phase (step 7.5).

7.7) Repeat step 7.6 and 7.5 three more times, but there is no need to save the aqueous phases resulting from the subsequent partitions.

7.8) Remove the final top layer (aqueous phase) as much as possible from the bottom layer (organic phase) and transfer the bottom layer (organic phase) into a separate new glass tube using clean Pasteur pipette.

7.9) Dry the organic phase under N_2 stream at 42 °C.

7.10) Cover the tube with parafilm and store at -20 °C until use.

The combined aqueous phase needs to be desalted by C18 column prior to MS analysis.

8. C18 Clean-Up of Permethylated Sulfated O-glycans from the Aqueous Phase

8.1) Equilibrate a C18 cartridge column with three volumes of ACN and five volumes of 5% AcOH.

8.2) Load the aqueous phases collected and combined from steps 7.5 and 7.6 onto the column.

8.3) Wash the column with 10 ml of H_2O for desalting.

8.4) Elute the permethylated sulfated O-glycans into a new glass tube with 2 ml of 50% ACN. An additional elution with 85% ACN will enhance recovery of permethylated sulfated O-glycans on larger oligosaccharides.

8.5) Dry eluates under nitrogen stream at 42 °C.

The dried material can be stored at -20 °C up to 6 months prior to MS analysis.

Representative Results

Effect of Ethyl Acetate Treatment Prior to In-Gel Reductive β-Elimination

A representative mass spectra of permethylated O-linked glycan samples released from bovine mucin using in-gel reductive β-elimination is shown in **Figure 4.3**. The EtOAc wash of gel piece effectively removes SDS and polyacryl contaminants which otherwise interfere with MS analysis.

Figure 4.3: Ethyl acetate wash of polyacrylamide gel piece prior to in-gel reductive β-elimination enhances detection of released glycans.

(A) Without wash with ethyl acetate, the mass spectrum of permethylated O-linked glycans released by in-gel β-elimination from bovine submaxillary mucin is dominated by an abundance of a polydisperse contaminant, which almost completely obscures the MS signals associated with O-linked glycans. (B) Washing the gel piece with ethyl acetate eliminates the contaminant peaks, allowing sensitive detection of glycans. Modified from Kumagai (Kumagai et al. 2013).

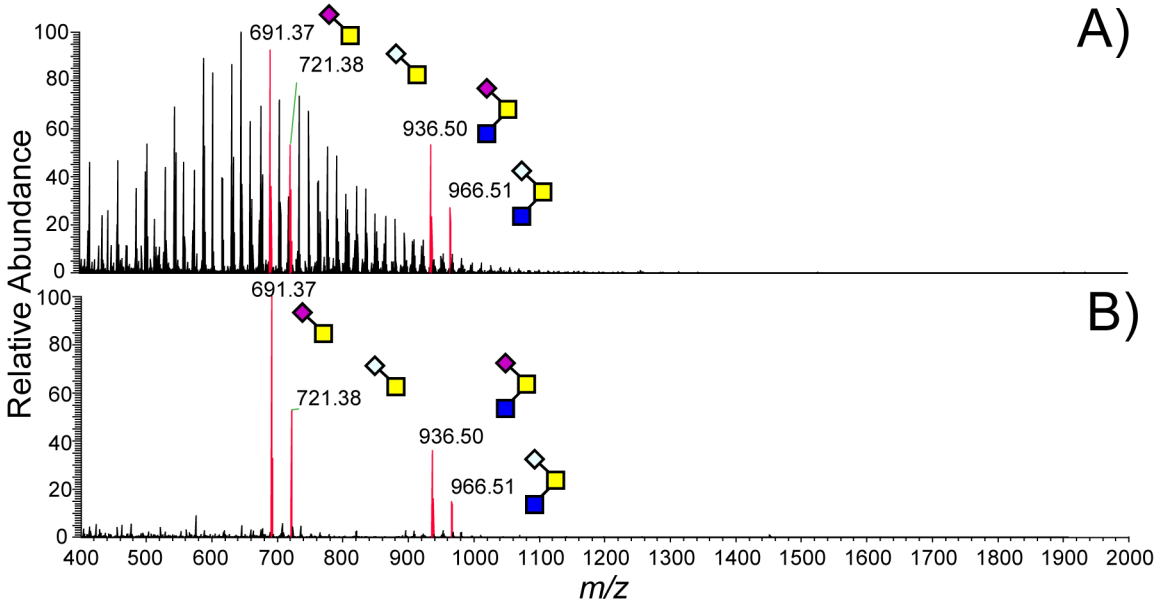

Recovery of O-linked Glycan is Greater from Small Gel Slices.

O-linked glycans were released from bovine submaxillary mucin by in-gel β-elimination using gel pieces that were either sliced small (~2 x 2 mm) or large (~5 x 5 mm). Following permethylation, a known amount of a permethylated external glycan standard (maltotri- and maltotetrasaccharide, Dp3 and Dp4) was added to each to facilitate quantification of glycan recovery. The recovery of O-linked glycans from small gel pieces was almost exhibits 10-fold greater than from large gel slices (**Figure 4.4**).

Figure 4.4: Glycan recovery from small gel pieces is more efficient than from larger pieces.

Small pieces (~2 x 2 mm) yielded more glycan than larger cubes (~5 x 5 mm). Bars show relative signal intensities for the sum of all O-linked glycan structures normalized to the signal detected for an external standard (maltotrisaccharide Dp3, set to 100%), which was added to the released glycan before MS analysis. Values are mean standard deviation for n=3. Modified from Kumagai (Kumagai et al. 2013).

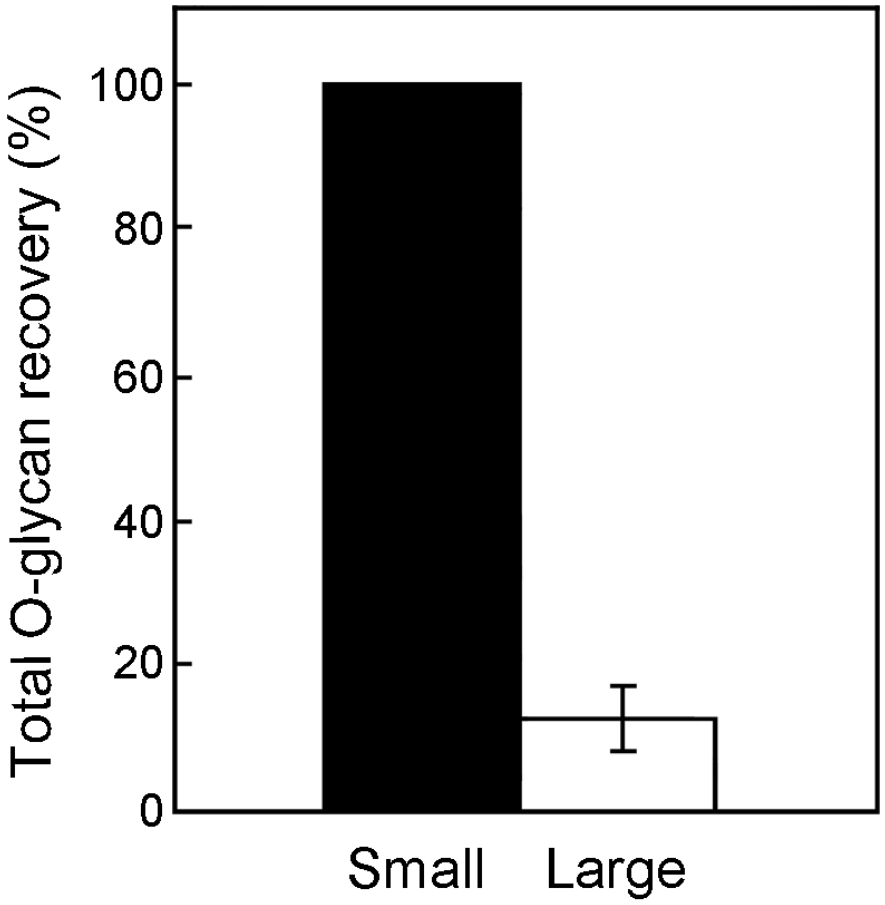

Enrichment of Sulfoglycans by Phase Partition

A permethylated sulfated glycan standard (sulfo-Le^a) was quantitatively recovered in the aqueous phase while permethylated sialylated glycans derived from the mucin glycoprotein partitioned into the DCM phase (**Figure 4.5**). The recovery of each permethylated glycans by aqueous-organic partition was comparable to that of the previously characterized C18 Sep-Pak clean-up method (Yu et al. 2009). But the speed and simplicity of the phase partition method, which quantitatively separates sulfated and non-sulfated permethylated glycan species without need for column chromatography, greatly facilitates sample throughput and subsequent analytic approaches.

Figure 4.5: Differential recovery of sulfo- and sialo-glycans by phase partition.

Bovine mucin glycoprotein was spiked with a known amount of a sulfo-glycan standard (sulfo-Lea) before being subjected to reductive β-elimination. Released glycans were permethylated and the permethylation reaction was adjusted to 1:1:water:DCM. The resulting organic and aqueous phases were separated and analyzed by MS. Glycan recovery was quantified relative to permethylated external glycan standards, which were spiked into the sample before MS analysis. Glycan recoveries into the organic (DCM) and aqueous (Water) phases are shown relative to the external standard, which was set to 100%. Sulfoglycans were undetectable in the organic phase but quantitatively recovered in the aqueous phase. Results represent the mean ± S.E. of three independent experiments. Modified from Kumagai (Kumagai et al. 2013).

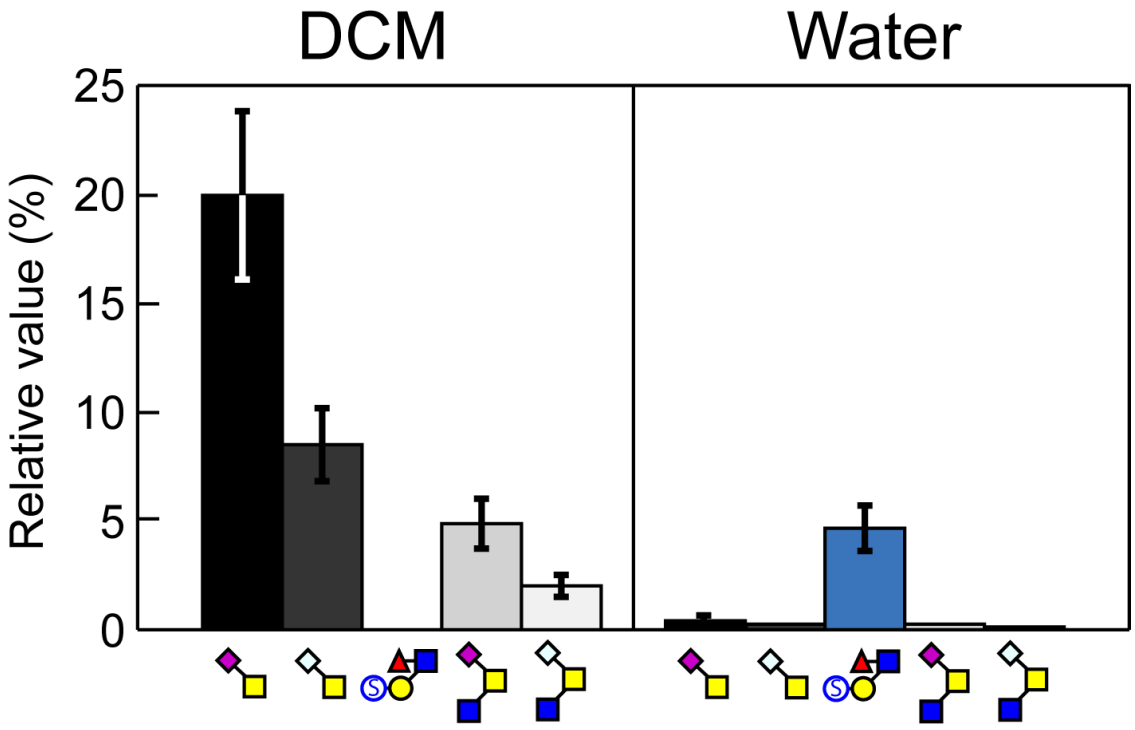

Application to In-Depth Proteomic and Glycomic Analyses in Biological Samples

Human saliva proteins were separated by SDS-PAGE and stained with Coomassie Brilliant Blue (G-250). A high molecular weight protein at MW ~600 kD was excised from the gel. A portion of the gel slice was subjected to in-gel tryptic digestion followed by LC-MS/MS based proteomic analysis, which validated the assignment of this band as MUC5B (Thomsson et al. 2002; Thomsson et al. 2005). The remainder of the gel piece was subjected to in-gel β-elimination for O-glycan analysis. Following permethylation and aqueous-organic phase partition (Water:DCM::1:1), permethylated glycans in the aqueous and organic phases were analyzed by NSI-MS. Non-sulfated permethylated O-glycans were almost exclusively recovered from the organic phase and all of the permethylated sulfoglycans were recovered from the aqueous phase, which facilitates the identification and characterization of nearly isobaric sulfated and non-sulfated glycans, e.g., $Fuc_1Hex_3HexNAc_2GalNAc\text{-}ol$ (m/z=1606.8, $[M+Na]^+$) and $(SO_3)_1NeuAc_1Fuc_1Hex_2HexNAc_1GalNAc\text{-}ol$ (m/z=1606.7, $[M+2Na-H]^+$) differ by only 0.1 mass units and would be difficult to resolve without physically separating the two species by phase partition (**Figure 4.6**).

Figure 4.6: Detection of isobaric complexity in neutral and sulfo-glycans separated by aqueous-organic partition.

MS^2 fragmentation patterns obtained from parent ions detected by total ion mapping (TIM) analysis of permethylated O-glycans released from human salivary mucin by in-gel β-elimination and water:DCM partition following permethylation. (A) MS^2 from TIM analysis of DCM phase for a 2.8 mass unit window around m/z = 1608. (B) The MS^2 spectrum of the same mass window for TIM analysis of the water phase. In the DCM-phase, the major fragment ions correspond to loss of Hex_1-O (m/z 1370.8), $Fuc_1Hex_3HexNAc_2$+Na (1331.8), loss of Fuc_1Hex_1-O (1196.7), loss of $Hex_1HexNAc_1$ (1143.6), loss of $Fuc_1Hex_1HexNAc_1$ (969.5), loss of $Fuc_1Hex_2HexNAc_1$-O (747.4), $Fuc_1Hex_1HexNAc_1$+Na (660.4), and $Hex_1HexNAc_1$+Na (486.3). Based on these fragment ions, a mixture of non-sulfated structures with a composition of $Fuc_1Hex_3HexNAc_2GalNAc$-ol is proposed as shown to the right of the spectrum. In contrast, the major fragment ions for the water phase are loss of SO_3Na (1486.8), loss of NeuAc (1231.5), loss of Fuc_1Hex_1-O (1196.7), loss of combination of NeuAc and SO_3Na (1111.8), and loss of $NeuAc_1Hex_1$-O (1009.4). A mixture of sulfated structures with a composition of $(SO_3^-)_1NeuAc_1Fuc_1Hex_2HexNAc_1GalNAc$-ol is proposed. Without physical separation of the neutral and sulfoglycans by phase partition, interpreting MS^2 spectra of such mixtures is significantly more challenging. Modified from Kumagai (Kumagai et al. 2013).

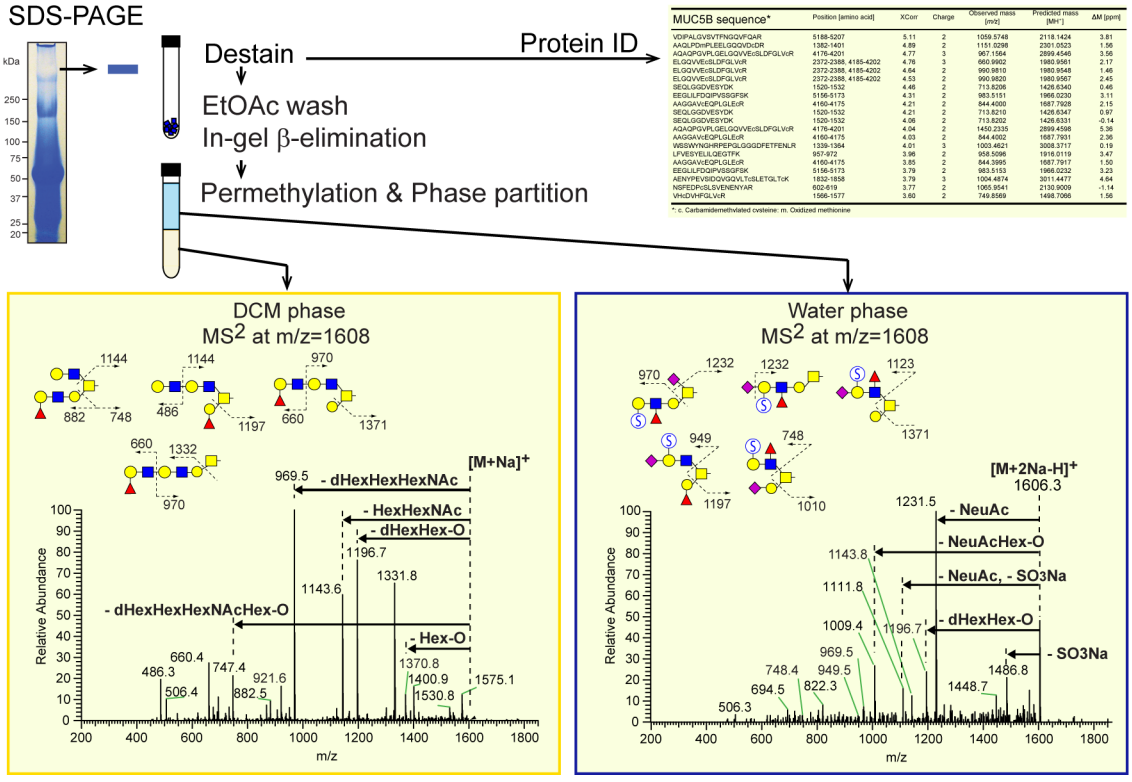

Discussion

Combining in-gel reductive β-elimination with aqueous-organic extraction enhances the sensitivity and depth of structural data that can be acquired for characterizing sulfated and non-sulfated O-linked glycans harvested from small amounts of mucin-type glycoproteins resolved from other proteins by SDS-PAGE. The essential advances of the technical approaches presented in this study are: (a) facile removal of gel-derived contaminants by simple washing steps (b) quantitative recovery of permethylated sulfoglycans in the aqueous phase following a rapid water-DCM partition. The workflow described here dramatically improves the sensitivity of detection for sulfated and non-sulfated glycans released from glycoproteins expressed at physiological levels in biological samples.

While the methods described here are robust and highly reproducible when applied with careful attention to standard analytic practices, a few considerations regarding possible sources of contamination are worth a brief mention. Ensuring that all glassware is exceptionally clean and free of dust and detergent is critical. Upon noticing contaminant peaks in MS spectra, all glassware should be washed thoroughly and rinsed with MeOH prior to final drying. Another source of contamination is the use of rubber-lined screw caps in place of PTFE-lined caps, which lack the required resistance to organic chemicals resulting in samples contaminated with an interfering polymeric compound. Although this protocol was specifically designed with the intention of utilizing MSn analysis by NSI-MS on an ion trap instrument, other types of mass

spectrometers, such as MALDI-TOF/TOF can be also applied to dissecting sulfoglycoforms in biological materials using the preparative methods described here.

In comparison to other methodologies currently in use for in-gel glycan release and analysis, the techniques described here do not require HPLC separation prior to MS analysis and are applicable to permethylated glycans, producing greater structural characterization than can be extracted from non-derivatized samples. Moreover, the methods described here are capable of separating permethylated forms of sulfated O-glycans from non-sulfated neutral and sialylated O-glycans by a simple phase partition. The optimized sample clean-up and simple phase partition methodologies minimize sample manipulation and losses that can occur through chromatography steps. Methods requiring greater sample handling may lead to an underestimate of sulfoglycan diversity due to losses during work-up. Furthermore, detection of permethylated sulfated glycans in negative mode is significantly less sensitive than detection of permethylated glycans in positive mode. Desulfation of permethylated sulfoglycans by solvolysis specifically removes sulfate groups, leaving naked hydroxyls that can be subsequently permethylated with deuterated methyl iodide, increasing MS-signal intensities approximately 5-fold and providing a unique isotopic mass tag at the site of sulfation (Kumagai et al. 2013).

References

Anumula, K.R. and Taylor, P.B. (1992). "A comprehensive procedure for preparation of partially methylated alditol acetates from glycoprotein carbohydrates." Anal Biochem **203**(1): 101-108.

Aoki, K., Perlman, M., Lim, J.M., Cantu, R., Wells, L. and Tiemeyer, M. (2007). "Dynamic developmental elaboration of N-linked glycan complexity in the Drosophila melanogaster embryo." J Biol Chem **282**(12): 9127-9142.

Aoki, K., Porterfield, M., Lee, S.S., Dong, B., Nguyen, K., McGlamry, K.H. and Tiemeyer, M. (2008). "The diversity of O-linked glycans expressed during Drosophila melanogaster development reflects stage- and tissue-specific requirements for cell signaling." J Biol Chem **283**(44): 30385-30400.

Ashline, D., Singh, S., Hanneman, A. and Reinhold, V. (2005). "Congruent strategies for carbohydrate sequencing. 1. Mining structural details by MSn." Anal Chem **77**(19): 6250-6262.

Ashline, D.J., Lapadula, A.J., Liu, Y.H., Lin, M., Grace, M., Pramanik, B. and Reinhold, V.N. (2007). "Carbohydrate structural isomers analyzed by sequential mass spectrometry." Anal Chem **79**(10): 3830-3842.

Domon, B. and Costello, C.E. (1988). "A systematic nomenclature for carbohydrate fragmentations in FAB-MS/MS spectra of glycoconjugates." Glycoconjugate Journal **5**(4): 397-409.

Hellman, U., Wernstedt, C., Gonez, J. and Heldin, C.H. (1995). "Improvement of an "In-Gel" digestion procedure for the micropreparation of internal protein fragments for amino acid sequencing." Anal Biochem **224**(1): 451-455.

Kozak, R.P., Royle, L., Gardner, R.A., Fernandes, D.L. and Wuhrer, M. (2012). "Suppression of peeling during the release of O-glycans by hydrazinolysis." Anal Biochem **423**(1): 119-128.

Kumagai, T., Katoh, T., Nix, D.B., Tiemeyer, M. and Aoki, K. (2013). "In-gel beta-elimination and aqueous-organic partition for improved O- and sulfoglycomics." Anal Chem **85**(18): 8692-8699.

Kuster, B. and Mann, M. (1999). "18O-labeling of N-glycosylation sites to improve the identification of gel-separated glycoproteins using peptide mass mapping and database searching." Anal Chem **71**(7): 1431-1440.

Kuster, B., Wheeler, S.F., Hunter, A.P., Dwek, R.A. and Harvey, D.J. (1997). "Sequencing of N-linked oligosaccharides directly from protein gels: in-gel deglycosylation followed by matrix-assisted laser desorption/ionization mass spectrometry and normal-phase high-performance liquid chromatography." Anal Biochem **250**(1): 82-101.

Lapadula, A.J., Hatcher, P.J., Hanneman, A.J., Ashline, D.J., Zhang, H. and Reinhold, V.N. (2005). "Congruent strategies for carbohydrate sequencing. 3. OSCAR: an algorithm for assigning oligosaccharide topology from MSn data." Anal Chem **77**(19): 6271-6279.

Lowe, J.B. and Marth, J.D. (2003). "A genetic approach to Mammalian glycan function." Annu Rev Biochem **72**: 643-691.

Morelle, W., Canis, K., Chirat, F., Faid, V. and Michalski, J.C. (2006). "The use of mass spectrometry for the proteomic analysis of glycosylation." Proteomics **6**(14): 3993-4015.

Moremen, K.W., Tiemeyer, M. and Nairn, A.V. (2012). "Vertebrate protein glycosylation: diversity, synthesis and function." Nat Rev Mol Cell Biol **13**(7): 448-462.

Mortz, E., Sareneva, T., Haebel, S., Julkunen, I. and Roepstorff, P. (1996). "Mass spectrometric characterization of glycosylated interferon-gamma variants separated by gel electrophoresis." Electrophoresis **17**(5): 925-931.

Ohtsubo, K. and Marth, J.D. (2006). "Glycosylation in cellular mechanisms of health and disease." Cell **126**(5): 855-867.

Rosenfeld, J., Capdevielle, J., Guillemot, J.C. and Ferrara, P. (1992). "In-gel digestion of proteins for internal sequence analysis after one- or two-dimensional gel electrophoresis." Anal Biochem **203**(1): 173-179.

Schulz, B.L., Packer, N.H. and Karlsson, N.G. (2002). "Small-scale analysis of O-linked oligosaccharides from glycoproteins and mucins separated by gel electrophoresis." Anal Chem **74**(23): 6088-6097.

Taylor, A.M., Holst, O. and Thomas-Oates, J. (2006). "Mass spectrometric profiling of O-linked glycans released directly from glycoproteins in gels using in-gel reductive beta-elimination." Proteomics **6**(10): 2936-2946.

Thomsson, K.A., Prakobphol, A., Leffler, H., Reddy, M.S., Levine, M.J., Fisher, S.J. and Hansson, G.C. (2002). "The salivary mucin MG1 (MUC5B) carries a repertoire of unique oligosaccharides that is large and diverse." Glycobiology **12**(1): 1-14.

Thomsson, K.A., Schulz, B.L., Packer, N.H. and Karlsson, N.G. (2005). "MUC5B glycosylation in human saliva reflects blood group and secretor status." Glycobiology **15**(8): 791-804.

Varki, A. (1993). "Biological roles of oligosaccharides: all of the theories are correct." Glycobiology **3**(2): 97-130.

Washburn, M.P. (2004). "Utilisation of proteomics datasets generated via multidimensional protein identification technology (MudPIT)." Brief Funct Genomic Proteomic **3**(3): 280-286.

Yan, A. and Lennarz, W.J. (2005). "Unraveling the mechanism of protein N-glycosylation." J Biol Chem **280**(5): 3121-3124.

Yu, S.Y., Chang, L.Y., Cheng, C.W., Chou, C.C., Fukuda, M.N. and Khoo, K.H. (2013). "Priming mass spectrometry-based sulfoglycomic mapping for identification of terminal sulfated lacdiNAc glycotope." Glycoconj J **30**(2): 183-194.

Yu, S.Y., Wu, S.W., Hsiao, H.H. and Khoo, K.H. (2009). "Enabling techniques and strategic workflow for sulfoglycomics based on mass spectrometry mapping and sequencing of permethylated sulfated glycans." Glycobiology **19**(10): 1136-1149.

CHAPTER 5

Conclusions and Future Directions

The work described herein is defined by two main themes: glycosylation of secretory epithelium and the impact this has on the inflammatory response from innate immune cells. The inflammatory response is often thought to, by default, be pro-inflammatory. It is becoming increasingly appreciated that inflammation is a significant contributing factor in most disease states, and that dampening the inflammatory response, or promoting anti-inflammatory activity, is critical to efficient therapy. No two organs or tissues will have the same change in glycosylation in response to a stimulus, but that isn't surprising since glycosylation is very often tissue specific. Tissue specific glycosylation is a reoccurring theme that holds true between different tissues in the same organism, but is also true for the same tissue from different species.

Here I present data that shows two tissues modifying their glyco-terrain – how choroid plexus is modified under chronic neuroinflammation and how airway bronchus changes during differentiation – when analyzed under certain conditions. Both stories are punctuated by an increase in anti-inflammatory glycan epitopes but for very different reasons. For AD brains under persistent stress it is believable to see an increase in these epitopes, albeit for unknown reasons and having currently unknown consequences, but logical nonetheless.

The increased expression for airway bronchus is more peculiar. It could be reasoned that any attempt to antagonize normal growth, thereby hampering proper development, would be counter productive for the cell. Currently, there is not a complete understanding of how cells or tissues change their glycosylation during development making these data important. Having a more complete view of the glyco-terrain and how it changes during development would provide insight into why these epitopes are important. It is currently known how these particular epitopes influence innate immune cells in the airway. What isn't known, and what I propose here, is how these epitopes may influence innate immune cells in the CNS.

Siglec-F may regulate the inflammation status in AD at the Choroid Plexus

Chapter two describes a change in brain glycosylation. These changes can be seen in the whole forebrain as a decrease in N-glycosylation, an increase in FOS - which likely results from ERAD - and a trend towards an increase in lactosylceramide and decrease in GD1 for AD mice. The increase in FOS suggests a disruption of the quality control mechanism in the ER for ensuring proper protein folding. Unfolded proteins are marked for degradation by the sequential and specific removal of mannose residues before being shuttled to the cytosol. Removal of the glycan is done by endo-β-*N*-acetylglucosaminidase (ENGase), producing a free oligosaccharide with a single GlcNAc at the reducing end (Overdijk et al. 1981; Chantret and Moore 2008). This points towards a general defect in protein glycosylation and protein homeostasis that cannot be

the result of changes in glycosyltransferase expression or localization (**Figure 5.1-5.2)** (Xiang et al. 2013). The decrease in N-glycans has other implications as well; many of the decreases observed are potential ligands for sialic acid binding immunoglobulin like lectins, or Siglecs. Probing frozen sections revealed a specific increase in ligands for Siglec-F at the choroid plexus in AD mice. This increase in ligand does not correspond to an increase in microglia at the epiplexus surface as would be expected. Interestingly, the cell type expressing Siglec-F is blood-derived macrophages that are extravasating and radiating away from the choroid plexus. These macrophages are activated as M2 type, or anti-inflammatory, and are uniquely capable of migration through the choroid plexus (Shechter et al. 2013). A major determinate in the activation and migration of macrophages is LRP1. Macrophages are primed toward M2 activation status (May et al. 2013) and interact with integrins for extravasation through LRP1 (Ranganathan et al. 2011), which was specifically increased at the basal surface of choroid plexus in AD mice. These data suggest a pleiotropic role for LRP1 in AD: both the priming of anti-inflammatory leukocytes and the recruitment of these primed leukocytes to the CNS for increased immune surveillance. Once these leukocytes, specifically M2 macrophages, are in the choroid plexus they can interact with the increased glycan ligand for Siglec-F that appears to be sporadically added to LRP1. This sporadic and uncontrolled addition of glycans is likely an incorrect paradigm, yet is widely accepted since there are many inconsistencies in glycosylation that do not have an accepted explanation. For example, not all sequons for N-linked glycosylation are occupied on any given

protein, nor is the specific glycan found at a sequon always the same. This microheterogeneity is commonly observed but not well described since analytical techniques are only now becoming sufficient to accurately quantify the phenomenon. Therefore, why LRP1 is differentially glycosylated at the apical surface is unknown. In addition, why LRP1 doesn't show increased expression at the apical surface is also unknown. It may be that LRP1 is very rapidly shed into the CSF preventing an accumulation at the apical surface, much is still uncertain. Regardless, this interaction has the potential to modulate the inflammatory milieu in an attempt to limit the damage from Aβ induced neurotoxicity. Given the current state, there are four directions for future work that will be outlined next.

Activation of naïve monocytes by differentially glycosylated LRP1

To determine the role differentially glycosylated LRP1 plays in the activation of macrophages we are employing a cell culture model. Here, we will isolate bone marrow mesenchymal stem cells from WT and Siglec-F $^{-/-}$ mice and culture them *in vitro*. These cells can be pushed towards a monocyte lineage by addition of macrophage colony stimulating factor (M-CSF) and further differentiated towards both M1 and M2 state macrophages using unique cytokines for each. Using these cells we would test naïve monocytes, M1, and M2 macrophages for altered cytokine secretion and cell fate by addition of LRP1 isolated from both AD and WT mice (**Figure 5.3**). We hypothesize that LRP1 isolated from AD mice will elicit a unique phenotype from naïve monocytes and cement the M2 status for cells isolated from WT mice. We also hypothesize that

cells isolated from Siglec-F $^{-/-}$ mice will not show the same cytokine secretion profile as those from WT mice. If successful, this experiment will implicate LRP1 and Siglec-F in the regulation of inflammation in Alzheimer's disease through increased CNS immune surveillance.

Immune surveillance of the CNS has received increased attention lately due to recent findings concerning regulatory T-cell activation and interaction with microglia (Baruch et al. 2013; Baruch et al. 2015). Here, T-regs are responsible for influencing microglial status and increasing the extravasation of macrophages into the CNS through the choroid plexus. This highlights the importance of the choroid plexus, again marking it as a unique and understudied cell type, and reinforces the idea of immune modulation in neurological disease.

Determining the major carrier of Siglec-F ligand

Confocal analysis of frozen sections showed a dramatic increase in the ligands for Siglec-F at the choroid plexus in AD. A carrier for this epitope was identified as LRP1 by LC-MS/MS following an in-gel digest of Siglec-F-Fc IP. Unfortunately, if frozen sections are double stained for LRP1 and Siglec-F-Fc there is very little colocalization, demonstratively showing that there are other proteins modified with the epitope that are still unknown. This isn't surprising since the proteomic identification also contained versican (**Figure 2.3)**. Additionally, when whole cell lysate is probed by Siglec-F-Fc overlay there is an additional nine bands visible (**Figure 5.4)**. The large banding above 250-kD appears to be the largest carrier of the epitope but our current efforts have not

proven this to be true. It may, however, carry an epitope with the highest affinity for Siglec-F. To better understand the nature of these ligands, enzymatic and chemical treatments with PNGaseF, sialidase, α2-3 specific sialidase, and solvolysis were used on lysate and probed with lectins. Many of the bands visible by Siglec-F-Fc overlay can also be visualized using MAA (binds α2-3 sialic acid) and SNA (binds α2-6 sialic acid) (**Figure 5.4)**. Identification of these proteins will require additional preparation since their molecular weights will not allow in-gel digests from whole lysate. Future efforts here should employ multidimensional chromatography to purify the proteins followed by LC-MS/MS for identification. These data will hopefully provide insight into the regulation of the Siglec-F ligand through pathway analysis.

Probing the glyco-terrain of the CSF and Choroid Plexus

Until recently, there was limited knowledge of the CSF proteome. It was assumed that the CSF would be identical throughout the CNS and would not change during development. This is now known to be false. The choroid plexus secretes unique proteins and growth factors into the CSF depending on its location in the ventricular system (Lun et al. 2015). Therefore, we want to understand the glyco-terrain of the CSF and choroid plexus for each ventricle. We propose to isolate both CSF and choroid plexus from adult mice and identify the N- and O-glycans using nanoelectrospray mass spectrometry. An attempt will be made to find and identify GSLs being harbored in extracellular vesicles. Similar to the previously mentioned proteomics data, we hypothesize that there

will be differences in the glycans identified depending on where the sample was taken in the CNS.

Neurodegeneration is not commonly thought of as a developmental disease, yet it has parallels in neuronal development. The process of cortical development and migration from the ventricle apical surface in developing brains is well described (Lehtinen et al. 2011), but its function and efficiency in AD is still debated. Therefore, we also aim to determine the glyco-terrain of CSF and choroid plexus from embryonic mice. We hypothesize that there will be differences between WT adult and embryonic CSF/choroid plexus glycosylation that will be further altered in AD. These data may provide key insights into how neurogenesis is altered in response to changes in glycosylation.

Targeting ciliogenesis for therapy

Cilia formation and function in Alzheimer's disease has not been a main focus for researchers. This is likely due to various reasons but chief among them is the long held belief that new neurons are not formed in the adult brain, which is partially regulated by the role primary cilia play in development. Therefore, a logical role for primary cilia in the brain was not known, especially since it is currently unknown which cells in the human brain have primary cilia. This is now known to be false since there are two main sites of neurogenesis in adult brains: the subgranular zone and the subventricular zone. In 3xtg-AD mice, these granule cells have significantly shortened primary cilia that results in reduced neurogenesis (Rodriguez et al. 2008; Chakravarthy et al. 2012).

Interestingly, the choroid plexus has an unpublished defect in ciliogenesis in 5xFAD mice (**Figure 5.5**). The apical surface of the choroid plexus is highly decorated with non-motile cilia that are thought to regulate CSF production (Damkier et al. 2013). Taken together, these data are intriguing since it has been proposed that a failure to produce CSF results in Alzheimer's disease (Silverberg et al. 2003). Oddly, the association between the CSF and Alzheimer's disease also includes interactions between shed LRP1 and Aβ. When Aβ binds LRP1 at the ChP apical surface the complex is shed by ADAM10 and ADAM17 into the CSF (Liu et al. 2009). This interaction prevents the oligomerization of Aβ thereby reducing the plauqe load in the brain. Therefore, a defect in ciliogenesis in 5xFAD mice - and subsequent decrease in CSF production - would lead to decreased removal of Aβ and increase the plauqe burden.

This ciliogenesis defect has a second complication. Cilia found on ChP are non-motile 9+0 type cilia, and are considered to be primary cilia, that are distinct from the motile 9+2 type cilia found on the ependyma (Narita and Takeda 2015). These non-motile, primary cilia are important for signaling as many molecules important for growth and development are found in the CSF (i.e. FGF, SHH, retinoic acid, LIF) (Guemez-Gamboa et al. 2014; Lun et al. 2015). The ciliogenesis defect will most likely play a role in diminished SHH signaling, which may be affected by differences in glycosylation. In bladder cancer stem cells, glycosylation of SHH by ppGalNT1 was required for signaling to occur and maintain self-renewal and tumorigenesis (Li et al. 2016). Therefore, I also suspect that differences in glycosylation found in 5xFAD forebrains, and

potentially the ChP and CSF, will affect SHH signaling through the primary cilia on choroid plexus.

The regulation of ciliogenesis has been described as a function of actin dynamics (Kim et al. 2010). Blocking the assembly of actin filaments promotes ciliogenesis by stabilizing the pericentrosomal preciliary compartment (PPC), a structure localized to the cilia and recycling endosomes. Pharmacological inhibition of actin assembly can be achieved through addition of a cocktail (latrunculin B, jasplakinolide, and Y27632) of inhibitors to the growth media of HL-60 cells, fibrosarcoma HT1080 cells, and 3T3 fibroblasts (Peng et al. 2011). To determine the affect of altered ciliogenesis in the 5xFAD mouse, intracerebroventricular (i.c.v.) cannula delivered microinjections of the listed inhibitors would provide samples for glycomic analysis and confocal microscopy.

Glycosylation is altered during differentiation of NHBE cells

Chapter three describes the changes observed in glycosylation of differentiating human bronchus epithelium. Overall, there are broad changes in glycosylation. Each class of glycan has a distinct alteration, that likely stems from separate regulatory elements. N-glycans show a change in the diversity and abundance hybrid and complex structures alongside changes in high mannose. O-glycans do not show any change in diversity but class wide increases in abundance as differentiation proceeds. Unique alterations in sulfated structures show an increase for highly regulated structures that are not found on mTECs. Finally, GSLs are reduced in complexity with globo series structures dominating

the profile. These changes occur concomitant with increases in anti-inflammatory epitopes.

Currently, there is a paucity of information on changes in glycosylation during differentiation and how infection and allergic disease are affected. Certain strains of bacterial and viral pathogens of the airway rely on glycans for survival and cell entry. For some, like *M. pneumoniae*, it is still unknown what mediates cell entry. Interestingly, *M. pneumoniae* can harvest host glycans and use them 1) a substrate for synthesizing their own glycans and 2) decorate their cell surface for avoidance of immunodetection (Daubenspeck et al. 2015). Therefore, further analysis of glycosylation and *M. pneumoniae* infection is needed. Additionally, the contribution of anti-inflammatory epitopes to their immune avoidance would provide new directions for therapeutic design.

Determine binding capacity of human Siglecs

The Siglec family of lectins is highly varied in what sialyloglycans they recognize (Macauley et al. 2014). Siglec-8 and Siglec-9 recognize very different epitopes with minor overlap on 6'-su-sLacNAc, yet signal for apoptosis for eosinophils and neutrophils, respectively. This apoptosis is the basis for therapeutics currently in design, to limit the allergic inflammation in Asthma and COPD. Removal of eosinophils and neutrophils in allergic disease is beneficial since they exacerbate the inflammation and damage. However, removal of eosinophils during *Pseudomonas aeruginosa* infection impairs clearance in mice (Hogan et al. 2013). The relationship between eosinophils and bacterial infection

is uncertain since there is a rapid decline in eosinophil numbers following sepsis, yet they have a clear capacity to clear some infections. Therefore, the relationship between Siglecs, glycosylation, and *M. pneumoniae* infection needs to be investigated.

Similar to Siglec-F overlays, determining the binding pattern of human Siglecs during differentiation of NHBE cells will provide a basis for immunomodulatory epitopes. This will allow NHBE cells that are infected with *M. pneumoniae* to be probed for loss of ligand. Conversely, *M. pneumoniae* isolated from infected NHBE ALI culture can be probed for Siglec ligands on the cell surface that were harvested from their host. If *M. pneumoniae* are capable of scavenging and displaying the glycan ligands for Siglecs, this provides an acquired mechanism of avoiding immunodetection in addition to limiting the number of leukocytes present.

Determine the ability of *M. pneumoniae* to bind NHBE lysate and secreted mucins during differentiation

Alternatively, *M. pneumoniae* are capable of binding and infecting NHBE cells through an undetermined, nonproteinacious molecule. Using protein lysate from differentiating NHBE cells and the mucins isolated from them, elucidating glycan-binding epitopes may be determined through *M. pneumoniae* overlays. Similar to a western blot, radioisotope labeled *M. pneumoniae* may be used as a cellular binding probe. This simple assay will provide new insights into what *M. pneumoniae* binds during infection.

Closing Remarks

Overall, this dissertation is focused on glycan-mediated disease and resolution since this is my main interest in research. I have greatly enjoyed the writing process, much to my surprise, since it has afforded me new enjoyment in my research. Hopefully, the reader also found value in these pages.

Figure 5.1: Quantitative RT-PCR of AD forebrain reveals no changes in glycosyltransferase abundance.

Whole forebrains with the olfactory bulb and cerebellum removed were used for qRT-PCR. Here, a detailed analysis of the most common initiating and branching enzymes for N- and O-glycosylation shows no significant changes between AD and WT.

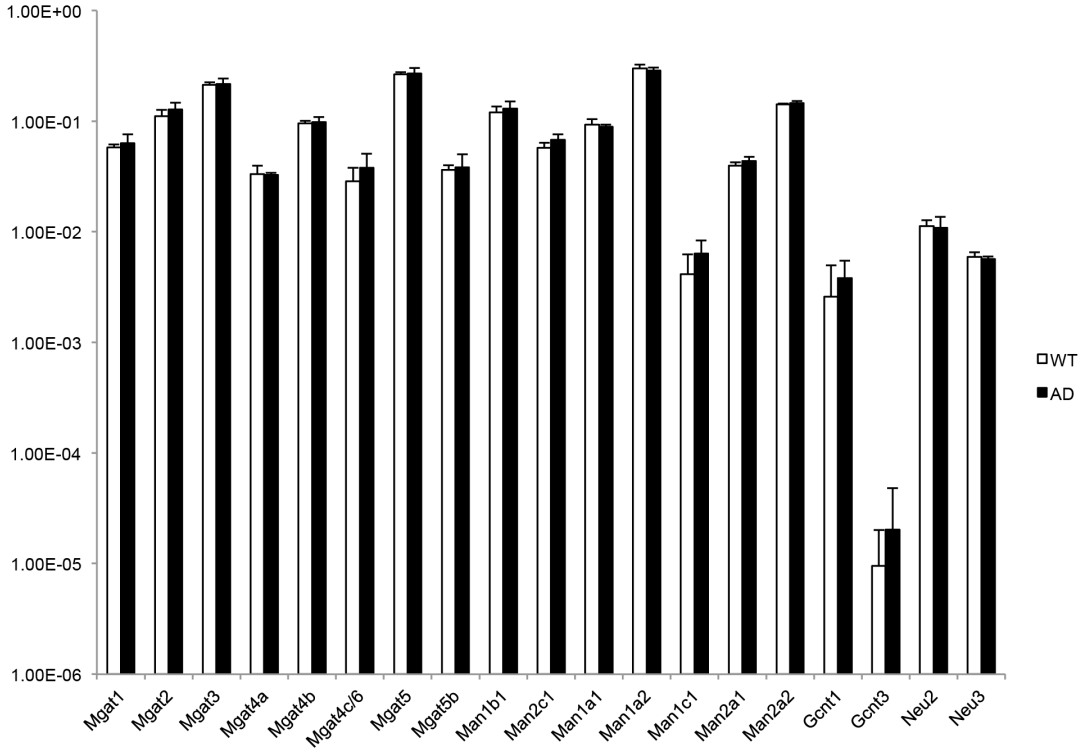

Figure 5.2: Quantitative RT-PCR of AD forebrain reveals no changes in glycosyltransferase abundance.

Whole forebrains with the olfactory bulb and cerebellum removed were used for qRT-PCR. Here, a detailed analysis of the most common initiating and branching enzymes for N- and O-glycosylation shows no significant changes between AD and WT.

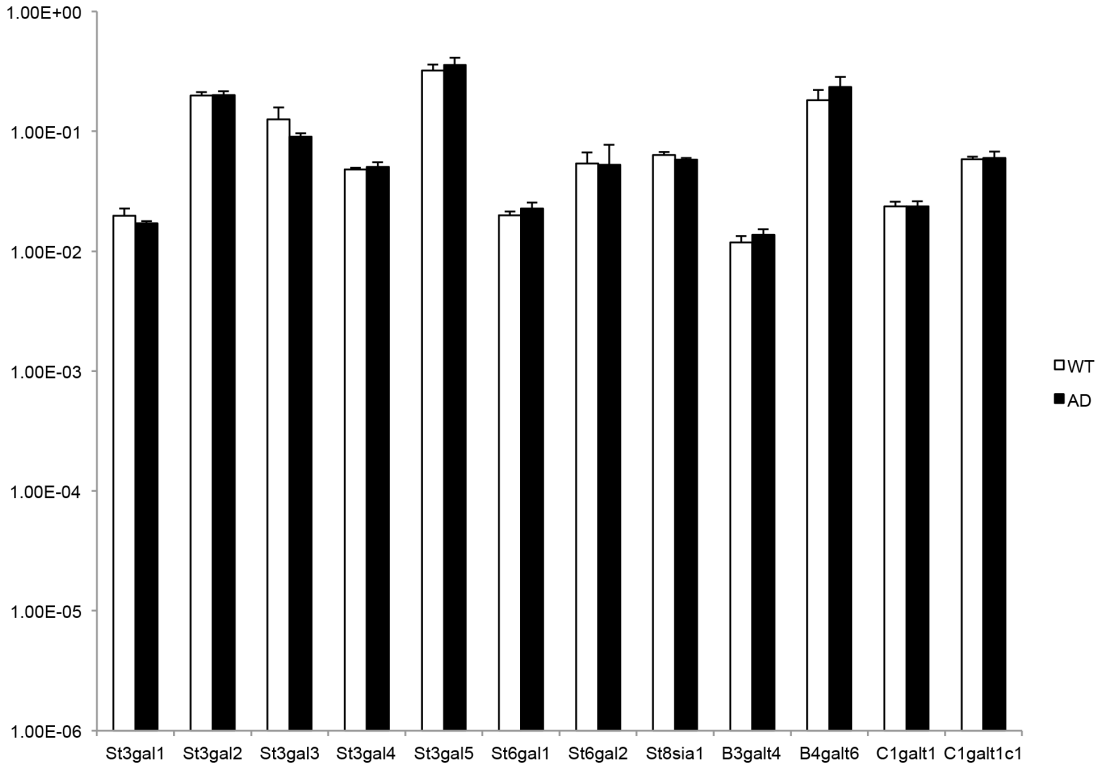

Figure 5.3: Determining the effect of LRP1

To determine how LRP1 influences monocytes and macrophages, primary cells are needed. Extraction of bone marrow from the femur and tibia of adult mice provides mesenchymal stem cells that can be differentiated into naïve monocytes, M1 macrophages, and M2 macrophages. These cells can be stimulated with LRP1 enriched from WT and AD mice to promote cell fate determination. Culture media can be used for cytokine analysis and FACS will determine cell type.

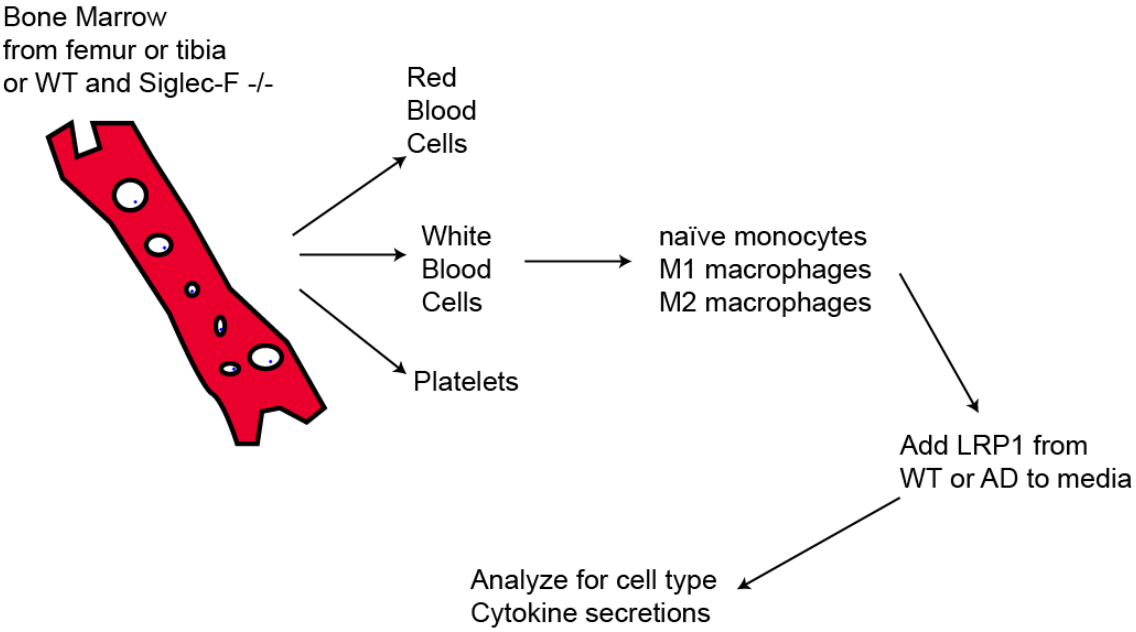

Figure 5.4: Probing whole brain lysate for Siglec-F ligands

Whole brain lysate analyzed by Siglec-F-Fc overlay shows an additional nine bands below 250-kD (A). To further characterize the nature of these ligands lectin blots were used with enzymatic treatment of the lysate. When lysate is probed with MAA, which binds α2-3 sialic acid, strong banding is observed at 150-kD (B). When probed with SNA, which binds α2-6 sialic acid, banding is seen at multiple locations that are distinct from what is seen for MAA (C).

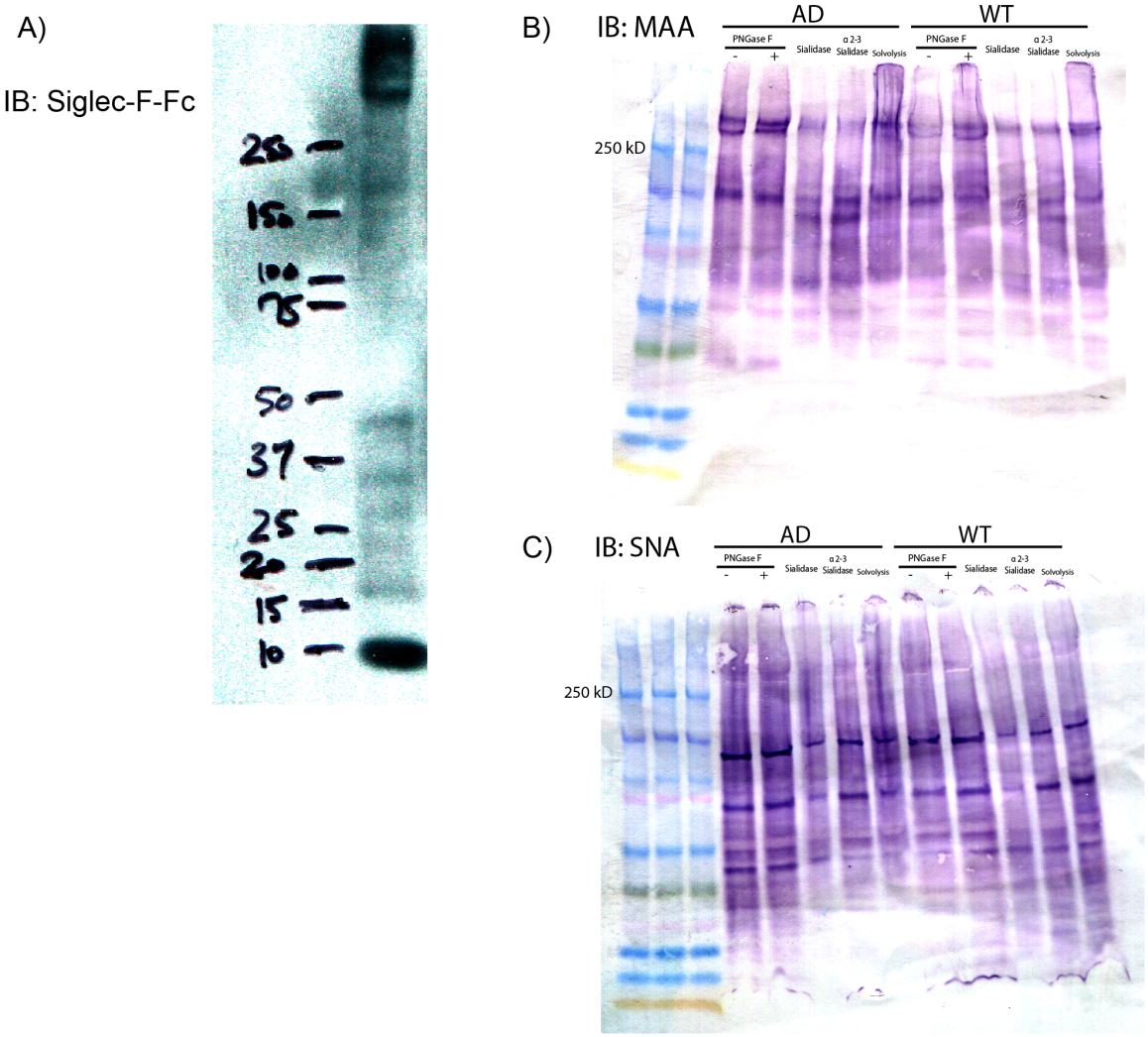

Figure 5.5: Ciliogenesis defect in 5xFAD mice

Frozen sections from WT and AD mice were stained with H&E and imaged. In WT mice the appearance of cilia at the choroid plexus' apical surface is readily apparent, while the apical surface of AD mice appears to have a defect. The lack of visible, defined cilia in AD sections speaks to the need for a more careful characterization of the structure.

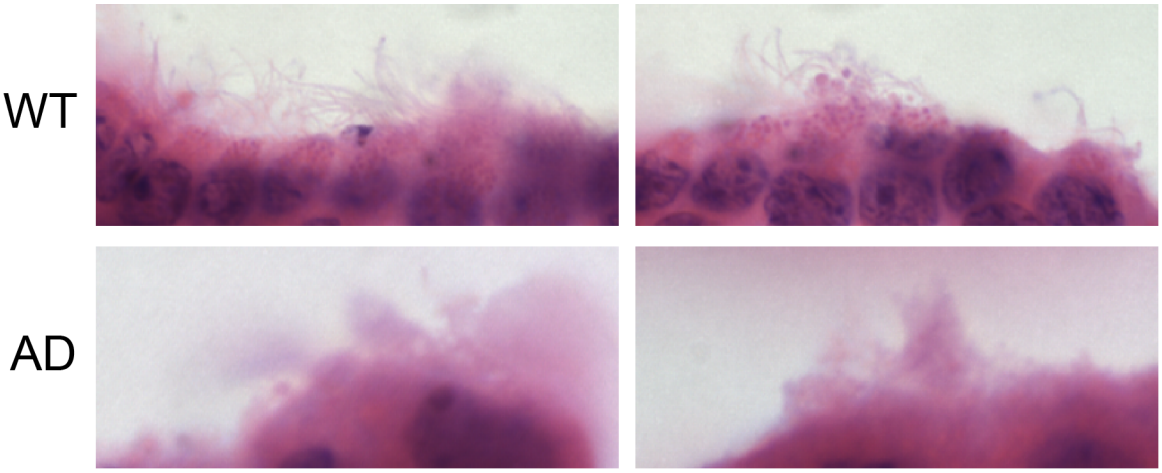

References

Baruch, K., Ron-Harel, N., Gal, H., Deczkowska, A., Shifrut, E., Ndifon, W., Mirlas-Neisberg, N., Cardon, M., Vaknin, I., Cahalon, L., Berkutzki, T., Mattson, M.P., Gomez-Pinilla, F., Friedman, N. and Schwartz, M. (2013). "CNS-specific immunity at the choroid plexus shifts toward destructive Th2 inflammation in brain aging." Proc Natl Acad Sci U S A **110**(6): 2264-2269.

Baruch, K., Rosenzweig, N., Kertser, A., Deczkowska, A., Sharif, A.M., Spinrad, A., Tsitsou-Kampeli, A., Sarel, A., Cahalon, L. and Schwartz, M. (2015). "Breaking immune tolerance by targeting Foxp3(+) regulatory T cells mitigates Alzheimer's disease pathology." Nat Commun **6**: 7967.

Chakravarthy, B., Gaudet, C., Menard, M., Brown, L., Atkinson, T., Laferla, F.M., Ito, S., Armato, U., Dal Pra, I. and Whitfield, J. (2012). "Reduction of the immunostainable length of the hippocampal dentate granule cells' primary cilia in 3xAD-transgenic mice producing human Abeta(1-42) and tau." Biochem Biophys Res Commun **427**(1): 218-222.

Chantret, I. and Moore, S.E. (2008). "Free oligosaccharide regulation during mammalian protein N-glycosylation." Glycobiology **18**(3): 210-224.

Damkier, H.H., Brown, P.D. and Praetorius, J. (2013). "Cerebrospinal fluid secretion by the choroid plexus." Physiol Rev **93**(4): 1847-1892.

Daubenspeck, J.M., Jordan, D.S., Simmons, W., Renfrow, M.B. and Dybvig, K. (2015). "General N-and O-Linked Glycosylation of Lipoproteins in Mycoplasmas and Role of Exogenous Oligosaccharide." PLoS One **10**(11): e0143362.

Guemez-Gamboa, A., Coufal, N.G. and Gleeson, J.G. (2014). "Primary cilia in the developing and mature brain." Neuron **82**(3): 511-521.

Hogan, S.P., Waddell, A. and Fulkerson, P.C. (2013). "Eosinophils in infection and intestinal immunity." Curr Opin Gastroenterol **29**(1): 7-14.

Kim, J., Lee, J.E., Heynen-Genel, S., Suyama, E., Ono, K., Lee, K., Ideker, T., Aza-Blanc, P. and Gleeson, J.G. (2010). "Functional genomic screen for modulators of ciliogenesis and cilium length." Nature **464**(7291): 1048-1051.

Lehtinen, M.K., Zappaterra, M.W., Chen, X., Yang, Y.J., Hill, A.D., Lun, M., Maynard, T., Gonzalez, D., Kim, S., Ye, P., D'Ercole, A.J., Wong, E.T., LaMantia, A.S. and Walsh, C.A. (2011). "The cerebrospinal fluid provides a proliferative niche for neural progenitor cells." Neuron **69**(5): 893-905.

Li, C., Du, Y., Yang, Z., He, L., Wang, Y., Hao, L., Ding, M., Yan, R., Wang, J. and Fan, Z. (2016). "GALNT1-Mediated Glycosylation and Activation of Sonic Hedgehog Signaling Maintains the Self-Renewal and Tumor-Initiating Capacity of Bladder Cancer Stem Cells." Cancer Res **76**(5): 1273-1283.

Liu, Q., Zhang, J., Tran, H., Verbeek, M.M., Reiss, K., Estus, S. and Bu, G. (2009). "LRP1 shedding in human brain: roles of ADAM10 and ADAM17." Mol Neurodegener **4**: 17.

Lun, M.P., Johnson, M.B., Broadbelt, K.G., Watanabe, M., Kang, Y.J., Chau, K.F., Springel, M.W., Malesz, A., Sousa, A.M., Pletikos, M., Adelita, T., Calicchio, M.L., Zhang, Y., Holtzman, M.J., Lidov, H.G., Sestan, N., Steen, H., Monuki, E.S. and Lehtinen, M.K. (2015). "Spatially heterogeneous choroid plexus transcriptomes encode positional identity and contribute to regional CSF production." J Neurosci **35**(12): 4903-4916.

Lun, M.P., Monuki, E.S. and Lehtinen, M.K. (2015). "Development and functions of the choroid plexus-cerebrospinal fluid system." Nat Rev Neurosci **16**(8): 445-457.

Macauley, M.S., Crocker, P.R. and Paulson, J.C. (2014). "Siglec-mediated regulation of immune cell function in disease." Nat Rev Immunol **14**(10): 653-666.

May, P., Bock, H.H. and Nofer, J.R. (2013). "Low density receptor-related protein 1 (LRP1) promotes anti-inflammatory phenotype in murine macrophages." Cell Tissue Res **354**(3): 887-889.

Narita, K. and Takeda, S. (2015). "Cilia in the choroid plexus: their roles in hydrocephalus and beyond." Front Cell Neurosci **9**: 39.

Overdijk, B., van der Kroef, W.M., Lisman, J.J., Pierce, R.J., Montreuil, J. and Spik, G. (1981). "Demonstration and partial characterization of endo-N-acetyl-beta-D-glucosaminidase in human tissues." FEBS Lett **128**(2): 364-366.

Peng, G.E., Wilson, S.R. and Weiner, O.D. (2011). "A pharmacological cocktail for arresting actin dynamics in living cells." Mol Biol Cell **22**(21): 3986-3994.

Ranganathan, S., Cao, C., Catania, J., Migliorini, M., Zhang, L. and Strickland, D.K. (2011). "Molecular basis for the interaction of low density lipoprotein receptor-related protein 1 (LRP1) with integrin alphaMbeta2: identification of binding sites within alphaMbeta2 for LRP1." J Biol Chem **286**(35): 30535-30541.

Rodriguez, J.J., Jones, V.C., Tabuchi, M., Allan, S.M., Knight, E.M., LaFerla, F.M., Oddo, S. and Verkhratsky, A. (2008). "Impaired adult neurogenesis in the dentate gyrus of a triple transgenic mouse model of Alzheimer's disease." PLoS One **3**(8): e2935.

Shechter, R., Miller, O., Yovel, G., Rosenzweig, N., London, A., Ruckh, J., Kim, K.W., Klein, E., Kalchenko, V., Bendel, P., Lira, S.A., Jung, S. and Schwartz, M. (2013). "Recruitment of beneficial M2 macrophages to injured spinal cord is orchestrated by remote brain choroid plexus." Immunity **38**(3): 555-569.

Silverberg, G.D., Mayo, M., Saul, T., Rubenstein, E. and McGuire, D. (2003). "Alzheimer's disease, normal-pressure hydrocephalus, and senescent changes in CSF circulatory physiology: a hypothesis." Lancet Neurol **2**(8): 506-511.

Xiang, Y., Zhang, X., Nix, D.B., Katoh, T., Aoki, K., Tiemeyer, M. and Wang, Y. (2013). "Regulation of protein glycosylation and sorting by the Golgi matrix proteins GRASP55/65." Nat Commun **4**: 1659.